

# Natural Late Holocene lake level fluctuations recorded in the Ipperwash strandplain, southern Lake Huron

by

Sean Morrison

A thesis

presented to the University of Waterloo

in fulfilment of the

thesis requirement for the degree of

Master of Science

in

Earth Science (Water)

Waterloo, Ontario, Canada, 2017

©Sean Morrison 2017

## **Author's Declaration**

I hereby declare that I am the sole author of this thesis. This is a true copy of the thesis, including any required final revisions, as accepted by my examiners.

I understand that my thesis may be made electronically available to the public.

## Abstract

The Laurentian Great Lakes (LGL) are the largest system of surface freshwater on Earth. Three factors, glacial isostatic adjustment (GIA), outlet conveyance, and climate processes contribute to natural rises and falls in LGL lake level over geologic time. Studying the natural history of prehistoric lake levels preserved in coastal landforms helps determine the context of current lake levels and predict potential future lake level changes.

Detailed records of lake level change during the late Holocene are preserved in strandplains of beach ridges. Each beach ridge forms as a result of a lake level rise and fall over many decades and preserves a record of relative lake level elevation at the time of deposition. Multiple beach ridges within a single strandplain contain an account of relative lake level changes over the past 4,500 years.

This study examined beach ridges in the Ipperwash strandplain, southern Lake Huron, that uniquely preserves natural lake level fluctuations at the only unregulated outlet in the LGL, the Port Huron/Sarnia outlet of Lake Michigan-Huron, which is particularly susceptible to natural lake level fluctuations. The Ipperwash strandplain is the closest strandplain with the most number of beach ridges to the Port Huron/Sarnia outlet and therefore best records natural lake level fluctuation experienced at the Port Huron/Sarnia outlet of Lake Michigan-Huron.

The study of the Ipperwash strandplain beach ridges used many methods to derive measured elevations and modelled ages of ancient lake levels. Elevation data is combined with age data to create the Ipperwash paleohydrograph. Thirty-six basal foreshore elevations were used to reconstruct the elevation of ancient lake levels. Elevation data shows an oscillatory lake level fall from a maximum elevation of 181.0 m to a minimum elevation of 177.8 m. Ten optically stimulated luminescence ages were used to create a linear age model of the Ipperwash strandplain. The resultant age model shows a maximum age of 3520 years ago and a minimum age of 710 years ago.

The multi-millennium trend shows a net linear fall at an average rate of 7 cm/century for the entire Ipperwash paleohydrograph. This trend is interpreted as a record of the rate of GIA at Ipperwash relative to Lake Michigan-Huron's outlet. The multi-millennium trend suggests the rate of GIA at Ipperwash is 7 cm/century; however, estimates of GIA based on water gauge data suggest the rate

of GIA at Ipperwash is 0 cm/century. This discrepancy could result from an underestimation estimated from contoured water level gauge data for the rate of GIA at Ipperwash, erosion at the Port Huron/Sarnia outlet during the deposition of the Ipperwash strandplain and/or the Chicago outlet being dominant during the deposition of the Ipperwash strandplain.

The multi-millennium trend may also be expressed as two millennium trends shown as two vertically offset phases of lake-level lowering from 3520 to 2180 years ago and 2020 to 710 years ago. These age ranges correspond with the Algoma and 1700-high lake level phases in Lake Michigan. Millennium patterns at Ipperwash corresponds to regional climate records and may represent a climate signal. However, the rate of linear lake level lowering for the older lake level phase at Ipperwash corresponds with the difference in rates of GIA, based on water gauge data, between the Chicago outlet and the Ipperwash strandplain. Therefore, the millennium trends may represent either natural climate change or the abandonment of the Chicago outlet of Lake Michigan-Huron. Detailed sedimentologic and lake level records at the Port Huron/Sarnia and Chicago outlets are needed to resolve this controversy.

Centennial lake level fluctuations represent rises and falls in lake levels lasting an average of 208 years  $\pm$  114 years with an average amplitude of  $0.8 \pm 0.4$  m about the linear millennium trends. The average timing of the centennial lake level fluctuation at Ipperwash are similar to centennial lake level fluctuations found in Lakes Superior and Michigan-Huron that are interpreted to represent climate driven lake level fluctuations.

Multi-decadal lake level fluctuations cause a single Ipperwash strandplain beach ridge to form average every  $73 \pm 35$  years. The subsurface stratigraphy of Ipperwash beach ridges shows a similarity of other LGL beach ridges which are interpreted to form as a result of a climate driven lake level fluctuations over many decades.

The Ipperwash paleohydrograph provides the context needed to adjust all strandplain data in Lake Michigan-Huron to resolve basin-wide relative lake level changes related to GIA, outlet conveyance, and climate. In addition, the Ipperwash paleohydrograph suggest lake-level may rise and fall on a multi-decadal time scale contributing to erosion and setting the stage to create a new beach ridge, assuming the rate of sediment supply is maintained.

## Acknowledgements

First and foremost, I would like to thank my supervisor, Dr John Johnston, for giving me the opportunity to explore the natural history of the Great Lakes while gaining valuable experience in the field and in the lab, and also for countless discussions, edits and insights about my Master's project.

I would also like to thank my committee members, Dr Harry Jol, Dr Martin Ross, and Dr Tony Endres, for their help during the project and review of this thesis.

I would like to thank Dr Todd Thompson and Dr Henry Loope for their discussions and observations about the ancient shorelines of the Great Lakes. And the Indiana Geological Survey for the use of lab equipment.

I would like to thank Dr Ken Lepper with the Optical Dating Dosimetry Lab at North Dakota State University for processing samples for OSL dating and for innumerable emails regarding OSL results.

I would like to thank Dale and Hugh Lausannen at Cobblestone Cottages for their encyclopedic knowledge of Ipperwash Beach, and their caring support. I would also like to thank the Centre Ipperwash Community Association for their assistance in networking with the local community.

I am also grateful to Paul Johnson for his help with core processing; Andrew Wiebe for helping to arrange equipment use; Riley Mulligan for making available high-resolution DEM data.

I would also like to thank my field assistants Cesar Garcia and Anthony Zamperoni for their tireless work trekking through swampy swales and over bramble filled ridges.

Finally, I would like to thank, and am forever grateful to, all my friends and family for their support, encouragement and amity.

# Table of Contents

Author’s Declaration.....	ii
Abstract .....	iii
Acknowledgements.....	v
Table of Contents.....	vi
List of Figures.....	ix
List of Tables.....	xiii
Chapter 1 Introduction .....	1
1.1 Significance and objectives .....	3
Chapter 2 Background .....	5
2.1 Glacial History and Glacial Isostatic Adjustment.....	5
2.2 Prehistoric Lakes .....	6
2.2.1 Algonquin Highstand.....	7
2.2.2 Stanley Lowstands and Mattawa Highstands .....	8
2.2.3 Nipissing Highstand.....	8
2.2.4 Modern Lakes .....	9
2.2.5 Drivers of Post-Nipissing Lake Level Change .....	10
2.2.6 Historic lake level drivers .....	11
2.3 Beach Ridges.....	12
2.3.1 Beach Ridges and LGL Lake Levels.....	13
2.3.2 Sedimentary Facies .....	13
2.3.3 Depositional Model.....	14
Chapter 3 Study Area .....	17
3.1 Lake Huron.....	17
3.2 The Thedford Embayment.....	18

3.3 The Ipperwash strandplain .....	19
Chapter 4 Methods .....	22
4.1 Field Observations and Satellite Image Interpretation.....	22
4.2 Ground Penetrating Radar.....	22
4.3 Topographic Surveying .....	23
4.4 Vibracoring .....	24
4.5 Lab Analysis.....	24
4.6 Optical Stimulated Luminescence .....	25
Chapter 5 Results and Discussion .....	27
5.1 Field Observations.....	28
5.2 Radar Stratigraphy.....	31
5.3 Topographic Survey.....	34
5.4 Modern Shoreline Facies.....	38
5.5 Ancient Shoreline Facies .....	39
5.6 Cross Strandplain Geomorphic and Sedimentological Characteristics.....	42
5.6.1 Ridge Groups and Interpretations.....	44
5.7 Age Modelling .....	47
5.8 Developing the Ipperwash Paleohydrograph.....	50
Chapter 6 The Ipperwash paleohydrograph .....	52
6.1 GIA, outlet conveyance and climate .....	54
6.2 Multi-millennium pattern.....	56
6.3 Millennium patterns.....	58
6.4 Centennial patterns .....	62
6.5 Multi-decadal patterns .....	63
Chapter 7 Conclusion.....	64

Chapter 8 Recommendations.....	67
References .....	68
Appendix A Ground Penetrating Radar Profiles .....	78
Appendix B Modern Beach Survey and Elevation Calibration.....	86
Appendix C Cross Strandplain Topographic Survey.....	87
Appendix D Modern Beach Sample Statistics.....	93
Appendix E Core Statistics.....	94
Appendix F Core Sediment Sample Statistics.....	95
Appendix G Reasoning for Facies Differentiation .....	110



## List of Figures

Figure 1: The five Laurentian Great Lakes (LGL) are shared water bodies between the USA and Canada. Important former and active outlets are labelled. Today, the entire LGL drains into the Atlantic Ocean via the St Lawrence River. The study area for this thesis is located in southern Lake Huron, near the Port Huron/Sarnia outlet. ....	1
Figure 2: Rate of GIA in cm/century based on water level gauge data nested within ICE-3G rates of GIA. Note the zero relative isobase passes through southern Lake Huron near the Port Huron/Sarnia outlet. (Modified from Mainville and Craymer, 2005).....	6
Figure 3: Outlet referenced paleohydrograph of Lake Huron over the past 13,000 years showing a wide range of lake level variations. Maps of shoreline position during the Lake Algonquin highstand, Stanley lowstands, Nipissing highstand, and the modern shoreline position. There is a similarity in shoreline position in southern Lake Huron of the Algonquin and Nipissing shorelines. (Modified from Johnston et al., 2014; and Clark et al., 2012) .....	7
Figure 4: Lake Michigan paleohydrograph showing the fall from the Nipissing highstand to the modern lake configuration. The lake level curve is mirrored 0.6 m below the paleohydrograph to indicate possible extent of low lake levels (From Baedke and Thompson, 2000). ....	10
Figure 5: Typical core showing common sediment facies within LGL beach ridges include dune, foreshore and upper shoreface deposits. Identification of the contact between foreshore and upper shoreface deposits (also called the plunge point) correlates with lake level at the time of deposition (from Thompson et al., 2014) .....	14
Figure 6: Conceptual model of LGL beach ridge development shows how beach ridges develop in response to lake level fluctuations. Colors show correlations between graphs and diagrams. A simple rise or fall in lake level will affect the rate of lake level change (A) and a change in the rate of sediment supply will affect shoreline behavior (B) together the rate of lake level change and sediment supply dictates how the coastline responds to lake level fluctuations (modified from Johnston et al., 2007). Diagrams of strandplain cross sections show how the beach responds to changing rates of lake level change (C). ....	15
Figure 7: The Thedford Embayment, southern Lake Huron, contains several ancient shorelines. The Ipperwash strandplain extends from Kettle Point to Grand Bend and extends from the Nipissing shoreline to the modern beach. Shorelines in Pinery Provincial Park are covered by large dunes, while beach ridges are exposed on the northern and southern ends of the Ipperwash strandplain.	

The study area is located on the southern end of the Ipperwash strandplain, near Ipperwash Beach. ....21

Figure 8: Aerial image of the southern Ipperwash strandplain with outline of surveyed area, major drainages and the Nipissing bluff. Road access is along W Ipperwash Road, Ipperwash Road, and Army Camp Road. ....21

Figure 9: A straight line, shore perpendicular transect was drawn in QGIS to develop a topographic profile across the Ipperwash strandplain. A DEM created from SWOOP 2015 data shows strandplain elevations. ....24

Figure 10: Map showing the location of GPR profiles, vibracores, OSL samples, and topographic survey collected on and in the Ipperwash Strandplain. As well as segments qualitatively assessed through field observations and satellite images. ....27

Figure 11: Location of GPR profiles collected on the Ipperwash strandplain. ....31

Figure 12: Raw (BEAN-2) and interpreted (BEAN-B) GPR profile collected in a shore perpendicular orientation across the modern beach. Color scheme of interpretations shown in figure 11. ....33

Figure 13: Generalized radar stratigraphic cross section across two, beach ridges based on analysis of modern and ancient Ipperwash beach ridges. Vertical exaggeration x3. Radar reflection patterns are described and interpreted to represent dune, disturbed areas, water table, erosional surface, foreshore and shoreface sediments. ....34

Figure 14: Comparison of cross strandplain elevation profiles developed from 2016 surveyed elevations, Johnston (1999), and drawn from the SWOOP 2015 DEM. Also plotted are core elevations and the Nipissing elevation from Thompson et al. (2014). A discrepancy between 2016 elevations, Johnston (1999) and SWOOP 2015 is minimal up to 630 m distance landward but then diverges. ....36

Figure 15: Comparison of the difference between core elevations determined from 2016 surveyed elevations and from the SWOOP 2015 DEM. Two groups of elevations (209-666 m and 699-1785 m landward) are consistently offset. Groups have a similar standard deviation and range but have means that differ by 3.1 m. ....36

Figure 16: Adjusted topographic profile shows good agreement across the entire length of the 2016 survey. Profiles were adjusted by subtracting 1 m from 2016 surveyed elevations between 630 and 690 m landward and 2.5 m from 690 m landward to the landward margin of the survey. SWOOP 2015 elevations were adjusted by adding 1 m to points landward of 660 m. ....37

Figure 17: Plot of topographic survey and grain size results (mean, sorting and skewness) from the modern Ipperwash Beach showing the foreshore-shoreface contact as an abrupt change in grain size parameters. ....38

Figure 18: Visual descriptions and grain size statistics from core 2025. Shoreface sediments (274-163 cm), foreshore sediments (163-119 cm) and dune sediments (119-0 cm) are characterized by differing sedimentary structures and grain size parameter. The abrupt contact between foreshore and shoreface sediments is used as a proxy for the ancient lake level elevation when that beach ridge formed. ....40

Figure 19: Surface elevation, core sediment facies and OSL ages from the Ipperwash strandplain. All data is plotted with respect to distance from the modern shoreline with ridge numbers labelled. ....42

Figure 20: Geomorphic and sedimentologic characteristics across the Ipperwash strandplain showing aerial imagery with OSL sample location labeled. Eight segments (A-H) were qualitatively identified based on field observations. Groups of 3 to 7 ridges identified as rises and falls below 1 standard deviation are also identified and bracketed. ....46

Figure 21: OSL element data used for dose rate calculation and OSL age results (from Lepper, 2017). ....48

Figure 22: Age model A connects all individual ages sequentially and shows slopes between individual ages. The average slope is 1.9 years/m and a standard error of 1.1. ....49

Figure 23: Age model B uses a linear regression through all ages. The resultant equation is  $y = 1.8 \pm 0.09x + 98.5 \pm 107.0$  and has a  $r^2$  is 0.98. ....49

Figure 24: Ipperwash paleohydrographs developed from age model A and B. ....51

Figure 25: Ipperwash paleohydrograph compared to Lake Huron’s annual average historic lake level. The Ipperwash paleohydrograph records lake level fluctuations from 3520 to 710 years ago and shows a net lake level decrease from a high of 181.0 m 3450 years ago to a low of 177.8 m 850 years ago. ....53

Figure 26: Historic hydrograph, Ipperwash paleohydrograph and the Lake Michigan paleohydrograph (Baedke and Thompson, 2000). If the Lake Michigan paleohydrograph is adjusted based on the rate of GIA at Ipperwash the two graphs plot closely. ....54

Figure 27: A linear regression through the entire paleohydrograph shows a relatively well confined pattern spanning the entire paleohydrograph. ....57

Figure 28: Ipperwash paleohydrograph with GIA removed and divided into two linear regressions which suggests two phases of lake level lowering. The two periods of lake level lowering are vertically offset by 0.5 m and a period of 160 years. ....59

Figure 29: Ipperwash paleohydrograph divided into centennial oscillations as defined by lake level rises and falls about the millennium pattern lines. Centennial oscillations are represented by groups of 3 to 5 ridges. ....62

## List of Tables

Table 1: Characteristics used to subdivide the Ipperwash strandplain into 8 segments based on field observations. ....	30
Table 2: Characteristics of modern beach facies.....	39
Table 3: Common characteristics used to differentiate core sediment facies .....	41
Table 4: Cross strandplain geomorphic and sedimentologic statistics.....	43
Table 5: Reported and modelled ages .....	50
Table 6: F-Test Two-Sample for Variances .....	51

# Chapter 1

## Introduction

The Laurentian Great Lakes (LGL) are the largest freshwater system in the world by surface area, and second largest by volume (Gronewold et al., 2013a). The LGL are a system of interconnected large lakes, as well as connecting and inflowing rivers, surrounding wetlands, and smaller water bodies, which extend along the border of the United States of America and Canada (Figure 1). At the head of the LGL, Lake Superior is the largest lake by volume, and outflows through the Sault Ste Marie rapids and locks (the Sault outlet) affecting lake levels in the lower basins (International Upper Great Lakes Study Board, 2009; 2012). Lakes Michigan and Huron are hydrologically connected and outflow through the only unregulated outlet (lacking any locks) in the entire LGL at Port Huron, Michigan and Sarnia, Ontario (Port Huron/Sarnia outlet) before draining into Lake Erie and then Lake Ontario then flowing down the 1,200 km-long St Lawrence River into the Atlantic Ocean (International Upper Great Lakes Study Board, 2009; 2012; Figure 1).



*Figure 1: The five Laurentian Great Lakes (LGL) are shared water bodies between the USA and Canada. Important former and active outlets are labelled. Today, the entire LGL drains into the Atlantic Ocean via the St Lawrence River. The study area for this thesis is located in southern Lake Huron, near the Port Huron/Sarnia outlet. Satellite imagery from Google Earth.*

The LGL contains nearly 20% of the world's surface freshwater supply, and provides drinking water for forty million people in the USA and Canada (Gronewold et al., 2015). Many commercial industries rely on water from the LGL including fishing, recreation, cargo shipping, hydropower, manufacturing and agriculture. In 2010, a quarter of million jobs supported the shipping of 322.1 million metric tons of cargo through a 3,700 km long deep draft navigation system, the longest in the world, which links the LGL to the global sea lanes (Martin Associates, 2011). If politically combined, the eight US states and two Canadian provinces which at least partially lie within the LGL basin would constitute the third largest economy in the world (Porter, 2015).

Commercial industry in the LGL rely on consistent, or at least predictable, lake levels; however, lake levels in the LGL naturally fluctuate on many scales ranging from seconds to millennia. Lake level changes are influenced by various processes including weather systems, regional climate patterns, vertical ground movement, and human activities (Gronewold and Stow, 2014; Johnston et al., 2014). In modern times, lake level changes damage near shore structures (Meadows et al., 1997), impact wetland habitats (Wilcox et al., 2007), and affect commercial shipping (International Upper Great Lakes Study Board, 2009; 2012;). Lake levels in Lake Michigan-Huron over the historic record (since 1860 CE) are recorded by water gauges which show lake levels have fluctuated up to 2 m on a decadal time scale primarily influenced by changes in regional precipitation and evaporation (Gronewold and Stow, 2014). Human modification and the relatively short historic lake level record means the historic record may not fully represent natural lake level patterns which are preserved in depositional coastal landforms. By studying preserved clues within preserved landforms geoscientists can reconstruct lake level fluctuations going back several millennia. These data provides a natural lake level record that can be used to calibrate models which predict future lake level changes, and can be used by shoreline communities and managers to understand the natural rates of erosion and deposition along a specific shoreline.

Of paramount interest is the outlet for Lake Huron, adjacent to Port Huron, Michigan and Sarnia, Ontario, which became the dominant outlet of Lake Huron during the Late Holocene (Thompson et al., 2014). No long-term lake level studies exist near this pivotal outlet (Johnston et al., 2014), therefore my thesis conducted a study of the Ipperwash strandplain, the nearest preserved lake level

record to the Port Huron/Sarnia outlet, to reconstruct natural lake level fluctuations during the Late Holocene.

## **1.1 Significance and objectives**

An understanding natural coastal processes is important when making management decisions. Wave action, storms, tides, ice and geology contribute to dynamic coastal systems, and human populations living along a coastline are particularly vulnerable as shoreline position changes with lake level fluctuations.

The LGL contains over 4,500 miles of coastline (Gronewold et al., 2013a), yet when compared to ocean coastlines, LGL coastlines offer a unique setting due to minimal tidal influence, frequent lake level fluctuations over the past 10,000 years and vertical ground movement causing lake levels to relatively rise and fall within the same basin (Rawling and Hansen, 2014). To quantify risk along the LGL coastlines coastal vulnerability indexes, developed for ocean coastlines, have been applied to the Apostle Islands National Lakeshore on Lake Superior, Sleeping Bear Dunes National Lakeshore on Lake Michigan and Indiana Dunes National Lakeshore on Lake Michigan (Pendleton et al., 2010). More commonly, engineering and policy based shoreline management plans have been created for individual LGL shoreline segments (i.e. Reinders, F.J. and Associates, 1989; Au-Sable-Bayfield Conservation Authority, 2000). Both coastal vulnerability indexes and shoreline management plans use the historic lake level record to base decisions on. By studying the natural history of shorelines in the LGL Earth scientists are able to reconstruct the natural lake level record as well as examine past shoreline behaviors preserved in coastal landforms. Natural records can then be used to improve coastal vulnerability indexes and shoreline management plans by incorporating natural lake level changes and shoreline behaviors.

Studying a specific LGL shoreline can provide insights into the natural history studied shoreline and the LGL as a whole. One example of a LGL shoreline is the Ipperwash strandplain, southern Lake Huron, which is the study site for this thesis (Figure 1). Indigenous peoples have occupied the region since time immemorial, and the Chippewa's of Kettle and Stoney Point still occupy the area. Ipperwash Beach has been a favored sit of cottage goers for well over a hundred years. In addition, the strandplain also hosts many important ecosystems such as some of Ontario's last remaining



Carolinian Forests (Javala et al., 2015). Pinery Provincial Park in the central portion of the strandplain preserves some of the largest dunes in Ontario as well as diverse ecosystems, while allowing the public to camp, hike, and paddle in the park.

This thesis furthers previous investigations of the Ipperwash strandplain (Johnston, 1999) by examining subsurface stratigraphy of 40 beach ridges and dating 10 individual beach ridges. Subsurface stratigraphy and age data is used to understand the long-term, natural history of the Ipperwash strandplain by 1) defining the natural limits of lake level for the Ipperwash strandplain and 2) deducing the natural patterns of deposition/erosion along Ipperwash beach in relation to natural lake level change.

## Chapter 2

### Background

#### **2.1 Glacial History and Glacial Isostatic Adjustment**

The contemporary extent of the LGL were shaped during the net southward advances and net northward retreats of the Laurentide Ice Sheet. The Wisconsin glaciation was the last glacial advance to erode and deposit material in the LGL basins and reached its maximum extent sometime between 25,270 and 21,290 cal BP before a net northward retreat (Lewis, et al., 2008b). Glacial sediment was sourced from metamorphic and igneous rock of the Canadian Shield in the north and sedimentary rock of the Michigan structural basin in the south. Shoreline outcrops provide an easily available sediment source to a variety of depositional coastal features (Larson and Schaetzl, 2001).

As the ice thinned and retreated the depressed land began to slowly adjust. This adjustment termed glacial isostatic adjustment (GIA), was recognized by early researchers (Gilbert, 1898). Areas of thicker and longer lasting ice were depressed more, and are currently rebounding faster, than areas of thinner shorter-lasting ice. Ice was thicker and longer lasting in the northern portions of the LGL, so today, shore features created by former lake levels in the LGL are generally at higher elevation in the northern portions of the basin (Lewis et al., 2005; Drzyzga et al., 2012). In addition, rising northern outlets were eventually abandoned as outflow transferred to the modern lower southern outlets (Leverett and Taylor, 1915; Lewis, et al., 2008b; Johnston et al., 2014).

Researchers have used GPS and geologic data (Peltier et al., 2015) to estimate rates of GIA on a continental scale. These estimates have been further refined in the LGL using water gauge data (Mainville and Craymer, 2005; Figure 2). Lake level reconstructions from ancient shorelines indicate a similar general pattern of GIA, but suggest some values estimated from water level gauge stations underestimate the long-term rate of GIA shorelines (Baedke and Thompson, 2000; Johnston, et al. 2012). GIA estimations from ancient shorelines and water level gauge data show the ongoing adjustment of the ground surface for the LGL has led to a general southward tilt of the basins, meaning that southern shores are undergoing a long term relative lake-level rise while northern shores experience a relative lake-level fall (Figure 2). The zero isobase or line of no relative uplift or

subsidence has been interpreted to pass through southwestern Lake Superior, northern Lake Michigan and southern Lake Huron (Figure 2).

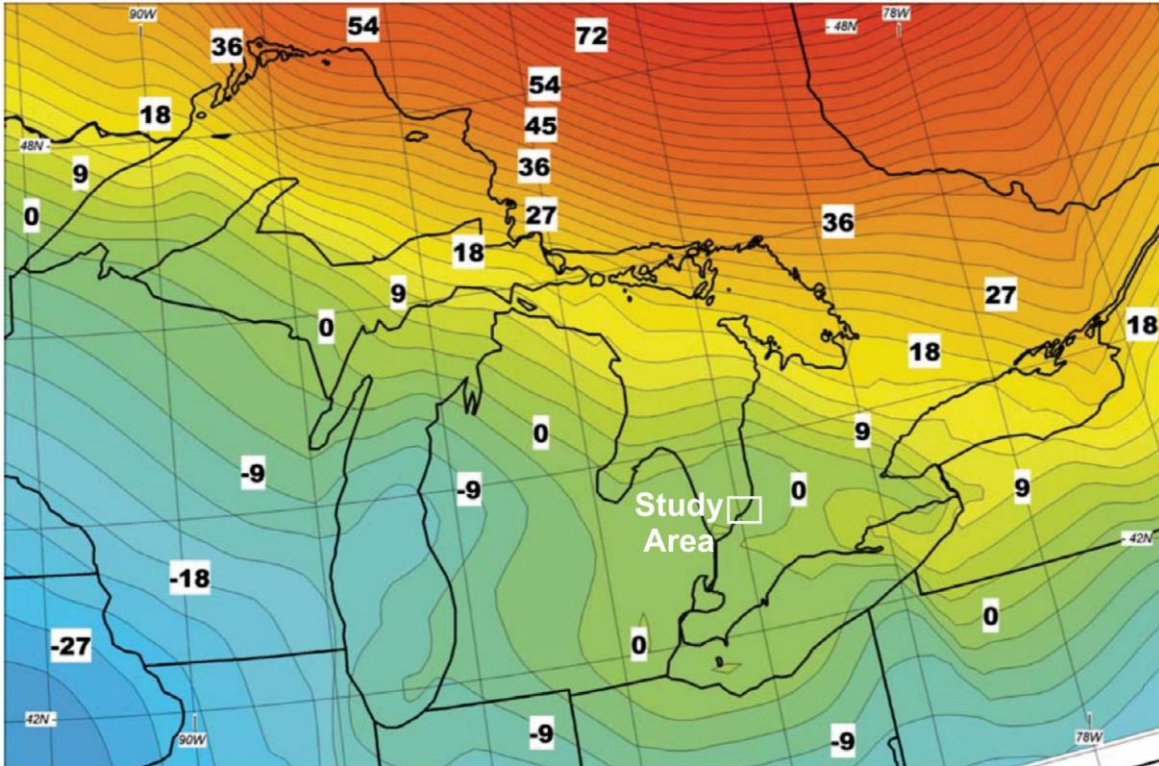


Figure 2: Rate of GIA in cm/century based on water level gauge data nested within ICE-3G rates of GIA. Note the zero relative isobase passes through southern Lake Huron near the Port Huron/Sarnia outlet. (Modified from Mainville and Craymer, 2005)

## 2.2 Prehistoric Lakes

Synthesis of pro-glacial and post-glacial lakes in the LGL basin were first compiled by Leverett and Taylor (1915). Later synthesis includes Hough (1958), Karrow and Calkin (1985), Teller (1987), Larson and Schaetzl (2001), Karrow and Lewis (2007), Kincare and Larson (2009), Clark et al. (2012), Lewis and King (2012), Johnston et al. (2014). A review of the pro-glacial and post-glacial lakes in the Huron basin by Lewis et al. (2008b) and refined by Lewis and Anderson (2012) compiles the current status of research exploring how changes in GIA, outlet conveyance, and climate affected basin wide lake level in ancestral Lake Huron. To elucidate variations in lake level, four well studied post-glacial lake phases in Lake Huron are briefly described: Algonquin highstand, Stanley lowstands and Mattawa highstands, Nipissing highstand, and the modern LGL (Figure 3).

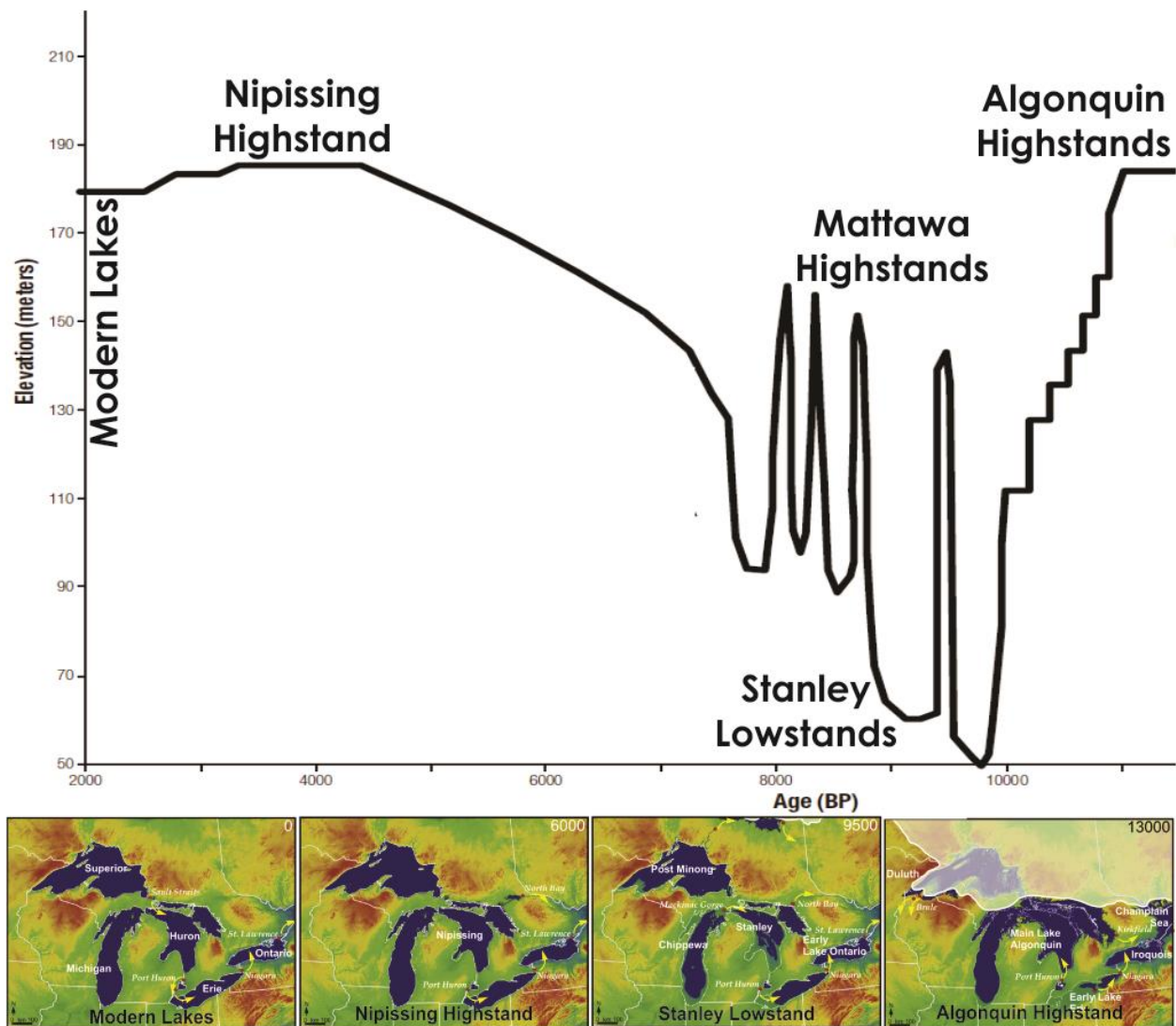


Figure 3: Outlet referenced paleohydrograph of Lake Huron over the past 13,000 years showing a wide range of lake level variations. Maps of shoreline position during the Lake Algonquin highstand, Stanley lowstands, Nipissing highstand, and the modern shoreline position. There is a similarity in shoreline position in southern Lake Huron of the Algonquin and Nipissing shorelines. (Modified from Johnston et al., 2014; and Clark et al., 2012)

### 2.2.1 Algonquin Highstand

The Algonquin highstand was the first hydrologically joined proglacial lake to occupy the Michigan-Huron basin and its shoreline can be traced around much of the basin (Lewis, et al., 2008b). The Algonquin highstand formed as the isostatically rising Kirkfield outlet (Figure 1) caused lake levels to slowly rise eventually reaching a highstand approximately 13,000 cal BP (Figure 3). At this time Lake Algonquin extended beyond the limits of lakes Superior, Huron and Michigan and was

bordered by the Laurentide Ice Sheet to the north (Figure 3). Following the Algonquin highstand, the retreating Laurentide Ice Sheet uncovered the isostatically depressed North Bay Outlet (Figure 1) and lake levels began to fall as Lake Algonquin began to drain through the North Bay Outlet.

### *2.2.2 Stanley Lowstands and Mattawa Highstands*

As water began to flow through the isostatically depressed North Bay outlet and the Laurentide Ice Sheet retreated from the LGL basin, water levels fell to the Stanley lowstands (Lewis, et al., 2008a; Lewis et al., 2008b; Figure 3). A lowstand was first identified when a deep water unconformity was interpreted as being caused by erosion during a relatively low lake level (Hough 1962). During this time (~10,000 to 8,000 cal BP) lake levels were primarily controlled by the slow ascent of the North Bay outlet (Figure 1; 3). However, sedimentological evidence suggests rapid rises in lake levels collectively known as the Mattawa highstands (Lewis et al., 2005; 2008b). These short highstands are associated with either the glacial outburst floods from the melting ice sheet or overflows from Glacial Lake Agassiz causing lake levels to rapidly rise up to 60 m above the mean elevation of the Stanley lowstands (Lewis and Anderson, 1989; Breckenridge and Johnson, 2009).

However, climatic factors also played a pivotal role, lake level decreased to a point when the Superior, Michigan, Huron and Georgia Bay basins became disconnected between ~8,900 to 8,200 cal BP (Lewis, et al., 2008b, McCarthy and McAndrews, 2012). The disconnected lakes are commonly linked with an increasingly warm and dry climate and demonstrates the LGL's sensitivity to climate changes (Lewis, et al., 2008a).

### *2.2.3 Nipissing Highstand*

The rise to the Nipissing highstand began with a transition to a wetter climate causing water to rise from the Stanley lowstand until drainage again flowed over the still rising North Bay outlet (Figure 1; Johnston et al., 2014). GIA caused the North Bay outlet to rise forming Lake Nipissing when the Huron, Michigan and Superior basins became confluent (Figure 3). However, the lake level rise to the Nipissing highstand, caused by GIA, was supplemented by persistent wet conditions over the LGL (Booth, et al., 2002). A rapid rise of 7.2 cm/year continued until 6,000 cal BP at which point the rate in lake level rise slowed to about 2.8 cm/year until 4,500 cal BP (Thompson et al., 2011) when the Nipissing reached a maximum of 183.3 m at the Port Huron/Sarnia outlet (Thompson et

al., 2014). The slowing of the lake level rise at 6,000 cal BP is attributed to the capture of the outlet by the Chicago and/or Port Huron outlet (Baedke and Thompson, 2000; Johnston et al., 2014).

#### *2.2.4 Modern Lakes*

Presently, Lake Superior drains through the Sault outlet into Lake Michigan-Huron which drains through the Port Huron/Sarnia outlet into Lake Erie (Figure 1). The modern configuration formed soon after the Nipissing highstand when lake levels decreased and began to fluctuate within the historic lake level range. Baedke and Thompson (2000) studied five strandplains of beach ridges around Lake Michigan using techniques developed by Thompson (1992) to reconstruct an outlet referenced record of lake level (paleohydrograph) since 4,500 cal BP (Figure 4). Following the Nipissing highstand, 4,500 cal BP, lake level underwent a rapid fall of 4.1 m until 3,400 cal BP (Baedke and Thompson, 2000). The end of the rapid fall is attributed to the abandonment of the Chicago outlet (Baedke and Thompson, 2000). Baedke and Thompson (2000) also propose lake levels rose and fell on a millennial rhythm over the next several thousand years. Lake levels rose from 3,300 to 3,000 cal BP, associated with the Algoma highstand, fell from 2,400 to 2,250 cal BP, and rose from 2,100 to 1,700 cal BP and fell from 1,700 to 1,000 cal BP (Figure 4). This millennial rise and fall is associated with changes in climate though the precise mechanism has not been identified (Baedke and Thompson, 2000). In Lake Huron, over the past millennium, lake level has fluctuated within historical measurements of 2.1 m (Lewis, et al., 2008a). Millennial oscillations were also found in Lake Superior and were a factor in the final separation of Lake Superior from Lake Huron-Michigan at approximately 1060 cal BP (Johnston et al., 2012).

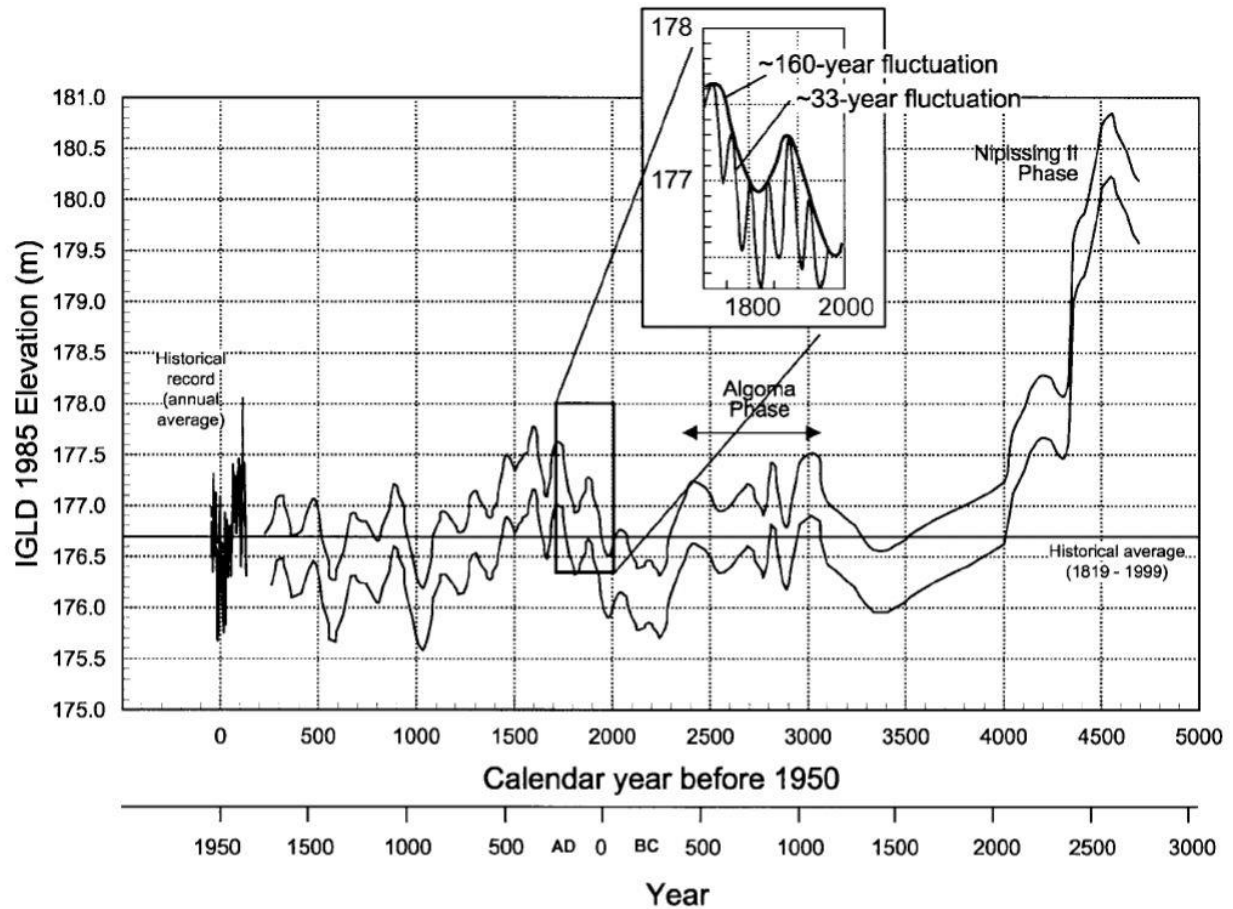


Figure 4: Lake Michigan paleohydrograph showing the fall from the Nipissing highstand to the modern lake configuration. The lake level curve is mirrored 0.6 m below the paleohydrograph to indicate possible extent of low lake levels (From Baedke and Thompson, 2000).

### 2.2.5 Drivers of Post-Nipissing Lake Level Change

Thompson and Baedke (1995) identified three lake level patterns by examining the geomorphology and sedimentology in five Lake Michigan strandplains of beach ridges (Figure 4). Millennium, centennial and multi-decadal lake level patterns are quasi-periodic and superimposed on one another. A millennium oscillation is observed as sets of beach ridges and correspond to the Algoma in the upper LGL and the Sault and sub-Sault lake phases in the Superior basin (Johnston et al., 2012). Lake levels fell from the Nipissing to Algoma to modern lake levels has been associated with outlet incision at Port Huron/Sarnia outlet (Hough, 1962) and/or climate (Booth et al., 2002). A shorter-term centennial pattern with a quasi-periodicity of approximately 160 years are composed of groups of 4-6 ridges. A similar pattern, lasting 100-150 years, is attributed to climate (Fraser et al., 1990).

The shortest quasi-periodic pattern repeats about every 30 years and is the average amount of time it takes for an individual ridge to be deposited.

Climate has been suggested as the cause of the three lake level patterns identified by Baedke and Thompson (2000). A correlation between atmospheric circulation patterns and quasi-periodic lake level fluctuations has been investigated but a consensus has not yet been reached. Millennial climate oscillations over the North Atlantic (Bond et al., 1997) drive atmospheric circulation patterns over North America effecting climate (Viau et al., 2002). The transition to the sub-Sault phase in Lake Superior is attributed to drought over North America during the transition from the Medieval Climate Anomaly to the Little Ice Age (Johnston et al., 2012).

Quasi-periodic decadal and multi-decadal lake level oscillations are attributed to changes in atmospheric circulation patterns over the LGL (Cohn and Robinson, 1976; Polderman and Pryor, 2004; Hanrahan et al., 2009; Watras et al., 2014). Quasi-periodic multi-decadal lake level fluctuations have been attributed to either the Pacific Decadal Oscillation (Watras et al., 2014), the North Atlantic Oscillation (Hanrahan et al., 2009), changes in large scale atmospheric circulation over the arctic (Polderman and Pryor, 2004) or the intermodulation of two near decadal atmospheric oscillations over the North Atlantic (Hanrahan et al., 2010). The linkage between climate and lake level emphasize how susceptible the LGL is to climate change.

### *2.2.6 Historic lake level drivers*

Historic drivers of lake level change are GIA, outlet conveyance, and climate with climate being the largest contributor (International Upper Great Lakes Study Board, 2009; 2012). The causes of climate driven historic lake level changes are examined and used to better understand possible climate influence on prehistoric lake levels.

The present area of the LGL basin contains roughly 33% surface water and 67% land (compared to other large lake basins which often contain 1-5% surface water), therefore, overlake evaporation, overlake precipitation as well as basin runoff are chief contributors to net basin supply and consequent lake level fluxes (Gronewold, et al., 2013b). Of particular consequence is the effect of seasonal changes in the frequency and intensity of weather patterns over the LGL (Argyilan and Forman, 2003; Polderman and Pryor, 2004). For instance, wide spread drought in North America



during the 1930s CE correlates with an extreme lake level low in Lake Huron caused by a reduction in spring and summer overlake precipitation and basin runoff (Argyilan and Forman, 2003). While the lake level low between the late 1990s CE and early 2010s CE has been related to increasing temperature reducing winter ice cover and subsequently increasing overlake evaporation (Gronewold and Stow, 2014). On the other hand, lake level rise in the 1980s CE is attributed to increased overlake precipitation and basin runoff during the autumn (Argyilan and Forman, 2003). While recent (2013-2014 CE) lake level rise is attributed to above average spring and fall overlake precipitation and basin runoff coupled with reduced summer and winter overlake evaporation caused by below average temperatures during those months (Gronewold et al., 2016). Over historic times, periods of persistent dry and warm climate correspond with lake level falls and periods of persistent wet and cool climate correspond with lake level rises (Argyilan and Forman, 2003; Gronewold et al., 2016). The relationship between high lake level with cool and wet climate and low lake levels with warm and dry climate is also postulated in the ancient lake level record (Fraser et al., 1975)

Numerous researchers have run computer simulation in an attempt to predict future LGL water levels under differing climate change scenarios and have calculated that lake levels are likely to fall as the climate warms (Lofgren et al., 2002; Angel and Kunkel, 2010; Hayhoe et al., 2010; Lofgren et al., 2001; MacKay and Seglenicks, 2013). However, since lake levels natural fluctuate it is important to have precise lake level records over prehistoric times to calculate natural lake level fluctuations and calibrate models predicting future lake level changes.

### **2.3 Beach Ridges**

Comprehensive reviews of marine and lacustrine beach ridges are found in Taylor and Stone (1996), Otvos (2000), Hesp et al. (2005) and Tamura (2012). Beach ridges are common features on many depositional coastlines that are topographically expressed as elongated sand and/or gravel ridges running parallel or subparallel to the shoreline and are separated by intervening low areas called swales. Beach ridges are composed of sand, gravel, and/or shingles (flat cobbles common in some coastal areas) and contain a core of waterlain sediments capped by windblown sediments. A series of beach ridges attached to the mainland is termed a strandplain (McCubbin, 1981).

### *2.3.1 Beach Ridges and LGL Lake Levels*

In the LGL, strandplains were noted and described by early researchers Goldthwait (1908) and Leverett and Taylor (1915). Decades later researchers began to utilize beach ridges to identify ancient lake levels (Larsen, 1985; Fraser et al., 1991). Thompson (1992) proposed the shoreface-foreshore contact (also called the basal foreshore) within an individual beach ridge correlates with lake level at the time of deposition. By coring and analyzing multiple beach ridges many ancient lake level elevations at one site are derived from one strandplain. Time constraints are attained through the dating of organic samples in swales or mineralogic sample in ridges. An age model is then created for each strandplain. Cross-strandplain elevations and ages are then used to produce a paleohydrograph extending back several millennia with a multi-decadal resolution.

### *2.3.2 Sedimentary Facies*

In cores collected from the individual beach ridges, normally less than five meters in length and four inches in width, genetic sediment facies in sandy LGL beach ridges are dune, foreshore and upper shoreface sediments (Figure 5; Thompson, 1992; Baedke et al., 2004). Upper shoreface deposits typically consist of moderately sorted upper very fine to lower fine sand with some beds of coarse sand and gravel. Shoreface deposits may also contain silt and clay laminae. Sedimentary structures typically include horizontal to high angled parallel laminae, ripple bedding and cross stratification with the entire sequence coarsening upward. Foreshore deposits are typically 1.0 to 1.8 m thick and consist of moderately sorted, upper fine to cobble size particles (sediment size dependent on sediment supply). Sedimentary structures include horizontal and lakeward-dipping subhorizontal laminae defined by alternations in grain size, with coarser grains concentrated at the base. The lower coarse-grain portion is called the basal foreshore and correlates with lake level at the time of deposition. The contact between the foreshore and upper shoreface is typically sharp and easily identified (Thompson, 1992) but may locally appear homogeneous (Johnston et al., 2007). Dune facies are 0.5 to 4 m thick and consist of moderately to well sorted, lower medium to lower fine grain quartz sands. Dune deposits are usually unstratified, but may locally contain heavy mineral laminae and/or horizontal to steeply dipping laminae. The upper portion typically contain rootlets. The contact between dune and foreshore deposits is sharp to gradational (Thompson, 1992).

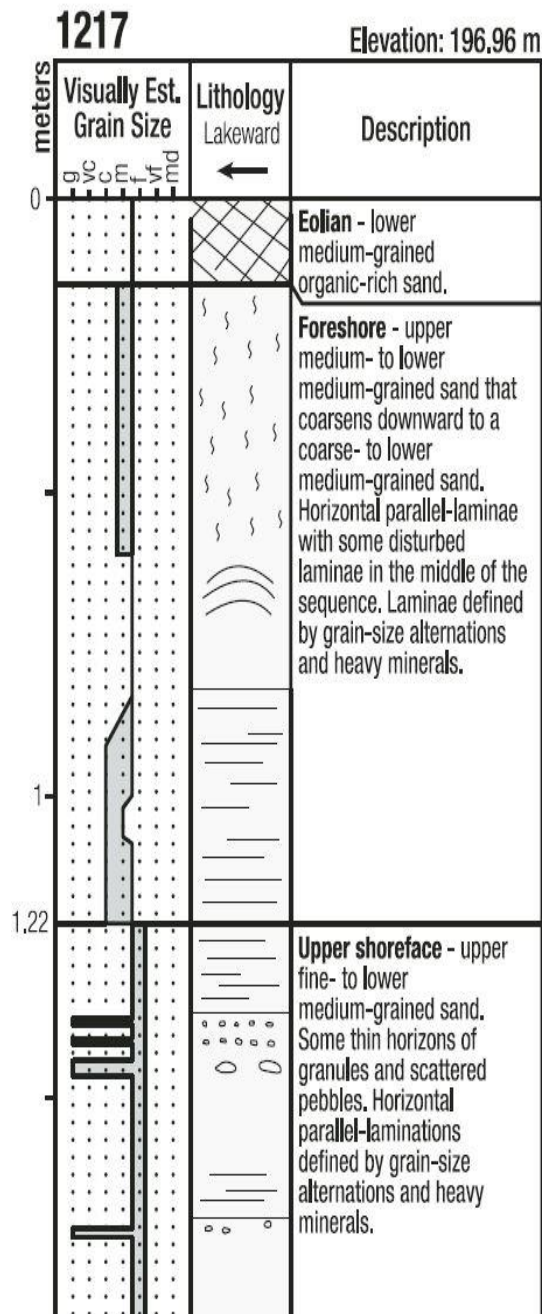


Figure 5: Typical core showing common sediment facies within LGL beach ridges include dune, foreshore and upper shoreface deposits. Identification of the contact between foreshore and upper shoreface deposits (also called the plunge point) correlates with lake level at the time of deposition (From Thompson et al., 2014)

### 2.3.3 Depositional Model

Thompson and Baedke (1995) modified Curray's (1964) model of shoreline behavior to provide a conceptual framework for the deposition of a beach ridge in response to lake level oscillations. The depositional or erosional behavior of a given coast is guided by the rate in water level change and the rate of sediment supply. Therefore, changes in the rate of lake-level rise or fall and changes in sediment supply will affect shoreline behavior. In an area where sediment supply exceeds the rate of lake level change the shoreline will prograde, build lakeward. Progradation can occur during rising lake levels if the rate of sediment supply exceeds the rate of lake level rise, but most readily happens as lake level falls.

Multi-decadal rises and falls in lake levels create beach ridges (Thompson and Baedke, 1995; Figure 6). When lake level change transitions from falling to rising lake levels the shoreline may eventually begin to erode. Then as the lake level rise reaches a peak elevation the rate of lake level change decreases and the shoreline will begin to aggrade, build upward. As lake levels fall, the shoreline will prograde forming the lakeward adjacent swale. Repetition of multi-decadal lake-level rises and falls have been shown to create a strandplain of beach ridges if sediment supply and accommodation space is sufficient for deposition (Figure 6; Thompson and Baedke, 1995; Johnston et al 2007).

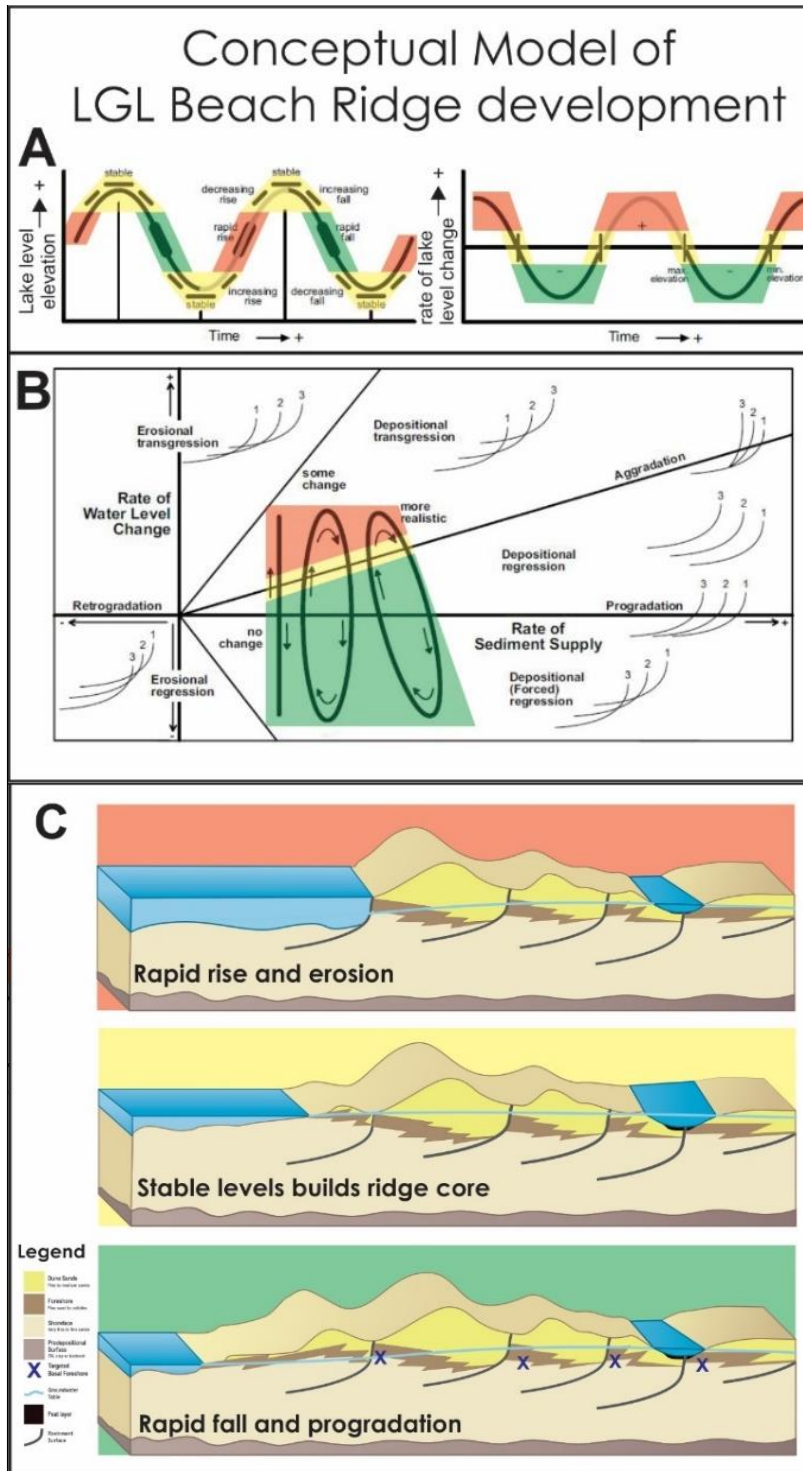


Figure 6: Conceptual model of LGL beach ridge development shows how beach ridges develop in response to lake level fluctuations and sediment supply. Colors show correlations between graphs and diagrams. A simple rise or fall in lake level will affect the rate of lake level change (A) and a change in the rate of sediment supply will affect shoreline behavior (B) together the rate of lake level change and sediment supply dictates how the coastline responds to lake level fluctuations (modified from Johnston et al., 2007). Diagrams of strandplain cross sections show how the beach responds to changing rates of lake level change (C).

Ground penetrating radar (GPR) has been used to understand stratigraphic patterns across several beach ridges in the LGL. Johnston et al. (2007) used GPR on a Lake Superior strandplain to image cross strandplain stratigraphy and identify a systemic pattern in LGL beach ridges to link a conceptual model of beach ridge formation with the preserved record. The water table is often imaged in GPR profiles as a continuous horizontal reflection. Beach ridge foreshore deposits are imaged as sigmoidal reflections that build upward and lakeward from a concave up reflection extending from below a beach ridge crest to the ground surface in the next landward adjacent swale. The reflections imaged across multiple beach ridges show the preserved stratigraphic patterns resulting from the deposition of multiple beach ridges.

Changes in the rate of lake level fluctuation and sediment supply cause individual LGL shorelines to erode and deposit over geologic time. This causes beach ridges to form in embayments along the LGL over a multi-decadal time scale, eventually forming a strandplain of many beach ridges. Because individual beach ridges form as a result of lake level fluctuations (and sediment supply) they preserve a lake level elevation at the time of deposition. Strandplains of many beach ridges can therefore be used to reconstruct lake level fluctuations over geologic time.

# Chapter 3

## Study Area

### 3.1 Lake Huron

Lake Huron is located at the downstream terminus of the upper LGL (considered lakes Superior, Michigan, and Huron). The major source of inflow to Lake Huron is from Lake Superior through the St Mary's River and the Sault outlet. Outflow from the Lake Huron and the entire upper LGL discharges through the Port Huron/Sarnia outlet in southern Lake Huron, and into the St Clair River, Lake St Clair and the Detroit River before draining into Lake Erie (Figure 1). Lakes Michigan and Huron are hydrologically joined through the Straits of Mackinaw. Flow through the Straits of Mackinaw is typically from west to east, though periodic changes in weather conditions over each lake disrupts net flow through the Straits (Saylor and Sloss, 1976; Saylor et al., 1991). Lake Michigan and Lake Huron are often considered separate basin because of their narrow connection (Lewis et al., 2008b). Lake Huron's surface area is 49,600 km<sup>2</sup>, while Lake Huron's total drainage area is 194,000 km<sup>2</sup>. The Lake's maximum depth is 229 m and its total water volume is 3,540 km<sup>3</sup> (Lewis, et al., 2008b). Lake Huron's mean yearly elevation based on water gauges (1918-2015 CE) is 176.42 m. Lake Huron has undergone noticeable lake level fluctuations, for instance a maximum lake level yearly average high was reached in 1986 at 177.29 m while a lake level minimum was reached in 1964 at 175.68 m (Gronwold, et al., 2013b).

The potential for outlet conveyance, a change in the water carrying capacity of a lake's outflow channel(s), could cause changes in lake level and prevent deep draft vessels passage through the outlet. From the Port Huron/Sarnia outlet to Lake Erie the average elevation drop is 3 m over 130 km. The relatively minor drop in elevation allows ships to pass from Lake Huron to Lake Erie without the necessity of locks. This is partly why the Port Huron/Sarnia outlet is the only unregulated outlet (lacking any locks or dams) in the entire LGL. The lack of any regulatory structures means cargo ships must vary their weight depending on lake level, lightening their load during low lake levels. The St Clair River channel has been dredged in the past to allow for passage of deep draft vessels during low lake levels. The last major dredging of the St Clair River occurred in 1963 and contributed to a permanent reduction in Lake Huron lake levels (International Upper Great Lakes Study Board, 2009). Since then an average decline of 23 cm has occurred in the difference of lake levels between Lake Huron and Lake Erie. Baird & Associates (2005) attributed

this drop to downcutting of the St Clair River, though further investigations identified active bedforms on the river bottom suggesting the river has not downcut in the recent past (Czuba et al., 2011). With the completion of the International Upper Great Lakes Study (International Upper Great Lakes Study Board, 2009; 2012) the decline in lake level between 1963 and 2006 was attributed in part to a change in outlet conveyance (7-14 cm), GIA (4-5 cm); however, the majority of recent lake level change was attributed to climate change (9-17 cm).

However, there is evidence of deposition in the Port Huron/Sarnia outlet in the form of spits (Campbell, 2016). The presence of the Port Huron/Sarnia spits means that sediment has accumulated in the Port Huron/Sarnia outlet in the past and could potentially accumulate in the outlet in the future. If sediment accumulates in the Port Huron/Sarnia outlet in the future it could prevent the passage of deep draft vessels. Quantifying past lake level fluctuations in southern Lake Huron will provide details needed to determine the timing and context of deposition of the Port Huron/Sarnia spits.

The study site for this thesis is strategically located in southern Lake Huron near the Port Huron/Sarnia outlet (Figure 1). Ipperwash is the closest strandplain to the Port Huron/Sarnia outlet with the most number of preserved beach ridges that document many past lake level fluctuations. Since the Ipperwash strandplain is located near the outlet (~40 km), the Ipperwash beach ridges preserve conditions experienced at the Port Huron/Sarnia outlet in geologic past.

### **3.2 The Thedford Embayment**

The Thedford embayment is located approximately 42 km northeast of the Port Huron/Sarnia outlet, 175 km west of Hamilton, Ontario and 130 km northeast of Detroit, Michigan. Towns in the area include the coastal towns of Grand Bend, Port Franks, Ipperwash Beach, and Kettle and Stoney Point First Nation communities, and the town of Thedford is located at the inland margin of the embayment (Figure 7).

Bedrock consists of the Middle Devonian Dundee Formation, Hamilton Group and Kettle Point Formation (Cooper, 1974). The only bedrock exposures are on Kettle Point and Stoney Points where the Kettle Point Formation outcrops before extending as offshore ridges. Between Port

Franks and Grand Bend a buried bedrock valley, called the Ipperwash trough, exists and is interpreted to have been eroded by subglacial/glacial meltwater (Gao, 2011).

Till exposures in the area primarily consist of St Joseph till (Cooper, 1974). The St Joseph till is a grey to yellowish-brown silt to clayey silt till with few pebbles (Cooper, 1974) and when exposed on the shoreline forms easily erodible bluffs (Au-Sable-Bayfield Conservation Authority, 2000). Erosion of bluffs of St Joseph till northeast of the Thedford embayment has historically supplied sediment to the littoral system at a rate of 68,000 m<sup>3</sup>/year (Reinders and Associates, 1989).

The Thedford Embayment comprises the area between an elevated wave cut bluff and the modern shoreline. Between Kettle Point and Stoney Point, the embayment extends 2 km landward from the modern shoreline and then increases to a maximum of 10 km landward from the modern shoreline in a broad arc between Port Franks and Grand Bend (Figure 7). Within the landward portion of the embayment at least two large gravel bars have been related to either the Nipissing or Algonquin lake phases (Cooper, 1979). Further studies postulated the gravel bars to contain an Algonquin age core capped by Nipissing deposits based on the identification of a paleosol in several gravel pits (Karrow et al., 1980).

### **3.3 The Ipperwash strandplain**

The Ipperwash strandplain consist of a 2 km wide strip of land between a prominent wave cut bluff/dune ridge landward from the modern Lake Huron shoreline and extends 25 km from Kettle Point northeast to Grand Bend (Figure 7). The northeastern and southwestern portions of the Ipperwash strandplain contain beach ridges while the central portion is masked by dunes in Pinery Provincial Park (Eyles and Meulendyk, 2012). The landward limit of the strandplain is a 10 m high bluff/dune ridge formed during the Nipissing (Cooper, 1979).

The southern Ipperwash strandplain, near Ipperwash Beach, contains a well-defined strandplain (Figure 8) and up to 40 individual beach ridges (Johnston, 1999). Drainage in the Ipperwash Beach area flows to the north-east along the natural Duffus Drain and manmade Ipperwash Drain (Figure 8). Road access is along West Ipperwash, and Ipperwash Road with numerous, hiking, ATV, and two-track trail allowing for relatively easy access to parts of the Ipperwash strandplain (Figure 8).



This thesis focuses on a surveyed shore perpendicular transect across the southern (Ipperwash Beach area) Ipperwash strandplain starting at the modern beach and ending at the Nipissing bluff approximately 2.2 km landward from the modern shoreline to reconstruct past relative lake levels preserved in beach ridges. The southern Ipperwash strandplain is an ideal location to study past lake level fluctuations for several reasons. 1) The Ipperwash strandplain is predicted to have a rate of GIA similar to the rate of GIA experienced at the Port Huron/Sarnia outlet (Figure 2). Therefore, the Ipperwash strandplain beach ridges will provide detailed information about lake level fluctuations at the outlet. 2) the 40 Ipperwash strandplain beach ridges are, at present, well preserved and have little dune covering allowing for easy access to waterlain sediments (Johnston, 1999). This thesis extends well beyond the Johnston (1999) topographic survey by coring 40 Ipperwash beach ridges to uniquely derive accurate elevations of past lake level stages and deriving the first age model for the Ipperwash strandplain to produce the most detailed record of post-Nipissing lake level fluctuations at Ipperwash created to date. The Ipperwash paleohydrograph provides a lake level record of past lake level fluctuations at Lake Huron's outlet which is required to understand past conditions (GIA, outlet conveyance, climate) in the Lake Huron basin and at specific sites around Lake Huron.

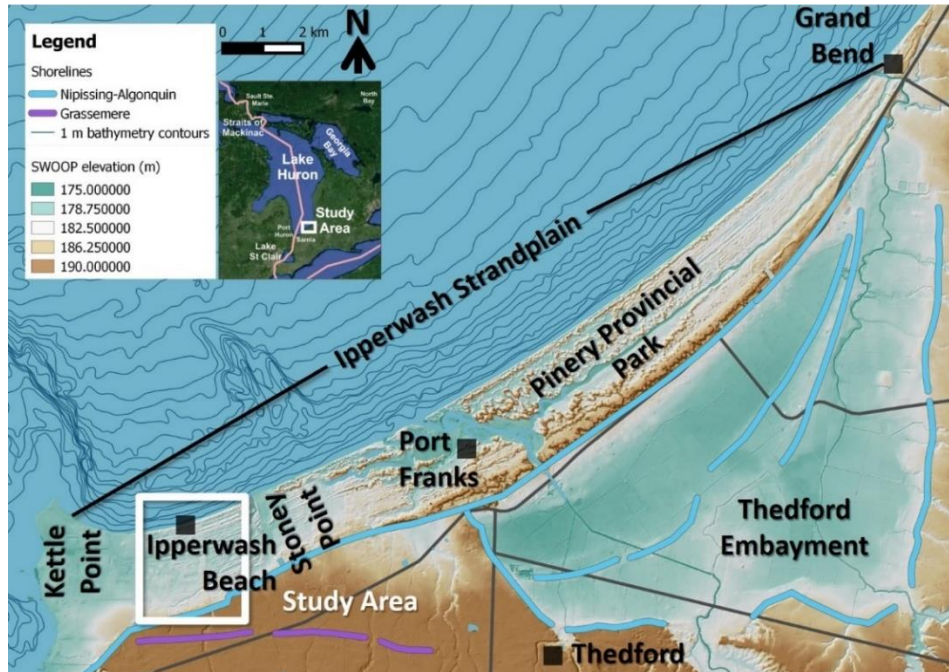


Figure 7: The Theedford Embayment, southern Lake Huron, contains several ancient shorelines. The Ipperwash strandplain extends from Kettle Point to Grand Bend and extends from the Nipissing shoreline to the modern beach. Shorelines in Pinery Provincial Park are covered by large dunes, while beach ridges are exposed on the northern and southern ends of the Ipperwash strandplain. The study area is located on the southern end of the Ipperwash strandplain, near Ipperwash Beach. Elevation data from Southwestern Ontario Orthimagery Project 2015.



Figure 8: Aerial image of the southern Ipperwash strandplain with outline of surveyed area, major drainages and the Nipissing bluff. Road access is along W Ipperwash Road, Ipperwash Road, and Army Camp Road. Satellite imagery from Google Earth

# Chapter 4

## Methods

To create an Ipperwash paleohydrograph, diverse methods were used to glean relevant data from the Ipperwash strandplain. These methods include field observations, satellite image interpretation, ground penetrating radar (GPR), topographic surveying, vibracoring, sediment analysis, and optical dating. These data were synthesized and systematically interpreted to create an Ipperwash relative paleohydrograph.

### ***4.1 Field Observations and Satellite Image Interpretation***

Field notes were collected along the surveyed transect from the modern beach landward 2.2 km to the Nipissing bluff (Figure 8). Field observations include estimations of swale width, water depth in swales, ridge width, ridge height, and ridge crest topography as well as notes describing the type and distribution of vegetation and human modifications. Width estimates from field observations were compared to satellite imagery available through GoogleEarth. Comments on GPR profile locations, core locations and the nature of vibracoring (i.e. how well the vibracore penetrated the subsurface) were also recorded.

### ***4.2 Ground Penetrating Radar (GPR)***

GPR is a noninvasive method to image the shallow subsurface. GPR utilizes electromagnetic (EM) waves which reflect from changes in dielectric properties of sediments (Jol and Bristow, 2003). The GPR set-up used in this study consists of a backpack mounted computer/console connected to a transmitter and receiver antennae with fiber optic cables. The GPR system was a pulseEKKO 100 with 100 and 200 MHz antennae and a 1000 V transmitter. For all transects, data was collected in step mode with a step size of 0.5 m or 0.1 m and antennae separation of 1.0 m or 0.5 m for 100 and 200 MHz antennae respectively. Relief measurements were collected using an optical surveying level to geometrically adjust the radar profile to reflect changes in topography. The data was processed using EKKO\_Project using dewow filtering, vertical and horizontal averaging and automatic gain control.

Estimates of propagation velocities of the EM wave through the sediment are needed to calculate depth. Common midpoint surveys (CMPs) were collected parallel to several transects to estimate propagation velocity through the sediment. However, CMP velocities were adjusted based on lithology and depth to water table.

For the Ipperwash strandplain, GPR was used as an exploratory method to determine the sedimentary architecture across multiple beach ridges. Defining the sedimentary architecture distinguishes natural and anthropogenically modified sediment to determine the viability of collecting near-surface foreshore sediments from vibracoring. In addition, the internal stratigraphy of the Ipperwash strandplain beach ridges were compared to another GPR transect through LGL beach ridges (Johnston et al., 2007).

### **4.3 Topographic Surveying**

A Sokkia total station survey was used to deduce the precise elevation of every beach ridge crest and swale, core location, and OSL pit. Elevations were corrected to a well-established datum in the LGL's (International Great Lakes Datum 1985 or IGLD85) by using a geodetic survey benchmark in Grand Bend to measure the water level elevation of Lake Huron at Grand Bend, then using this water level elevation at Ipperwash as a known elevation to link the Ipperwash transect to IGLD85. Waves were dampened to better measure water level elevation by using a large plastic cylinder with a tube at its base to allow for the passage of water. Lake level elevation was also compared to the lake level recorded at the water level gauge station in Goderich, Ontario (62 km NNW of Ipperwash), to ensure elevations were consistent. A 0.05 m discrepancy is observed between Grand Bend and Goderich. Elevations, relative to IGLD85 were established for each core site, OSL pit and beach ridge crest and swale.

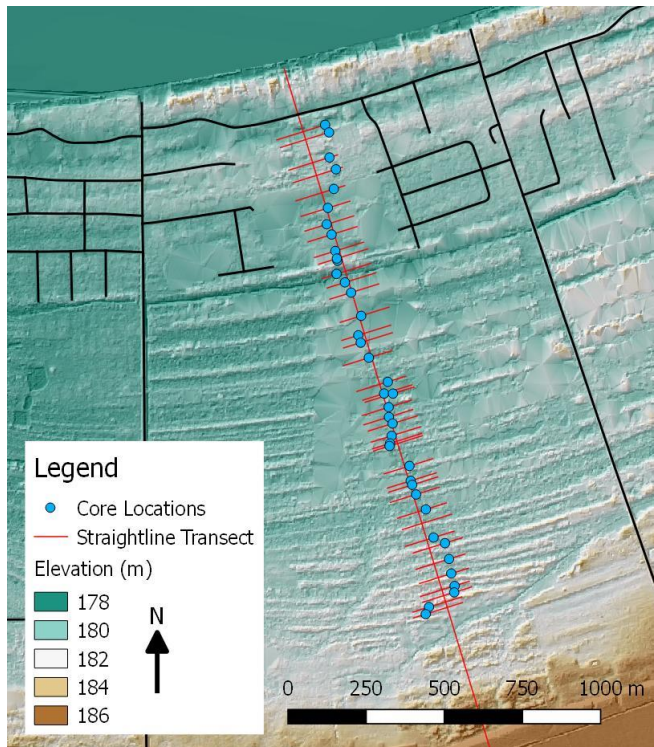


Figure 9: A straight line, shore perpendicular transect was drawn in QGIS to develop a topographic profile across the Ipperwash strandplain. A DEM created from SWOOP 2015 data shows strandplain elevations.

To develop a topographic profile across the Ipperwash strandplain a shore perpendicular transect was constructed. However, cores were not collected in a strict shore perpendicular orientation and the surveyed transect following core locations. A Garmin handheld GPS was used to determine core locations and these locations were then laterally adjusted to a shore perpendicular transect, roughly equidistant from all core locations, drawn in QGIS (Figure 9). Crest and swale midpoints were determined along the transect by examining aerial photographs. By adjusting GPS based core locations to a shore perpendicular transect and determining crest and swale locations along the transect, a topographic profile of the Ipperwash strandplain was created.

#### 4.4 Vibracoring

Vibracoring is a proven method to extract subsurface sediment from beach ridges and identify relic beach facies (Thompson, 1991; 1992). A 3 m tall, land-based vibracore system was used to collect cores 1-4 m in length. Cores were collected from the lakeward margin of each, individual beach ridge to minimize the amount of dune sand recovered and penetrate deep enough to collect the contact between foreshore and upper shoreface facies. The lakeward side of each core was marked on each core tube so the orientation of sedimentary structures could be examined once the cores were returned to the laboratory and opened.

#### 4.5 Lab Analysis

Cores were analyzed following the methods of Thompson (1991; 1992). Cores, once returned to the lab, were split, described (for visual grain size estimates, sedimentary structures, composition),

logged, photographed, preserved and sampled. Grain size was determined through visual estimation, and laser diffraction. Graphs of grain size distribution were produced to identify grain size changes within cores and across multiple cores. Latex peels were used to enhance sedimentary structures and produce a permanent record of the cores. Once sampled and described, facies were interpreted based on visual descriptions, grain size distribution and sedimentary structures.

Core samples, of approximately 2 cm<sup>3</sup> were collected every ~20 cm starting below the soil horizon. Additional samples were also collected above and below visibly identifiable contacts and in areas with unique sediments or stratigraphy. Over 200 samples from cores were analyzed to determine the grain size using the Malvern3000 laser diffractor system at the Indiana State Geological Survey. Samples collected on the modern beach were analyzed for grain size using a Fritsch laser diffractor system at the University of Waterloo. Laser diffraction is a proven method to analyze particle size of very fine grained to coarse sand sized, naturally occurring sediments (Sperazza, et al., 2004; Di Stefano et al., 2009). Analyzed samples were collected from cores chosen to bracket visually described facies and better define the contact between facies.

Once analyzed, samples were statistically described using GRADISTAT v. 08 (Blott and Pye, 2010). Statistical parameters were calculated using the Folk and Ward (1957) method. Final statistics were displayed in phi and described.

Sedimentary structures and statistical parameters are used to define facies interpreted as dune, foreshore and shoreface deposits. The study of other LGL strandplains suggests mean grain size, sorting, skewness and coarsest 1% (D(99)) are the most useful grain size statistics to differentiate facies (Thompson et al., 1997; Baedke and Thompson, 2000; Johnston et al., 2004, 2012, 2014). The contact between foreshore and shoreface sediments serves as a proxy for ancient lake level for each individual beach ridge (Thompson, 1992). Modern beach facies are used as an analogue and used to interpret ancient beach ridge facies.

#### **4.6 Optical Stimulated Luminescence**

Optical stimulated luminescence (OSL) is a technique to measure when certain minerals, typically quartz, feldspar or aluminum oxides, were last exposed to sunlight. OSL relies on mineral grains

being sufficiently exposed to sunlight to “bleach” the grains. Once bleached, the minerals absorb radiation from the decay of surrounding radioactive isotopes. This radiation causes the trapping of electrons within imperfections of the crystal lattice. Stimulating samples with certain wavelengths of light and measuring released energy allows for the calculation of burial time (Aitken, 1998). OSL is a proven dating method in both marine (Murray-Wallace et al., 2002) and lacustrine (Argyilan et al., 2005) coastal landforms. In the LGL OSL has been used in recent studies as an alternative to  $^{14}\text{C}$  dating of organics found in the swales of beach ridges (Argyilan et al., 2005) to develop paleohydrographs for lake basins (Johnston et al., 2012). Samples were collected from approximately 1 m below the crest of beach ridges. Temporal and monetary constraints allow only every third to fifth beach ridge in the Ipperwash strandplain to be age-dated using OSL methods.

The OSL samples from the Ipperwash strandplain were sent to Dr Lepper at the Optical Dating and Dosimetry Lab at North Dakota State University. OSL ages were determined from quartz grains and “derived from data collected from between 93 and 144 individual aliquots per field sample and represent over 12,000 individual OSL measurements” (Lepper, 2017). OSL ages are in calendar years before 2017 CE, but the abbreviation BP is not used to avoid confusion with other published ages reported as calendar years before 1950 CE.

## Chapter 5

### Results and Discussion

Field data and samples were collected from the Ipperwash strandplain during the 2015 and 2016 field seasons. Data collected includes field observations, 14 GPR profiles totaling over 1 km in length, a 2 km survey line, 6 sediment samples from the modern Ipperwash beach, 40 vibracores with an average depth of penetration of  $2.82 \text{ m} \pm 0.68 \text{ m}$ , and 10 OSL samples collected in a roughly shore normal orientation across the Ipperwash strandplain (Figure 10).

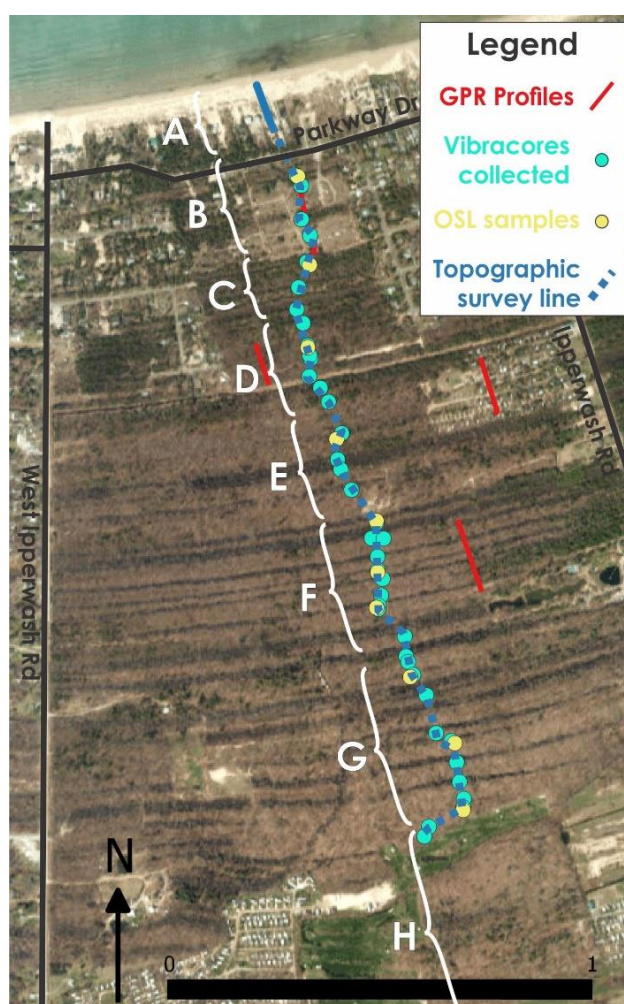


Figure 10: Map showing the location of GPR profiles, vibracores, OSL samples, and topographic survey collected on and in the Ipperwash Strandplain. As well as segments qualitatively assessed through field observations and satellite images.

These data are used to develop a relative paleohydrograph for the Ipperwash strandplain. Field observations were compared to satellite imagery and used to qualitatively divide the survey into segments based on ground surface observations. GPR is used as an exploratory tool used to describe subsurface stratigraphy. Topographic surveying allows the precise elevation of sample locations to be determined and to examine topographic patterns across the Ipperwash strandplain. Sediment samples from the modern beach are used to describe modern shoreline sediment facies. Vibracores from individual ancient shorelines are used to describe ancient shoreline sediment facies. Modern and ancient facies are interpreted either as dune, foreshore or shoreface deposits which are splayed laterally along the modern shoreline and vertically in cores from ancient shorelines. The contact between the foreshore and shoreface facies is of paramount interest since it approximates the elevation of the modern and ancient lake level when individual beach ridges



formed. OSL is used to date individual shorelines and develop an age model to reconstruct the timing of natural lake level oscillations over the past several millennia.

### **5.1 Field Observations**

A field survey was collected in the summer of 2016 beginning at the modern Lake Huron shoreline and extending in a roughly shore perpendicular orientation 2200 m to the Nipissing bluff. The field survey can be qualitatively divided into 8 segments based on field notes and verified by satellite imagery. The 8 segments are described and separated based on swale width, swale water depth, ridge width, ridge height/crest topography, vegetation, and human modification (Table 1).

Segment A extends from the modern shoreline to 209 m landward and contains approximately 3 ridges and the modern foredune. Swales and ridges are variable in width. Swales are dry and ridges are up to 4 m high. Vegetation is dominated by beach grasses and has been modified by humans including privately owned homes and cottages, publicly maintained beach access paths and washrooms, as well as roads and underground utilities. Cores were not collected from this segment due to human modification.

Segment B extends from 209 m to 354 m landward from the modern shoreline and contains 4 ridges from which cores 2001-2004 were collected. Swale and ridge width and height are unknown due to human modification. The area crossed by the survey is a former parking lot, and is currently used for hiking and ATV/dirt biking. Elsewhere on the strandplain, segment B contain residential housing. With the exception of a central swale, swales have been infilled but ridge crests are still apparent in certain areas. The segment is open with patches of juniper bushes with cedar trees along a central swale.

Segment C extends from 354 m to 513 m landward from the modern shoreline and contains 3 ridges from which cores 2005-2007 were collected. Wide widths are observed for swales (10-30 m) and ridges (15-30 m). Swales contain deep water (~0.5 m) and ridges are low (~1 m above swales) with relatively flat crests. Swales are well vegetated with closely spaced, short, thin, woody plants with cedar and birch trees at the swale-ridge contact. Ridge crests are covered by grasses and juniper bushes. Human modification is limited to hiking trails.

Segment D extends from 513 m to 736 m landward from the modern shoreline and contains 6 ridges from which cores 2008-2013 were collected. Swale and ridge width is variable. Swales are dry and ridges are high (up to 2 m) and steadily rise landward often with bench topography (i.e. a low ridge followed by a high ridge with no discernable swale between ridges). The area is dominated by Carolinian Forest, a particular forest type dominated by deciduous trees. Human modification is limited to hiking trails in most areas, but the segment is split by the Ipperwash Drain which was cut parallel to ridge crests.

Segment E extends from 736 m to 951 m landward from the modern shoreline and contains 4 ridges from which cores 2014-2017 were collected. Wide widths are observed for swales (15-30 m) and ridges (20-30 m). Swales are dry to shallow (~0.2 m water depth), and ridges are variable height with relatively flat to hummocky crests. The segment is dominated by Carolinian Forest. Human modification is minimal except for a cleared area on the crest of ridge 2017 which contains a concrete foundation, presumably the base of an old cabin.

Segment F extends from 951 m to 1379 m landward from the modern shoreline and contains 12 ridges from which cores 2018-2029 were collected. Narrow widths are observed for swales (5-20 m), but ridge width is variable. Swales are dry to shallow (~0.5 m water depth), and ridges are variable height with relatively flat to hummocky crests. Segment F is dominated by Carolinian Forest. Human modification is minimal, limited to two-track trails and selective logging.

Segment G extends from 1379 m to 1785 m landward from the modern shoreline and contains 4 ridges from which cores 2030-2038 were collected. Wide widths are observed for swales (15-40 m) and ridges (20-40 m). Swales are shallow to deep (0.2-1.0 m water depth), and ridges are variable height often with bench topography. The segment is dominated by Carolinian Forest. Human modification is minimal, limited to a two-track trail and selective logging.

Segment H extends from 1785 m to 2200 m landward from the modern shoreline, ending at the Nipissing bluff identified by Cooper (1979) and contains ~8 ridges from which cores 2038-2040 were collected from the lakeward most two ridges. Ridges landward of the Ponderosa Pines Golf Course were not cored. Ridge and swale width and height are variable and rise steadily landward.

Swales are dry to shallow (0-0.2 m water depth), and ridges are variable height often with hummocky topography. The segment is dominated by Carolinian Forest. Human modification is minimal, limited two-track trails, except for the area occupied by the Ponderosa Pines Golf Course.

Table 1: Characteristics used to qualitatively divide the Ipperwash strandplain into 8 segments

Transect Segment	A	B	C	D	E	F	G	H
Cores Collected	0	2001-2004	2005-2007	2008-2013	2014-2017	2018-2029	2030-2038	2038-2040
Number of Ridges	~3	4	3	6	4	12	10	~6
Distance Landward	0-209 m	209-354 m	354-513 m	351-736 m	736-951 m	951-1379 m	1379-1785 m	1785 m - 2200 m Nipissing Bluff
Swale Width	Variable	Unknown	Wide (10-30 m)	Variable	Wide (15-30 m)	Narrow (5-20 m)	Wide (15-40 m)	Variable
Swale Water Depth	Dry Swales	Dry Swales (infilled)	Deep wetlands (~0.5 m water depth)	Dry Swales	Shallow (0-0.2 m water depth)	Shallow (0-0.5 m water depth)	Shallow to deep (0.2-1 m water depth)	Dry to Shallow (0-0.2 cm)
Ridge Width	Variable	Unknown	Wide (15-30 m)	Variable	Wide (20-60 m)	Variable	Wide (20-40 m)	Variable
Ridge Crest Height/ Topography	High (up to ~4 m) dunes	Unknown	Flat low crests (~1 m)	Steadily rising, high (up to ~2m) crests often with bench like topography	Hummocky to flat topography	Variable	Variable often with bench like topography	Hummocky
Vegetation	Beach grasses	Open with cedars in central swale	Vegetated wetlands, cedars at wetland edge, open crests	Carolinian Forest	Carolinian Forest	Carolinian Forest	Carolinian Forest	Carolinian Forest
Human Modification	Privately owned houses and publicly maintained beach access points and washrooms	Former parking lot, ATV trails. Swales infilled but ridges still apparent	Minimal	Hiking trails. Cut through by Ipperwash Drain	Minimal expect for cleared area on ridge 2017	Minimal, selective logging and two-track trails	Minimal, selective logging and two-track trails	Minimal, two-track trails, with exception of Ponderosa Pines Golf Course

## 5.2 Radar Stratigraphy

Seven GPR profiles totaling 1069 m in length were collected in shore normal orientations across the modern beach (1 profile) and ancient shorelines (6 profiles) as well as 4 GPR profiles totaling 205 m in length were collected shore parallel on the modern beach (Figure 11). Relief measurements were collected with a Topcon laser level to geometrically adjust each GPR profile to changes in ground surface elevation.



*Figure 11: Location of GPR profiles collected on the Ipperwash strandplain.*

EM wave propagation velocity is needed to estimate depth and is determined with CMPs. However, velocity is adjusted based on lithology. For example, the BEAN-CMP was collected on the modern beach, above a near surface water table, and used to calculate a velocity of 0.05 m/ns, a velocity typical of saturated sand (Jol and Bristow, 2003). However, since the majority of the BEANR profile was above the water table a velocity typical of dry sands (0.15 m/ns) was used. All other CMPs were collected along transects well above the water table and show a velocity of 0.1 m/ns which is the velocity used to estimate depth in all other GPR profiles. Profiles collected with 100 MHz antennae show reflections up to 10 m depth while profiles collected with 200 MHz antennae show reflections 5-8 m depth but with a greater resolution.

Profile were collected in a shore perpendicular orientation across the modern beach and the most lakeward beach ridge. GPR profiles consist of multiple reflections which are grouped into reflection patterns based on configuration, continuity, amplitude and terminations. Reflection patterns are described using radar stratigraphic terminology (van Heteren et al., 1998; Jol and Bristow, 2003), which is a modification of seismic stratigraphic terminology developed by Mitchum (1977). Reflection patterns are then grouped into radar facies. Radar facies are a mappable sedimentary unity composed of reflection patterns which differ from adjacent facies (Mitchum, 1977).

The GPR profile shown in Figure 12 resolves all radar facies common in the Ipperwash strandplain. Modern and ancient shorelines in the Ipperwash strandplain show five reflections patterns grouped into three radar facies (Figure 13). Reflection pattern A extends from 5-10 m depth and reflections consist of horizontal to lakeward dipping (apparent angle less than  $10^\circ$ ), continuous reflections. Reflection pattern B extends for 0-5 m depth and consists of sigmoidal, concave up reflections which truncate radar facies A and approach an asymptote at  $\sim 5$  m depth. Reflection pattern C is at 0-2 m depth and consists of a single horizontal continuous reflection. Reflection pattern D occurs at 0-2 m depth, is discontinuous separated by the relief of beach ridges and consists of lakeward dipping to landward dipping to horizontal continuous reflections. Reflection pattern E occurs at 0-2 m depth, is discontinuous separated by the relief of beach ridges and consists of undulating to landward dipping semi-continuous reflections.

GPR profiles are interpreted based on comparison to other GPR studies in similar environments (van Heteren et al., 1998; Johnston et al., 2007). Ipperwash profiles are limited to 10 m depth, however other 100 MHz GPR surveys in similar environments have resolved structures up to 37 m depth (Smith and Jol, 1995). Therefore, the depth of penetration at Ipperwash is likely limited. GPR signals are limited by sediments of high conductivity, such as fine grain sediments (Jol and Bristow, 2003). There are three potential sources of fine grain sediments in the Ipperwash area: shale bedrock, St Joseph till, and offshore silts. Any of these could potentially limit the depth of penetration, however, local well log records describe underlying material as “blue clay” at 11 m depth which suggest either St Joseph till or offshore silts. The lower radar facies consists of reflection patterns A and B and is interpreted as shoreface and foreshore sediments. Reflection pattern A is interpreted as progradational and aggradational beach sand and reflection pattern B is

interpreted as a ravinement surface. Reflection pattern C is interpreted as the water table which is commonly exposed at surface in the swales of beach ridge. The first upper radar facies consists of reflection pattern D and is interpreted as disturbed areas because the facies is observed under paths allowing access to the beach. The second upper radar facies consists of reflection pattern E is interpreted as dune sediments and is found internally under the crest of beach ridges. Radar facies are similar to radar facies described in other LGL strandplains; therefore, the model for LGL strandplain formation (Thompson and Baedke, 1995; Johnston et al., 2007) can be applied to Ipperwash.

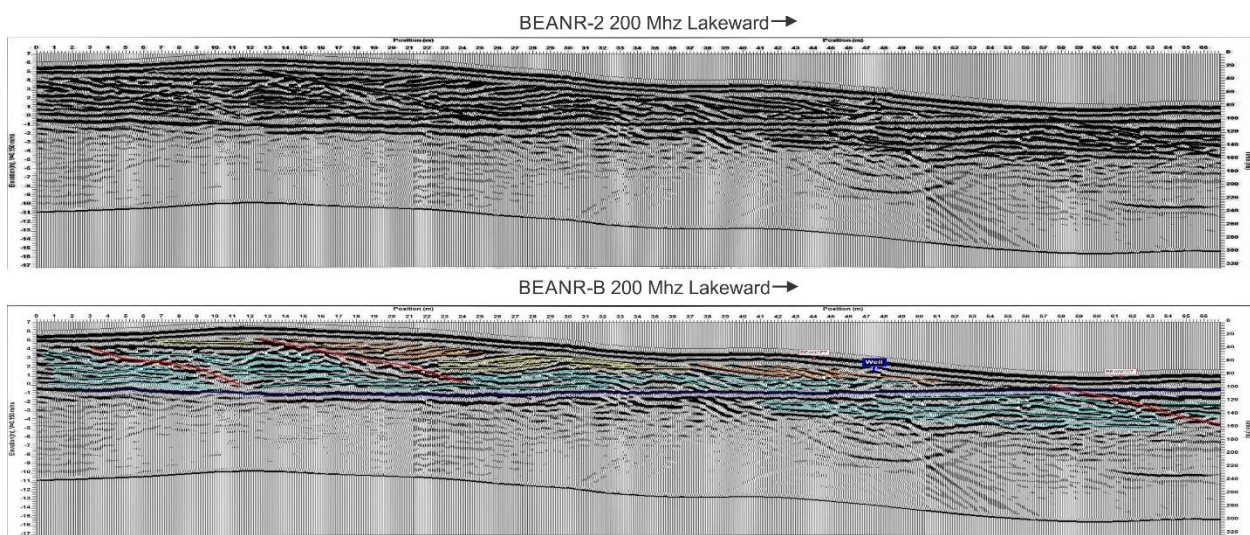


Figure 12: Processed (BEAN-2) and interpreted (BEAN-B) GPR profile collected in a shore perpendicular orientation across the modern beach. Color scheme of interpretations shown in Figure 13.

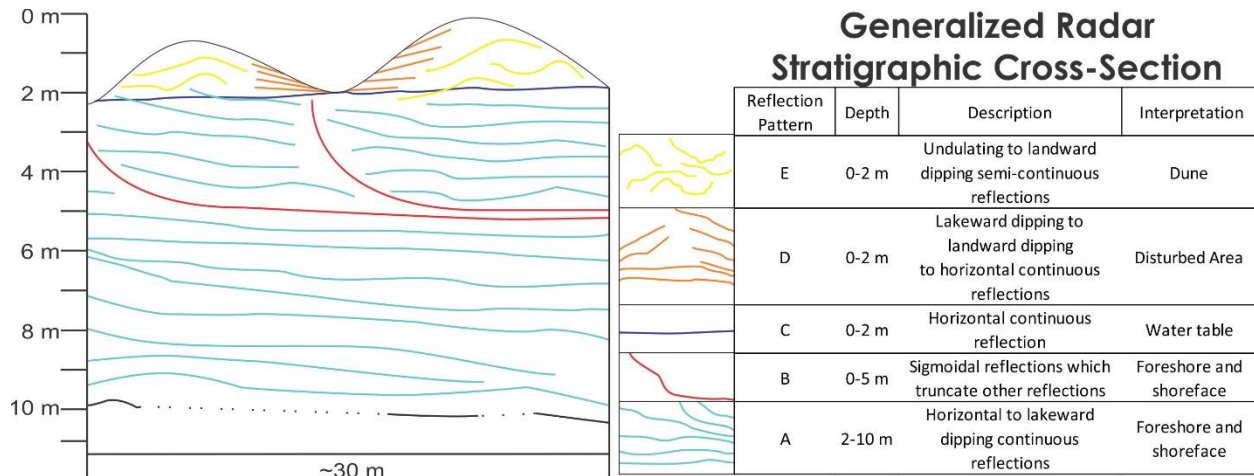


Figure 13: Generalized radar stratigraphic cross section across two, beach ridges based on analysis of modern and ancient Ipperwash beach ridges. Vertical exaggeration 3x. Radar reflection patterns are described and interpreted to represent dune, disturbed areas, water table, erosional surface, foreshore and shoreface sediments.

### 5.3 Topographic Survey

The topographic survey for this thesis collected elevations of ridge crests, swales, core surface location and OSL pit locations during the 2016 field season. The 2016 survey began at the modern shoreline and ended at core 2040 near the Ponderosa Pines Golf Course. The 2016 survey yielded results that decrease lakeward with a maximum of 186.5 m at 1772 m landward and a minimum of 179.3 m at 355 m landward. The transect consistently intersects the known peak Nipissing water level elevation of 183.3 m at the Port Huron/Sarnia outlet (Thompson et al., 2014) starting 800 m landward from the modern shoreline; however, previous research (Cooper, 1974; Johnston, 1999) indicates the peak Nipissing water level extended to a bluff 2.2 km landward from the modern Ipperwash shoreline. The discrepancy in the location of the peak Nipissing water level elevation lead to the comparison of the 2016 survey to other elevations measurements collected along the same transect (Figure 14) because accurate core elevations are needed to determine basal foreshore elevations and generate a paleohydrograph.

Two data sources (Johnston, 1999; southwestern Ontario orthophotography project, SWOOP2015) provide independent surface elevation data in the study area. Johnston (1999) used an optical level to survey a transect across the Ipperwash strandplain and adjusted ground surface ridge crest and swale elevation measurements to a nearby Geodetic Survey of Canada benchmark to convert measurements to a well-established LGL datum, IGLD85. SWOOP 2015 is a 2 m horizontal

resolution DEM (CGVD28) based on orthophotographs. Since SWOOP 2015 is based on photographs it only preserves the surface elevation of water bodies and uses a “steam-rolling” algorithm which “allowed for some raised features to be reduced closer to ‘bare-earth’ elevations (e.g. small buildings, small blocks of forest cover)” (SWOOP 2015 User Guide). The height of trees and any standing water must be accounted for when interpreting the SWOOP 2015 DEM. At Ipperwash, the landward portion of the strandplain is more densely forested and many of the swales contain between 0.1-1.0 m of standing water (Table 1).

The Johnston (1999) survey began at the then modern (1999) shoreline and only roughly parallels the 2016 survey. The topographic profile based on SWOOP 2015 was generated in QGIS along the same shore perpendicular line used to generate the 2016 topographic profile. However, the 2 m raster cell resolution of the DEM and “steam-rolling” algorithms simplifies and averages over an area larger than the Johnston (1999) survey. Lateral and vertical elevation differences in all three data sets were first visually assessed to determine where the transect elevations diverged (Figure 14). For all transects, ridge crest heights were used for comparison to negate the effect of standing water in SWOOP 2015 data. Crests location laterally vary by up to ten meters throughout the strandplain (Figure 14). The lateral offset is attributed to differences in horizontal data resolution.

Johnston (1999), SWOOP 2015 and 2016 survey elevations show good agreement up to 630 m distance landward, roughly plotting within a meter above or below one another (Figure 14). Johnston (1999) diverges from the 2016 survey elevations at 630 m landward consistently plotting ~1 m below 2016 elevations from 630-690 m and consistently plotting ~2.5 m below the 2016 elevations from 690 m to the landward margin of the survey. SWOOP 2015 elevations consistently plot ~3.5 m below the 2016 survey elevations from 660 m to the landward margin of the strandplain. Johnston (1999) elevations consistently plot ~1 m above SWOOP 2015 elevations from 660 m to the landward margin of the strandplain. The visual analysis suggests the elevations are consistently offset.

Core elevations from the 2016 survey and GPS based core locations overlaid on the SWOOP 2015 DEM were also compared to verify if elevations are consistently offset (Figure 15). Core elevations between the 2016 survey and the SWOOP 2015 DEM differ across the entire strandplain with a range of 5.4 m, a mean of 2.4 m and a standard deviation of 1.5 m (Figure 15). However, a clear



offset is noted. From 209-666 m landward, elevation differences range by 2.1 m with a mean difference of 0.2 m and a standard deviation of 0.6 m. From 699-1785 m landward, elevation differences range by 2.4 m about a mean difference of 3.3 m and a standard deviation of 0.6 m. Values on both sides of the offset show similar ranges and identical standard deviations, but have means that differ by 3.1 m showing that the elevations are consistently vertically offset.

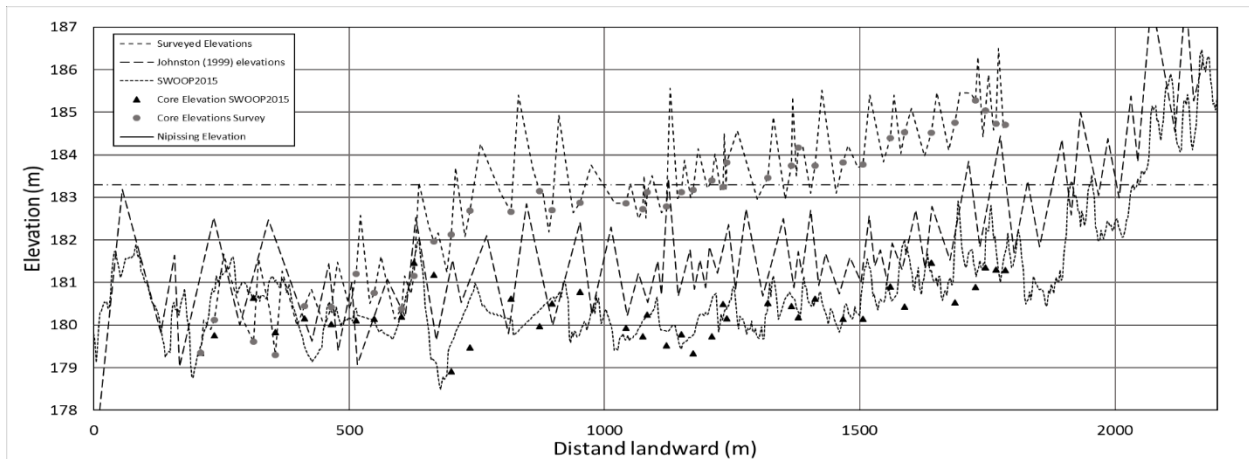


Figure 14: Comparison of cross strandplain elevation profiles developed from 2016 surveyed elevations, Johnston (1999), and drawn from the SWOOP 2015 DEM. Also plotted are core elevations and the Nipissing elevation from Thompson et al. (2014). A discrepancy between 2016 elevations, Johnston (1999) and SWOOP 2015 is minimal up to 630 m distance landward but then diverges.

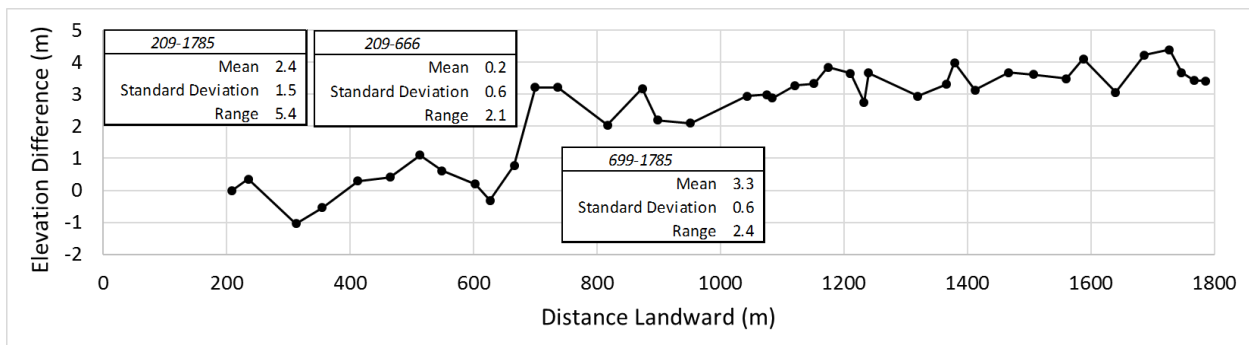


Figure 15: Comparison of the difference between core elevations determined from 2016 surveyed elevations and from the SWOOP 2015 DEM. Two groups of elevations (209-666 m and 699-1785 m landward) are consistently offset. Groups have a similar standard deviation and range but have means that differ by 3.1 m.

In order to adjust the 2016 survey which is needed to determine core elevations, the most realistic survey was determined. Johnston's (1999) survey is considered the most realistic elevation survey because Johnston's (1999) directly surveyed the ground surface. The Johnston (1999) survey is used

to adjust the 2016 survey that is consistently offset, most likely due to human or instrument error. The SWOOP 2015 survey is also adjusted to match the Johnston (1999) survey. The “steam-rolling” algorithm used in the SWOOP 2015 is suspected to have overestimated the height of forest cover in the landward portion of the strandplain.

All elevations are vertically adjusted to better match the Johnston (1999) survey. Consistency in the vertical offset of elevations allow for the adjustment of each dataset to better match one another by subtraction of a set value for a portion of the dataset (Figure 16). SWOOP 2015 elevations are adjusted by adding 1 m in elevation to all points landward of 660 m from the modern shoreline. 2016 surveyed elevations were adjusted by subtracting 1 m between 630 and 690 m landward from the modern shoreline (affecting 1 core, 2011) and subtracting 2.5 m for all points beyond 690 m landward from the modern shoreline (affecting 19 cores, 2012-2040). Once adjusted, all profiles show good agreement across the entire length of the survey (Figure 16). Adjusted 2016 survey elevations were used to determine core elevations and in all other analysis for this thesis.

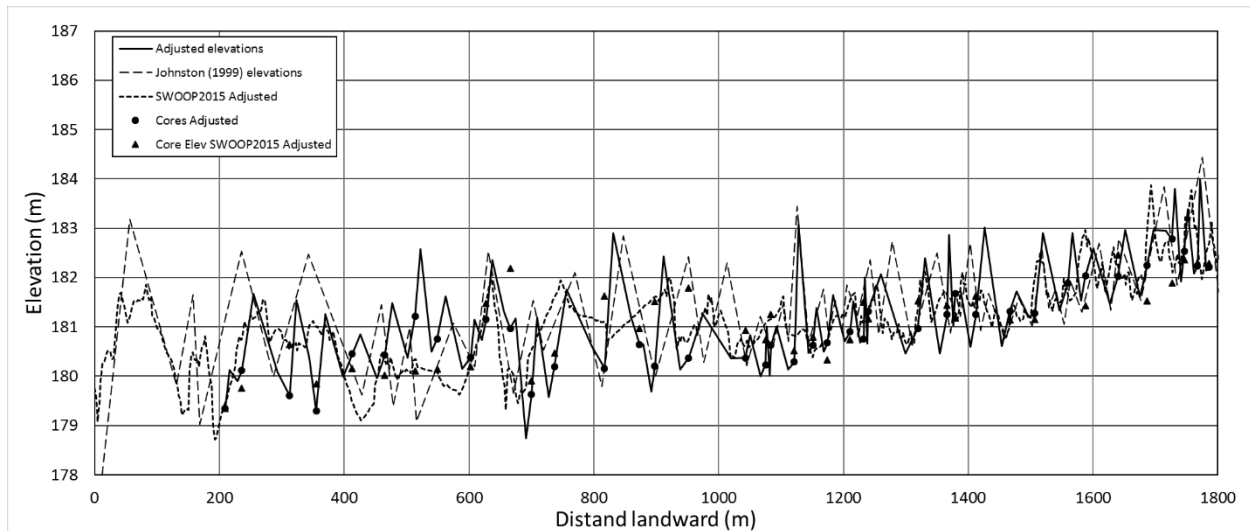


Figure 16: Adjusted topographic profile shows good agreement across the entire length of the 2016 survey. Profiles were adjusted by subtracting 1 m from 2016 surveyed elevations between 630 and 690 m landward and 2.5 m from 690 m landward to the landward margin of the survey. SWOOP 2015 elevations were adjusted by adding 1 m to points landward of 660 m.

## 5.4 Modern Shoreline Facies

Surface elevations across the modern beach were surveyed along the same transect as the cores (Figure 10). Surface sediment samples were collected along a 6 m transect beginning offshore and continuing ending on the foredune crest. Sediment samples were analyzed for grain size, sorting and skewness (Figure 17) using the University of Waterloo's Fritsch laser diffraction system. The survey is divided into three facies, dune, foreshore and shoreface, based on surface topography, sedimentary structures, mean grain size, sorting and skewness. The foreshore extends from the swash zone (the area of breaking waves) to the maximum wave runup on the modern beach. Dune facies extend landward from foreshore facies and shoreface facies extend lakeward from the foreshore facies. The plunge point exists at the foreshore-shoreface contact and can be used as a lake level proxy for ancient shorelines (Thompson, 1992).

In total, surface elevations decrease lakeward 2.9 m, with a total elevation decrease of 2.4 m occurring over the landward most 4 m, across the dune and foreshore. A 1.0 m tall erosional scarp separates the lakeward dipping foreshore surface from the undulating dune surface 1.0 m landward from the plunge point. From the plunge point lakeward elevations decrease a maximum of 0.5 m, however, a 0.4 m fall is observed over the first 0.1 m, near to the plunge point.

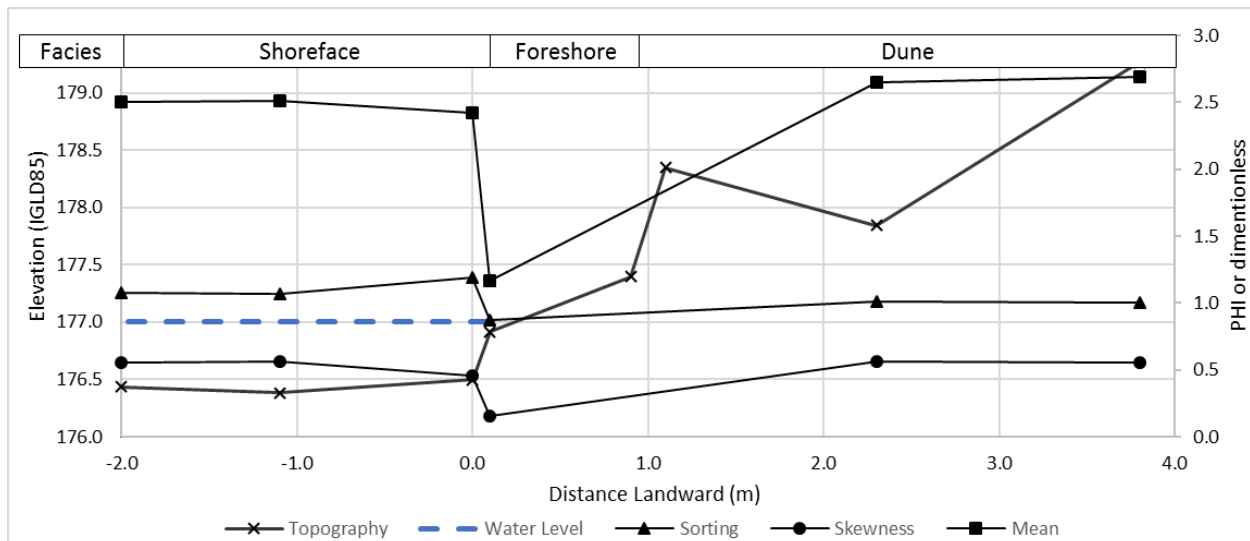


Figure 17: Plot of topographic survey and grain size results (mean, sorting and skewness) from the modern Ipperwash Beach showing the foreshore-shoreface contact as an abrupt change in grain size parameters.

All modern beach samples consisted of predominately sand sized particles. However, variations occur between dune, foreshore and shoreface facies (Table 2). Shoreface sediments consist of fine sand (2.425-2.509  $\Phi$ ), are poorly sorted (1.072-1.190), are very fine skewed (0.454-0.557  $\Phi$ ) and contain ripple marks. Foreshore sediments contain gravel size shell fragments; however these sediments were sieved out and only those particles finer than 2 mm were analyzed because they consisted of mollusk shells (presumably invasive zebra or quagga mussels) not found in cores of ancient shorelines. Foreshore sediments consist of medium sand (1.168  $\Phi$ ), are moderately sorted (0.875) and are fine skewed (0.152  $\Phi$ ). Dune sediments consist of fine sand (2.688-2.652  $\Phi$ ), are poorly sorted (1.006-1.009) and are very fine skewed (0.551-0.560  $\Phi$ ).

*Table 2: Characteristics of modern beach facies*

	Shoreface	Foreshore	Dune
Topography	Near horizontal	Lakeward dipping	Undulating
Sedimentary Structures	Ripple marks	None	Bioturbation
Mean Grain Size	Fine sand	Medium Sand	Fine Sand
Sorting	Poorly sorted	Moderately sorted	Poorly sorted
Skewness	Very fine skewed	Fine skewed	Very fine skewed

### **5.5 Ancient Shoreline Facies**

Forty cores were collected on the lakeward margin of each individual beach ridge in the Ipperwash strandplain except for the ridges nearest the modern shoreline which are modified by human activity (developed for permanent residence, paved roads, and dirt trails). Core depth of penetration ranges from 1.37-3.36 m with an average of 2.82 m. Sedimentary structures and color (determined by visual core descriptions, photographs and latex peels), and mean grain size, coarsest 1%, sorting, and skewness determine with the Indiana Geological Survey Malvern3000 laser diffraction system are used to define sediment facies. Cores were systematically interpreted and divided into dune, foreshore and shoreface facies based on changes in grain size statistics, visual descriptions, and color observed in core, photographs and latex peels (Appendix G). Core 2025 (Figure 18) is considered a typical core and described in detail to explain how sedimentary facies are defined and differentiated.

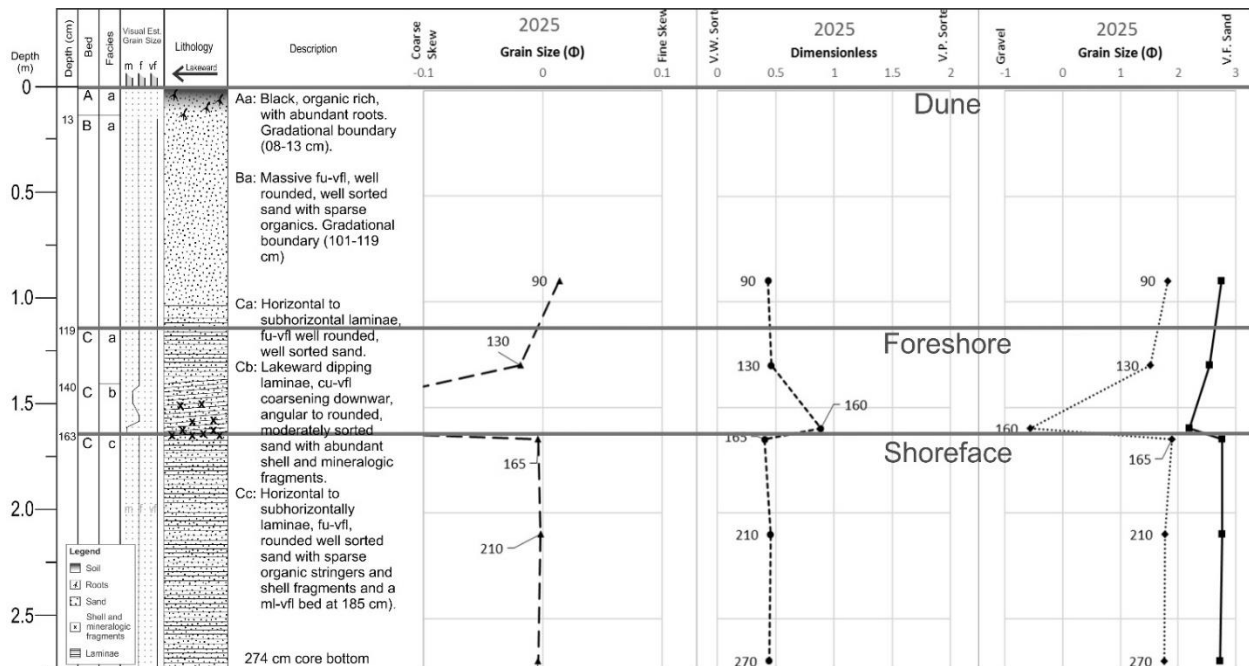


Figure 18: Visual descriptions and grain size statistics from core 2025. Shoreface sediments (274-163 cm), foreshore sediments (163-119 cm) and dune sediments (119-0 cm) are characterized by differing sedimentary structures and grain size parameter. The abrupt contact between foreshore and shoreface sediments is used as a proxy for the ancient lake level elevation when that beach ridge formed.

In core, shoreface facies are the lowest facies and typically include horizontal laminae, ripple marks and thin (1-2 mm wide) organic stringers and are noted as having a grey color. Statistically, the shoreface is characterized by a fine sand (mean grain size 2.76-2.72  $\Phi$ ) with the coarsest 1% of medium sand (D(99) of 1.75 to 1.89  $\Phi$ ), is well sorted (sorting 0.41-0.45) and symmetrically skewed (skewness 0.95-0.96  $\Phi$ ).

Foreshore facies contain horizontal to lakeward dipping laminae and a basal bed of coarse grain mineralogic and shell (gastropod) fragments with an abrupt lower boundary and are noted as having a brown color. Statistically, the foreshore is characterized by a fine sand (mean grain size 2.54-2.19  $\Phi$ ) with the coarsest 1% normally grading from fine to very coarse sand (D(99) of 1.52 to 0.57  $\Phi$ ), from well sorted to moderately well sorted (sorting 0.46-0.98) and from symmetric to coarse skewed (skewness 0.95-0.96  $\Phi$ ).

Dune facies are the uppermost facies and typically contain massive sand and noted as having a light brown color.. Statistically, the dune is characterized by fine sand (mean grain size 2.75-2.54  $\Phi$ ) with the coarsest 1% of medium sand (D(99) of 1.82 to 1.52  $\Phi$ ), is well sorted (sorting 0.43-0.46) and is symmetric to fine skewed (skewness 0.24-0.02  $\Phi$ ). The foreshore dune contact is typically gradational, however, the appearance of the laminae is considered the top of the foreshore when calculating foreshore thickness because dune sediment is commonly structureless.

In summary, the shoreface, foreshore and dune facies are identified based on sedimentary structures, color (determined by visual core descriptions, photographs and latex peels), and grain size parameters: mean grain size, coarsest 1%, sorting, and skewness (Table 3). Shoreface sediments are typically fine, well sorted and contain poorly to well defined laminae and is typically grey in color. Foreshore sediments are normally graded, moderately to well sorted, lakeward dipping to horizontal laminated with brown color and a basal layer of coarse to medium grain shell and mineralogic fragments. Dune sediments are fine grained, well sorted, structureless and light brown in color. Of the 40 cores collected, 36 yielded shoreface-foreshore contacts (basal foreshore depths). The 4 cores which did not yield basal foreshore depth likely did not penetrate deep enough to reach the basal foreshore. The 36 basal foreshore depths were subtracted from core location elevations to yield basal foreshore elevations (the approximate elevation of past lake levels when each beach ridge formed).

*Table 3: Common characteristics used to differentiate core sediment facies*

	Sedimentary structure	Mean grain size	Coarsest 1%	Sorting	Skewness	Color
Dune	Structureless	Fine sand	Medium Sand	Well sorted	Symmetrical to fine skewed	Light Brown
Foreshore	Lakeward dipping to horizontal laminae with basal bed of shell and mineralogic fragments	Fine sand	Normally grading from medium to very coarse sand	Well to moderately sorted	Symmetrical to coarse skewed	Brown
Shoreface	Horizontal laminae, ripple marks, organic stringers	Fine sand	Medium Sand	Well sorted	symmetrical	Grey

## 5.6 Cross Strandplain Geomorphic and Sedimentological Characteristics

Across the Ipperwash strandplain, changes occur in basal foreshore elevations, foreshore thickness, foreshore average grain size, beach ridge width (core to core spacing), and ridge height (swale-crest difference). These changes are quantified and statistically described.

Ground surface elevations (Figure 19) show a net increase from the lakeward to landward margin of the strandplain from a minimum of 178.1 m at the bottom of the Ipperwash Drain 700 m landward from the modern shoreline to a maximum of 184.0 m on the crest of the landward most ridge. The most lakeward ~3 beach ridges are not included because of intense human modification and were not cored. The topographic survey and core facies (Figure 19) were used to quantify the geomorphic and stratigraphic characteristics of the strandplain respectively (Table 4).

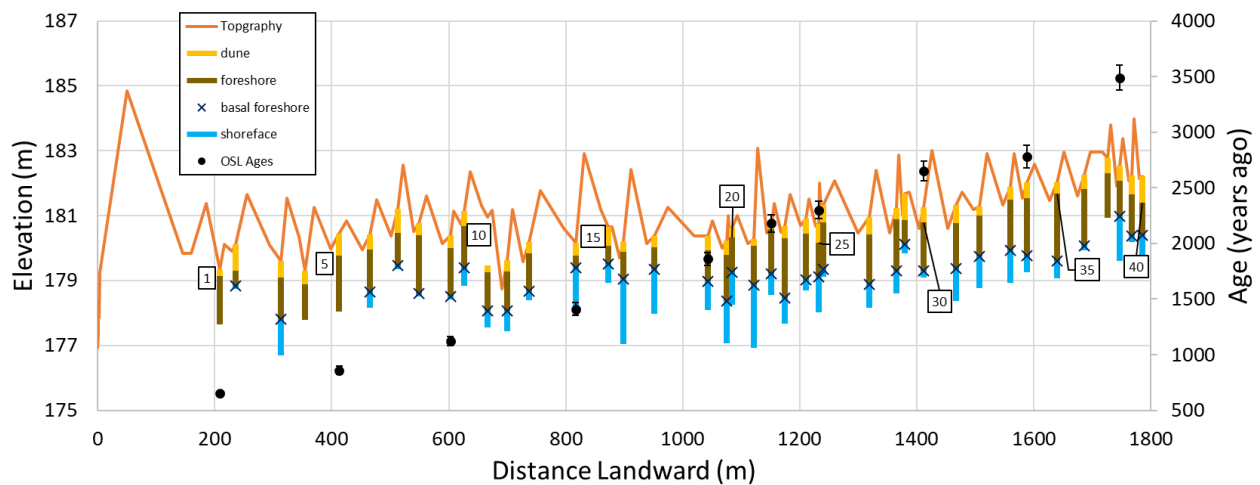


Figure 19: Surface elevation, core sediment facies and OSL ages from the Ipperwash strandplain. All data is plotted with respect to distance from the modern shoreline with ridge numbers labelled.

Basal foreshore elevations (Figure 19; Table 4) have a mean of 179.2 m with a standard deviation of 0.7, but show a net increase landward (slope 0.0006, y-intercept  $178.3 \pm 0.4$ ) with a maximum near the landward margin of the strandplain (180.99 m at 1746 m landward) and a minimum near the lakeward margin of the strandplain (177.8 m elevation at 312 m landward from modern shoreline). Foreshore thicknesses (Figure 19; Table 4) have a mean thickness of 0.9 m with a standard deviation of 0.4 with a relatively horizontal trendline (slope 0.00005, y-intercept  $0.7 \pm 0.2$ ). The maximum foreshore thickness is 2.0 m thick at 1637 m landward from modern shoreline and the minimum is

0.2 m thick at 817 m landward from modern shoreline. Foreshore average grain sizes (Figure 19; Table 4) have a mean of 2.0  $\Phi$  phi with a standard deviation of 0.1, but show a net increase landward (slope 0.0002, y-intercept  $2.4 \pm 0.1$ ) with a maximum of 2.7  $\Phi$  at 873 m landward and a minimum of 2.0  $\Phi$  at 312 m landward.

Beach ridge width (Figure 19; Table 4) have a mean of 40.4 m with a standard deviation of 0.7 and show a net decrease landward (slope -0.009, y-intercept  $50.8 \pm 8.1$ ), but have a maximum (91.1 m at 1043 m landward) and minimum (7.5 m at 1239.7 m landward) near the center of the strandplain. Ridge heights (Figure 19; Table 4) have a mean of 1.4 m with a standard deviation of 19.7 and have a landward decreasing trendline (slope -0.00003, y-intercept  $1.4 \pm 0.3$ ), but have a maximum (3.0 m height at 603 m landward) and minimum (0.02 m at 627 m landward) near the center of the strandplain.

*Table 4: Cross strandplain geomorphic and sedimentologic statistics*

	x-value of (maximum y-value)	x-value of (minimum y-value)	Mean	Standard Deviation	Trend line equation
Basal Foreshore Elevation (m)	1746 (181.0)	312 (177.8)	179.2	0.7	$y = 0.0006x + 178.0$
Foreshore Thickness (m)	1637 (2.0)	817 (0.2)	0.9	0.4	$y = 0.00005x + 0.7$
Foreshore Average Grainsize ( $\Phi$ )	873 (2.7)	312 (2.0)	2.5	0.1	$y = 0.0002x + 2.4$
Beach Ridge Width (m)	1043 (91.1)	1239.7 (7.5)	40.4	0.7	$y = -0.009x + 50.8$
Ridge Height (m)	627 (0.02)	603 (3.0)	1.4	19.7	$y = -0.00003x + 1.4$

Basal foreshore elevations and foreshore thickness have lakeward sloping trendlines through all data points. Foreshore average grain size, beach ridge width and ridge height have relatively horizontal trendlines which vary within 1 standard deviation of the mean. No visually apparent correlation is observed between quantified geomorphic and sedimentological characteristics.



### 5.6.1 Ridge Groups and Interpretations

A pattern is noted in the variations of parameters above and below one standard deviation (Figure 20). Groups of 3 to 7 ridges are defined by variations above and below 1 standard deviation. Patterns in beach ridge groupings are interpreted to represent relatively short-term fluctuations in lake level likely driven by climate (Baedke and Thompson, 2000). The five geomorphic and sedimentological parameters (Table 4) are described in regards to what past conditions the parameter likely record.

Basal foreshore elevation is a record of lake level at the time of deposition (Thompson, 1992). The lakeward sloping trendline (Figure 20) suggests that lake level has undergone a net regression during the deposition of the Ipperwash strandplain. However, the effects of GIA contributing to this relative, long-term lake level fall in elevation will be discussed in detail later.

Foreshore thickness is a factor of wave energy/height (Howard and Reineck, 1981) and wave energy/ height is a factor of wind direction, speed, fetch (Komar, 1998) collectively these parameters are referred to as wave climate (Johnston et al. 2007). Wave climate describes the average condition of waves in a certain location at a certain time, and foreshore thickness is related to wave climate when a specific beach ridge was deposited (Johnston et al., 2004).

Foreshore average grain size shows similar patterns to foreshore thickness (Figure 20) indicating a change in wave climate (Fox et al., 1966; Komar, 1998) or a change in sediment supply (Johnston et al., 2007). The close agreement between foreshore thickness and foreshore average grain size at Ipperwash is interpreted as a record of a climate oscillation.

Beach ridge width is related to shoreline behavior. Simplistically, beach ridge width is a factor of the rate of lake level change and sediment supply as well as predepositional slope (Thompson and Baedke, 1995; Figure 5). A wide beach ridge can therefore be thought to represent a period of relatively significant progradation, and a narrow ridge can be thought to represent a period of relatively minor progradation. However, due to varying erosion rates along the coast even a narrow ridge may be the result of a period of significant progradation of the coast and subsequent erosion removed much of the progradational record. Beach ridge groupings based on beach ridge width are well expressed across the entire strandplain and suggest an oscillation in shoreline behavior across several beach ridges during the deposition of the Ipperwash strandplain (Figure 20).

Beach ridge height is also related to shoreline behavior and variable dune cap (Figure 5). Since the core of a beach ridge is built by aggradation the height of a beach ridge is a factor of how long the shoreline aggrades (Figure 5). However, the presence of the dune cap complicates matters. Wind-blown sands accumulate on top of the beach ridge and increase the height of the beach ridge. Beach ridge height shows well defined beach ridge groups lakeward of 1200 m (Figure 20), this suggests oscillations in shoreline behavior and/or climate during the deposition of the Ipperwash strandplain.

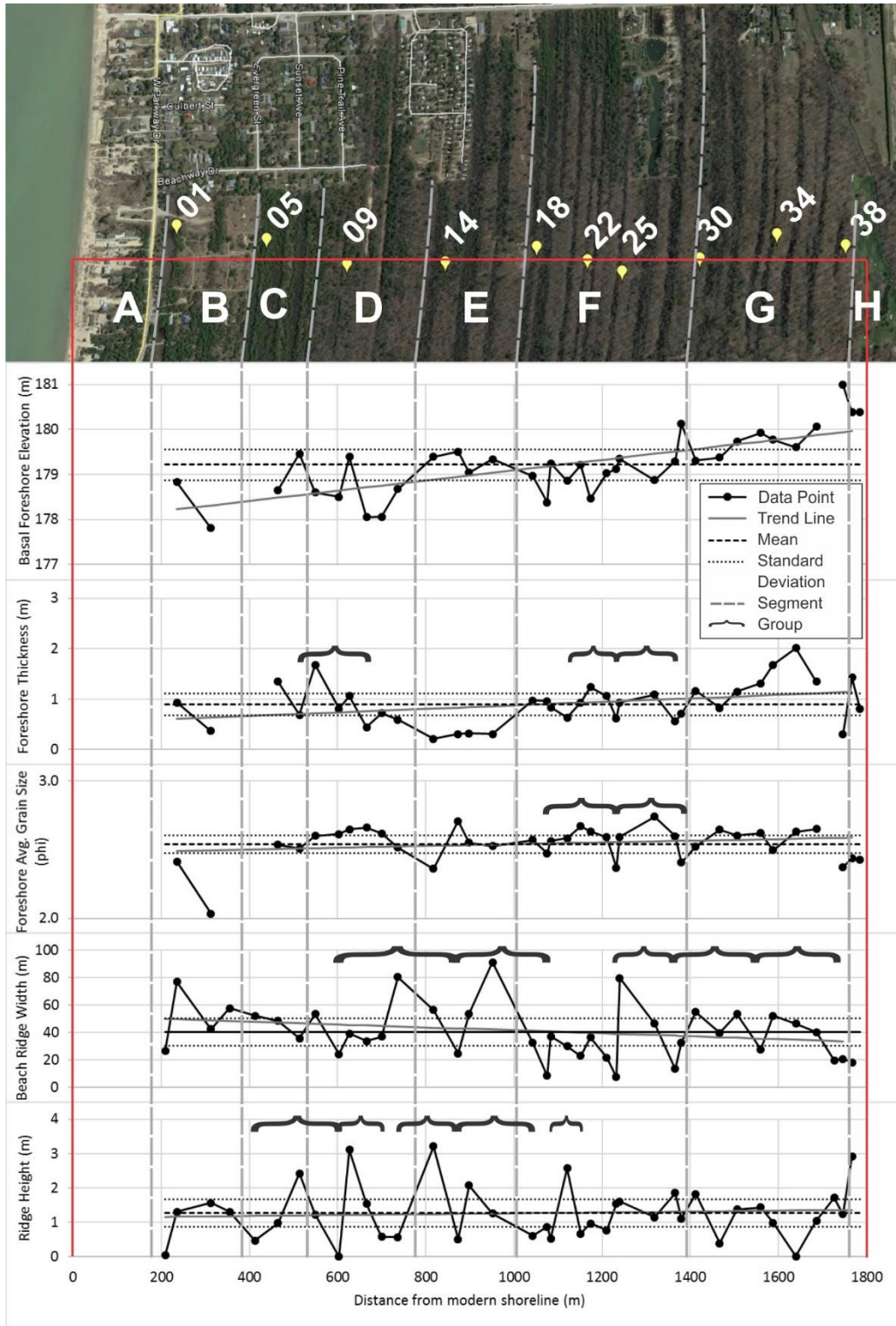


Figure 20: Geomorphic and sedimentologic characteristics across the Ipperwash strandplain showing aerial imagery with OSL sample location labeled. Eight segments (A-H) were qualitatively identified based on field observations. Groups of 3 to 7 ridges identified as rises and falls below 1 standard deviation are also identified and bracketed. Satellite imagery from Google Earth.

## 5.7 Age Modelling

Ten OSL ages (in calendar years before 2017 CE) were collected approximately 1 m below the ground surface of ridge crests on every third to fifth ridge. OSL samples were collected in an attempt to bracket ridge segments based on field observations (Figure 20). Error is reported as the standard error of equivalent dose ( $D_e$ ) distributions divided by the environmental dose rate (Figure 21). This method of error reporting allows for a more direct comparison of OSL measurement to other dating methods (such as radiocarbon) by placing emphasis on the variability of OSL  $D_e$  measurements (Lepper et al., 2011). Propagated age uncertainty (Aitkens, 1985), which takes into account geologic uncertainties is also reported (Figure 21).

Ages sequentially decrease from a maximum landward most (sample 2038, collected 1746 m landward from the modern shoreline) age of  $3490 \pm 110$  to a minimum landward most (sample 2001, collected 209 m landward from the modern shoreline) age of  $650 \pm 20$  years (Figure 19; 21).

Beach ridge number and distance the from modern shoreline were recorded for each OSL sample location. When beach ridge number is plotted against age, the average rate of beach ridge development is calculated. When distance landward from the modern shoreline is plotted against age, the average rate of long-term progradation is calculated. Distance landward is used to create the Ipperwash paleohydrograph because 1) beach ridges are variably spaced across the strandplain so plotting the ages against beach ridge number misrepresents the data and 2) during surveying it is possible that beach ridges were missed, buried, misinterpreted (i.e. dunes ridges misinterpreted as beach ridges), or discontinuous meaning the sampled ridges may over or under represent the true amount of beach ridges.

Sample ID	depth (m)	H <sub>2</sub> O (%)	K concentration (ppm)	Rb concentration (ppm)	Th concentration (ppm)	U concentration (ppm)
LH2001	1.06	30 ± 3	11625 ± 1328	34.47 ± 5.13	1.266 ± 0.125	0.471 ± 0.051
LH2005	0.84	30 ± 3	14108 ± 1508	43.35 ± 6.11	1.341 ± 0.135	0.566 ± 0.059
LH2009	1.02	25 ± 5	13190 ± 1511	43.94 ± 6.86	1.997 ± 0.190	0.586 ± 0.069
LH2014	1.03	25 ± 5	15375 ± 1701	40.70 ± 4.82	1.179 ± 0.116	0.523 ± 0.062
LH2018	0.65	25 ± 5	14841 ± 1323	41.25 ± 5.38	1.221 ± 0.121	0.553 ± 0.063
LH2022	0.93	25 ± 5	14295 ± 1269	41.15 ± 5.38	1.172 ± 0.118	0.467 ± 0.054
LH2025	0.98	25 ± 5	13789 ± 1218	39.61 ± 4.23	1.386 ± 0.133	0.673 ± 0.062
LH2030	0.68	25 ± 5	13534 ± 1185	43.34 ± 5.24	1.356 ± 0.134	0.593 ± 0.064
LH2034	1.22	25 ± 5	14790 ± 1319	38.78 ± 5.07	1.031 ± 0.105	0.555 ± 0.058
LH2038	1.22	15 ± 3	13768 ± 1250	44.87 ± 3.85	1.154 ± 0.108	0.465 ± 0.043

Irradiations for INAA were performed at the Ohio State University Research reactor. INAA data reduction was carried out by Scientific Consulting Services, Dublin, OH.

Sample ID	N <sup>1</sup>	M/m <sup>2</sup>	v <sub>t</sub> <sup>3</sup>	v <sub>d</sub> <sup>4</sup>	v <sub>g</sub> <sup>5</sup>	δD <sub>c</sub> <sup>6</sup>	Equivalent Dose <sup>5</sup> (Gy)	Dose Rate (mGy/yr)	Age <sup>7</sup> (yr)	Uncert. <sup>8</sup> (yr)
LH2001*	67/96	0.98	0.29	0.28	0.01	0.6%	0.724 ± 0.026	1.123 ± 0.122	650 ± 20	70
LH2005	74/96	0.97	0.39	0.35	0.04	0.1%	1.118 ± 0.050	1.298 ± 0.135	860 ± 40	100
LH2009	75/96	1.06	0.29	0.30	---	1.3%	1.491 ± 0.050	1.329 ± 0.150	1120 ± 40	130
LH2014	74/96	1.01	0.36	0.31	0.05	6.5%	2.012 ± 0.083	1.428 ± 0.165	1410 ± 60	170
LH2018	76/95	1.02	0.27	0.29	---	2.1%	2.618 ± 0.081	1.406 ± 0.141	1860 ± 60	200
LH2022	81/93	1.04	0.33	0.28	0.05	1.8%	2.925 ± 0.106	1.342 ± 0.135	2180 ± 80	230
LH2025	76/96	1.01	0.32	0.33	---	2.3%	3.116 ± 0.114	1.354 ± 0.132	2300 ± 80	240
LH2030	97/142	1.07	0.34	0.32	0.02	2.4%	3.513 ± 0.121	1.326 ± 0.130	2650 ± 90	280
LH2034	90/144	1.07	0.34	0.23	0.11	1.6%	3.839 ± 0.138	1.379 ± 0.139	2780 ± 100	300
LH2038	77/95	1.02	0.28	0.24	0.04	1.0%	4.989 ± 0.159	1.430 ± 0.133	3490 ± 110	340

\*OSL measurements were made on sand grains in the 150-250 μm fraction with the exception of LH2001, in which case the 90-150 μm fraction was used.

<sup>1</sup>No. of aliquots used for OSL D<sub>e</sub> calculation / no. of aliquots from which OSL data was collected (filtering criteria given in Lepper et al., 2003).

<sup>2</sup>Mean/median ratio: a measure of dose distribution symmetry/asymmetry (see supplement to Lepper et al., 2007).

<sup>3</sup>Total equivalent dose data dispersion (Std. dev./Mean)

<sup>4</sup>Data dispersion attributable to radiation dosimetric properties of the sample and dose recovery procedures.

<sup>5</sup>Simple residual data dispersion or geologic process data dispersion

<sup>6</sup>Dose recovery fidelity (refer to "check dose" in Lepper et al., 2000 and supplement to Lepper et al., 2007).

<sup>7</sup>Ages are based on the mean and std. err. of the D<sub>e</sub> distributions (Lepper et al., 2011)

<sup>8</sup>Fully propagated uncertainty (Aitken, 1985)

Figure 21: OSL element data used for dose rate calculation and OSL age results (Modified from Lepper, 2017).

Age models were created to extrapolate the 10 OSL ages collected in the Ipperwash strandplain to assign ages to the 36 recovered basal foreshore elevations used to create the Ipperwash paleohydrograph. To identify outliers and produce the most representative and realistic age model for the Ipperwash strandplain, two age models were created.

Age model A was developed as an initial examination of a linear relationship between individual ages connected sequentially (Figure 22). Slopes are calculated from the mean sample age of individual ages. Age model A shows slopes (in years per meter) ranging from 0.7 to 4.5 with an average slope between all 10 ages of 1.9 years/m ± 1.1 years. The maximum and minimum slope between ages occurs between the landward most three ages. And the lakeward most four ages have a consistent slope between ages, within 0.4 year/m of each other. This shows that slopes (i.e. the

average progradation rate) are most variable in the landward most portion of the strandplain and least variable in the lakeward portion of the strandplain (Figure 22).

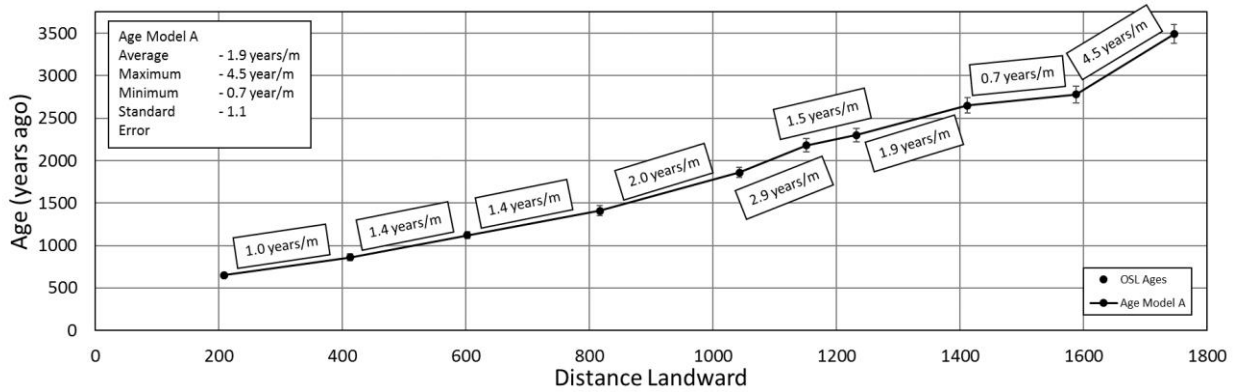


Figure 22: Age model A connects all individual ages sequentially and shows slopes between individual ages. The average slope is 1.9 years/m and a standard error of 1.1.

Age model B uses all ten ages in a single linear regression (Figure 23). For age model B  $r^2$  is 0.98, with a slope of  $1.8 (\pm 0.09)$  years/m +  $98.5 (\pm 107.0)$  years. Significance F is  $6.31 \text{ E} -08$  and the average of all residuals is 98.9 years. All age error bars lie at least partially within the confidence intervals and wholly within the prediction intervals (Figure 23). The  $r^2$  and confidence intervals suggest this age model is a good representation of the data. Ages within age model B are generally younger than reported ages in age model A (Table 5).

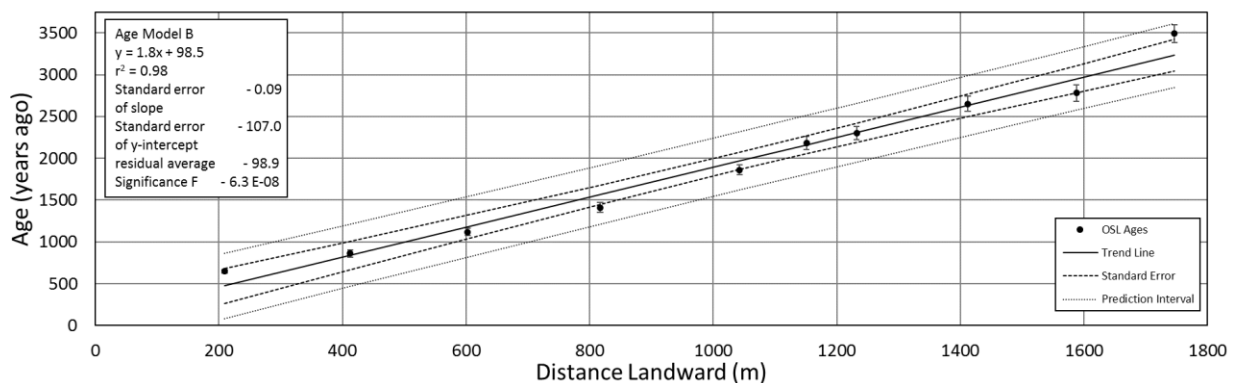


Figure 23: Age model B uses a linear regression through all ages. The resultant equation is  $y = 1.8 \pm 0.09x + 98.5 \pm 107.0$  and has a  $r^2$  is 0.98.

Table 5: Reported and modelled ages

Ridge Number	Distance from modern shoreline (m)	Reported Age/ Age Model A	Age Model B	Age Model A – Age Model B
01	209.2	650 ± 20	475	175
05	412.6	860 ± 40	841	19
09	602.6	1120 ± 40	1183	-63
14	816.9	1410 ± 60	1568	-158
18	1042.6	1860 ± 60	1975	-115
22	1151.1	2180 ± 80	2170	10
25	1232.3	2300 ± 80	2317	-17
30	1412.0	2650 ± 90	2640	10
34	1587.7	2780 ± 100	2956	-176
38	1746.4	3490 ± 110	3242	248

### 5.8 Developing the Ipperwash Paleohydrograph

An Ipperwash relative paleohydrograph can be developed by using measured elevations and modelled ages. Measured basal foreshore elevations (the ancient lake level proxy) are determined by analysis of vibracores from individual beach ridges. OSL ages are used to create an age model to assign ages to individual beach ridges. Since both basal foreshore elevations and modelled ages are plotted against distance landward from the modern shoreline, distance landward is used to relate elevation and age data.

Two Ipperwash relative paleohydrographs, one based on age model A (paleohydrograph A) and the other based on age model B (paleohydrograph B), were developed. Paleohydrographs are visually similar (Figure 24). F-tests, which test the equality of variances (Davis, 2002), are used to statistically compare paleohydrographs A and B. F-tests show the F-statistic to be less than the F Critical one-tail value; therefore, the null hypothesis is accepted, and the variance of the two populations is statistically similar (Table 6).

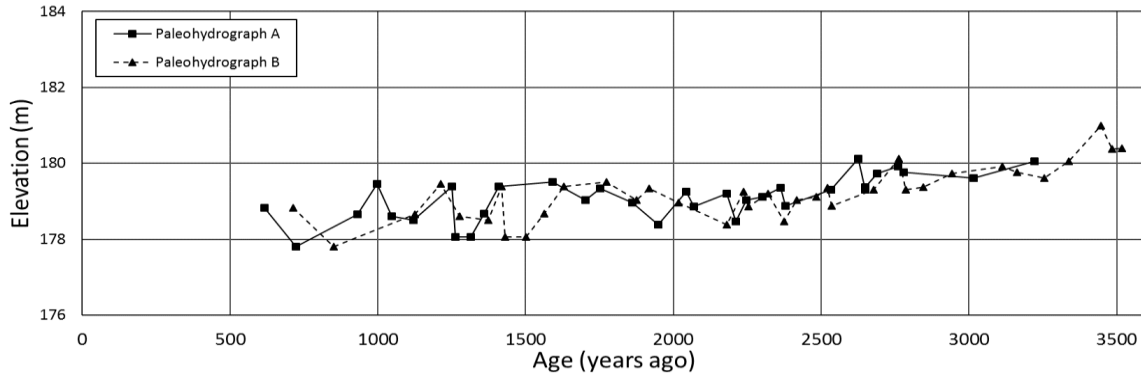


Figure 24: Ipperwash paleohydrographs developed from age model A and B.

Table 6: F-Test Two-Sample for Variances

	<i>Paleohydrograph A</i>	<i>Paleohydrograph B</i>
Mean	1973.35	2156.63
Variance	559372.90	558099.12
Observations	34	34
df	33	33
F-Statistic	1.002282357	
P(F<=f) one-tail	0.497407417	
F Critical one-tail	1.787821747	
F-Statistic < F critical one-tail	Variance of two populations equal	

Though the age models are statistically similar, geologically the age models have different implications. Age model A implies a variable long-term rate of progradation through time. Age model B implies a constant long-term progradation rate for the Ipperwash strandplain.

Age model B is used to reconstruct the most realistic Ipperwash paleohydrograph because 1) slopes between individual ages in age model A are similar, with most slopes falling within 2.2 year/m of one another suggesting a linear relationship across the entire strandplain, 2) age model A does not include the landward most two ridges since the landward most OSL sample was collected on ridge 38 (1746 m landward from the modern shoreline), 3) a linear model serves as a good, simple approximation of beach ridge age for the Ipperwash strandplain, and 4) age model B allows for the comparison to other LGL strandplain paleohydrographs since other paleohydrographs used linear age models (Baedke and Thompson, 2000; Johnston et al., 2012).



## Chapter 6

### The Ipperwash paleohydrograph

Thirty-six basal foreshore elevations and ten OSL ages were combined to create the Ipperwash paleohydrograph. Patterns within the Ipperwash paleohydrograph are described and interpreted in the context of known drivers of lake level change during historic times (International Upper Great Lakes Study Board, 2009; 2012) and geologic times (Baedke and Thompson, 2000; Johnston et al., 2012).

The Ipperwash paleohydrograph chronicles relative lake level fluctuations from 3520 to 710 years ago (Figure 25). The maximum relative lake level is 181.0 m which occurred 3450 years ago and the minimum relative lake level is 177.8 m which occurred 850 years ago. Prehistoric lake level elevations are higher than historic lake level elevations. Historic (since 99 years ago or 1918 CE) lake levels in Lake Huron have fluctuated between a lake-wide yearly average high of 177.3 m 31 years ago (or 1986 CE) and a lake-wide yearly average low of 175.7 m 53 years ago (or 1964 CE) (Gronewold et al., 2013a). Recent International Joint Commission Studies have concluded historic lake level changes has been driven by GIA, outlet conveyance, and climate with the largest contributing factor being climate (International Upper Great Lakes Study Board, 2009; 2012). GIA, outlet conveyance and climate are also important drivers of prehistoric lake level fluctuations (Johnston et al., 2014). Therefore, GIA, outlet conveyance, and climate are briefly reviewed to give context to interpretations of patterns within the Ipperwash paleohydrograph. It should be noted that though the terms millennium, centennial, and decadal are used these terms should not be taken as an exact length of time, but rather as a rough estimate of natural patterns observed through geologic time.

The Ipperwash paleohydrograph is compared to the Lake Michigan paleohydrograph which reflects lake levels at the Port Huron/Sarnia outlet (Figure 4; 26). The Lake Michigan paleohydrograph is an outlet-referenced paleohydrograph created by combing strandplain data from 5 sites around Lake Michigan and adjusting overlapping strandplain paleohydrographs to reconstruct lake level fluctuations in one hydrologically connected lake (Lake Michigan-Huron) at the Port Huron/Sarnia outlet. The Lake Michigan paleohydrograph shows that following the Nipissing highstand, 4,500 cal BP, lake level underwent a rapid fall of 4.1 m until 3,400 cal BP (Baedke and Thompson, 2000). The end of the rapid fall is attributed to the abandonment of the Chicago outlet (Baedke and

Thompson, 2000). Baedke and Thompson (2000) also propose lake levels rose and fell on a millennial rhythm over the next several thousand years. Lake levels rose from 3,300 to 3,000 cal BP, associated with the Algoma highstand, fell from 2,400 to 2,250 cal BP, and rose from 2,100 to 1,700 cal BP, associated with the 1,700 high, and fell from 1,700 to 1,000 cal BP (Figure 4; 26).

Ipperwash is the nearest preserved strandplain with the most beach ridges to the Port Huron/Sarnia outlet. The rate of GIA between the Ipperwash strandplain and the Port Huron/Sarnia outlet is expected to be similar (Figure 2; Mainville and Craymer, 2005). The Ipperwash paleohydrograph and the outlet referenced Lake Michigan paleohydrograph are expected to be similar as both reconstruct lake levels experienced at the Port Huron/Sarnia outlet. However, the Ipperwash paleohydrograph consistently plots above the Lake Michigan paleohydrograph (Figure 26). Johnston et al. (2012) and Thompson et al. (2014) suggested too much GIA was collectively removed when creating one outlet-referenced paleohydrograph for Lake Michigan. This thesis reevaluates the Lake Michigan paleohydrograph using the Ipperwash paleohydrograph.

The Ipperwash paleohydrograph is also compared to the historic lake level record for Lake Huron to determine the relationship between historic and prehistoric lake levels which can be used to more accurately predict potential future lake level changes at Ipperwash.

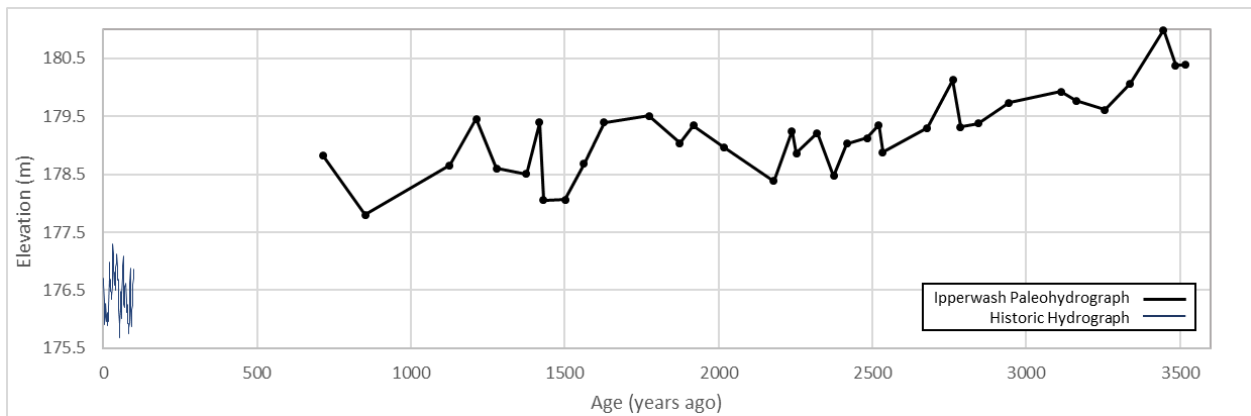


Figure 25: Ipperwash paleohydrograph compared to Lake Huron's annual average historic lake level. The Ipperwash paleohydrograph records lake level fluctuations from 3520 to 710 years ago and shows a net lake level decrease from a high of 181.0 m 3450 years ago to a low of 177.8 m 850 years ago.

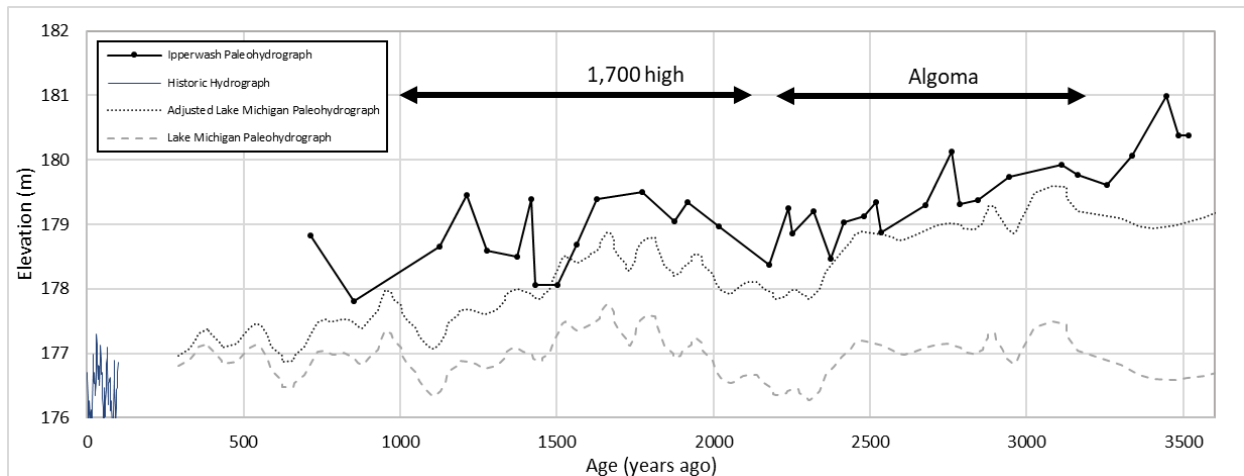


Figure 26: Historic hydrograph, Ipperwash paleohydrograph and the Lake Michigan paleohydrograph (Baedke and Thompson, 2000). If the Lake Michigan paleohydrograph is adjusted based on the rate of GIA at Ipperwash the two graphs plot more closely.

## 6.1 GIA, outlet conveyance and climate

GIA is the ongoing rate of land surface elevation change (expressed in cm/century) during and following glacial advances and retreats which influence relative lake level change in the LGL. Various methods have been used to estimate the rate of GIA in and around the LGL. Geologic data has been used in some areas of the LGL to estimate rates of GIA in a single basin relative to that basin's outlet (Lewis, 1970; Baedke and Thompson, 2000; Johnston et al., 2012). The analysis of geologic data suggests a linear rate of GIA over at least the past 3500 years and is interpreted as the longest pattern in LGL paleohydrographs (Johnston et al., 2014). Various geologic and GPS datasets have been used to model the absolute rate of GIA at a continental scale (Peltier et al., 2015), and these models have been further refined in the LGL through the inclusion of the lake level gauge record since 1918 CE (Mainville and Craymer, 2005; Figure 2) which forms the basis for rates of GIA in used in international management plans (International Upper Great Lakes Study Board, 2009; 2012). Though records vary on the exact rate of GIA at a precise location, all records show the same general pattern of GIA, the land surface rising (up to 54 cm/century) in the northern LGL and subsiding (down to -27 cm/century) in the southern LGL. Based upon the most recent GIA models at continental scales (Peltier, et al., 2015) and over the LGL (Mainville and Craymer, 2005) the rate of GIA is zero cm/century near the Port Huron/Sarnia outlet relative to a point representing the center of the Earth. Ipperwash is located 40 km from the Port Huron/Sarnia outlet, and is also estimated to have a rate of GIA of zero cm/century. In other words, the ground surface at

Ipperwash is not moving up or down relative to a fixed point in the center of the Earth and is identical to the ground surface at the Port Huron/Sarnia outlet through geologic time.

Outlet conveyance is a change in the water carrying capacity of a lake's outflow channel(s) due to channel activation or abandonment, or when the active channel experiences erosion or sedimentation. For example, Hough (1958) suggested the fall from the peak Nipissing, approximately 4500 years ago, was a result of natural erosion at the Port Huron/Sarnia outlet, and Johnston et al., (2007) suggested the outlet at Sault Ste Marie began regulating Lake Superior's lake level at 1100 calendar years ago. During historic times only a relatively small portion of the lake level change has been attributed to erosion, caused by dredging, in the Port Huron/Sarnia outlet (International Upper Great Lakes Study Board, 2009). These examples show the importance of a lake's outlet in regulating lake level in the LGL. A recent study by Campbell (2016) initiated investigation of natural changes in outlet conveyance preserved in three depositional coastal landforms (spits) located in the Port Huron/Sarnia outlet that were deposited sometime in the last 4500 years. Since the Port Huron/Sarnia spits lie at a similar elevation to the beach ridges in the Ipperwash strandplain (i.e. between the modern lake and the peak Nipissing), deposition of the spits likely occurred between 3520 and 710 years ago, the period of record in the Ipperwash paleohydrograph. The ages and subsurface stratigraphy of the Port Huron/Sarnia spits is therefore very important to determine past natural times of outlet conveyance caused by longshore drift and sedimentation in the Port Huron/Sarnia outlet that may have restricted outflow from Lake Michigan-Huron. No studies have investigated outlet conveyance caused by sedimentation in the Port Huron/Sarnia outlet. The Ipperwash paleohydrograph provides the context needed to interpret the Port Huron/Sarnia spits and how the spits may relate to natural outlet conveyance through geologic time.

Climate also influences LGL lake levels. Historic data and paleoclimate data suggests lake level fluctuate on the order of many decades (Argyilan and Forman, 2003; Gronwold and Stow, 2014) and many centuries (Fraser et al., 1990) and may be related to climate. Warm and dry climate have been related to low lake levels during historic (Argyilan and Forman, 2003; Gronewold and Stow, 2014) and prehistoric times (Fraser et al., 1990; Lewis et al., 2008a). Cool and wet climate have been related to high lake levels during historic (Gronwold et al., 2016) and prehistoric times (Fraser et al., 1990; Booth et al., 2002). Lows and highs in the Ipperwash paleohydrograph may therefore record at least

a partial climate record. Analysis of 40 paleoclimate records (Shuman and Marsieck 2016) show mid-latitude North America (i.e. the belt in which the LGL predominately lie) experienced relatively dry and warm conditions from 2900 to 2100 cal BP then a rapid transition to relatively wet and cool climate conditions which last until 1800 cal BP.

GIA, outlet conveyance and climate all affect lake levels, but with different temporal and lateral scales in a lake basin (Johnston, et al. 2014). GIA is an ongoing, linear, geologic process unique to different sites around a lake basin. Outlet conveyance also occurs over historic and prehistoric time scales but should be experienced and preserved at all strandplain sites around a lake basin. Similar to outlet conveyance, climate naturally changes on time scales ranging from decades to millennium and effects lake levels in an entire lake basin.

The Ipperwash paleohydrograph is analyzed to discern trends and patterns in lake level fluctuations. Multi-millennium, millennium, centennial, and multi-decadal patterns within the Ipperwash paleohydrograph are interpreted to represent GIA, outlet conveyance, and/or climate.

## **6.2 Multi-millennium pattern**

A long term, multi-millennium pattern identified by using all 36 data points in the Ipperwash paleohydrograph is simplistically described by a single linear regression. The resultant equation is  $y = 0.0007x + 177.8$  and  $r^2$  is 0.56 (Figure 27). Standard error of the slope is 0.001 and standard error of the y-intercept is 0.2. The slope of the trend line suggests a net lake level fall at a rate of 7 cm/century with oscillations above and below the trend line. The multi-millennium pattern shows a net, linear, relative lake level fall of 1.8 m from 3520 to 710 years ago.

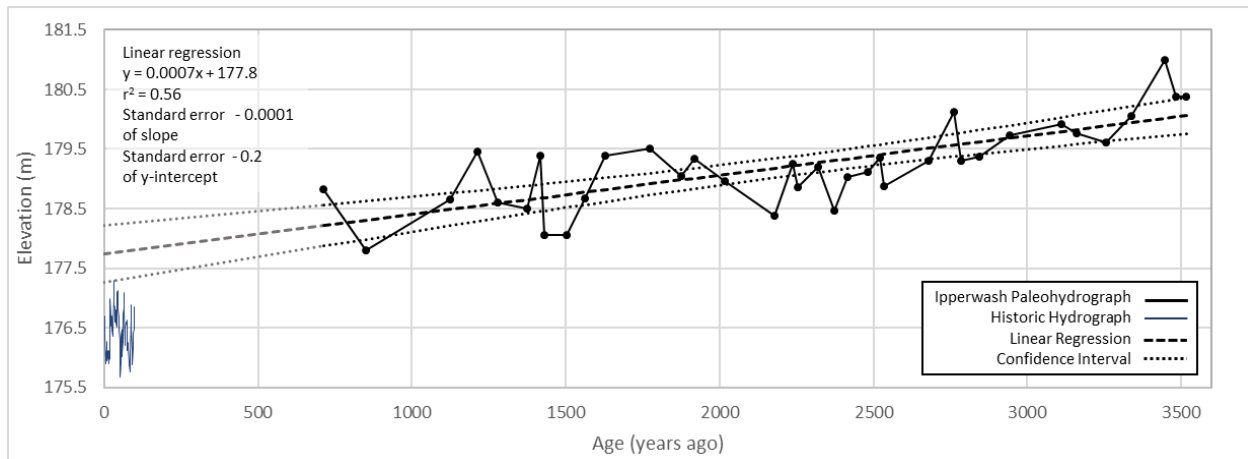


Figure 27: A linear regression through the entire paleohydrograph shows a relatively well confined pattern spanning the entire paleohydrograph.

GIA is regarded as the driver of the longest trend in LGL paleohydrographs (Johnston, et al., 2014) and is therefore interpreted as the dominant driver of the multi-millennium lake level lowering at Ipperwash. The multi-millennium linear pattern calculated from Ipperwash beach ridges suggests a rate of GIA near  $7 \pm 1$  cm/century. However, the rate of GIA, based on the current understanding in published literature, at Ipperwash is expected to be 0 cm/century (Mainville and Craymer, 2005). This difference in rates of GIA at Ipperwash could stem from three reasons or a combination of the three reasons. 1) Interpolation between water gauge stations underestimates the rate of GIA at Ipperwash. This could stem from insufficient water gauges near Ipperwash (the closest water gauge station is located at Lakeport, Michigan, approximately 43 km from Ipperwash) to accurately resolve the rate of GIA at Ipperwash. 2) The rate of lake level lowering at Ipperwash could stem from erosion at the Port Huron/Sarnia outlet during the deposition of the Ipperwash strandplain. If this is the case, all strandplains around Lake Michigan-Huron should reflect this rate of lake level lowering. However, strandplains in Lake Michigan show a varying rate of lake level change through geologic time (Thompson and Baedke, 1997). In addition, recent studies have found no active erosion in the Port Huron/Sarnia outlet in historic times (International Upper Great Lakes Study Board, 2009). 3) An outlet other than Port Huron/Sarnia was active and dominant during the time period recorded in the Ipperwash paleohydrograph. The Chicago outlet is the most likely outlet to be active during the deposition of the Ipperwash strandplain and interpretation of the millennium patterns within the Ipperwash paleohydrograph (discussed below) may support the dominance of the Chicago outlet during the time period recorded in the Ipperwash paleohydrograph.

Interestingly, applying a consistent rate of 7 cm/century to the outlet-referenced Lake Michigan paleohydrograph (Baedke and Thompson, 2000) helps the Lake Michigan and Ipperwash paleohydrographs match more closely (Figure 26). This argues for a readjustment of the Lake Michigan paleohydrograph to better represent the conditions experienced at the Port Huron/Sarnia outlet and is the first verification of an idea presented in previous studies which suggested too much GIA was removed when creating the Lake Michigan paleohydrograph (Johnston et al., 2012; Thompson et al., 2014).

When the multi-millennium long, linear pattern is extended to the present, the confidence interval minimum (177.3 m) intersects the historic yearly average lake level high (177.3 m) 31 years ago or 1986 CE (Figure 27). The intersection of the lower confidence interval of the multi-millennium pattern in the Ipperwash paleohydrograph and the historic annual Lake Huron lake level high, may support that the multi-millennium pattern is represented in the historic record. The multi-millennium pattern extended above the historic record potentially because subsurface elevation measure in Ipperwash beach ridges record multi-decadal lake level highs (Thompson and Baedke, 1995; Johnston et al., 2007). To equate the historic and prehistoric lake level records the multi-decadal historic lake level high is needed for comparison. The potential multi-decadal lake level high (occurring in 1986 CE or 31 years ago) is close to the statistical range calculated from Ipperwash beach ridges (Figure 27).

### **6.3 Millennium patterns**

Field observations and geomorphic and sedimentologic data suggests a break between a landward and lakeward set of beach ridges. The landward set of Ipperwash beach ridges consists of cores 2040 - 2014 (1785 – 817 m landward from the modern shoreline) and is characterized by swales filled with shallow to deep water (0 – 1 m deep), well defined beach ridge groups based on foreshore thickness and average grain size, and beach ridge width that is typically narrower than the lakeward set of ridges (Table 1; Figure 20). The lakeward set of Ipperwash beach ridges consists of cores 2013 – 2001 (737 to 209 m landward from the modern shoreline) and is characterized by either dry swales or swales filled with deep water (~1 m deep), well defined beach ridge groups based on ridge

height, and beach ridge with that is typically wider than the landward set of ridge (Table 1; Figure 20).

When the Ipperwash paleohydrograph is divided based on field observations, geomorphic and sedimentological evidence, two lowering patterns are observed each lasting approximately 1300 years. Patterns are vertically offset by 0.5 m over 160 years. These patterns are termed millennium patterns for the sake of simplicity and to differentiate them from the multi-millennium patterns which spans several millennium. The oldest period of relative lake level record lasts from 3520 to 2180 years ago, has an equation of  $y = 0.001x + 175.9$  with an  $r^2$  of 0.76. Standard error of the slope is 0.0002 and standard error of the y intercept is 0.5. The youngest period of relative lake level record lasts from 2020 to 710 years ago, has an equation of  $y = -0.0006x + 177.9$  with an  $r^2$  of 0.19. Standard error of the slope is 0.0004 and standard error of the y intercept is 0.5. The two patterns are vertically offset by 0.5 m.

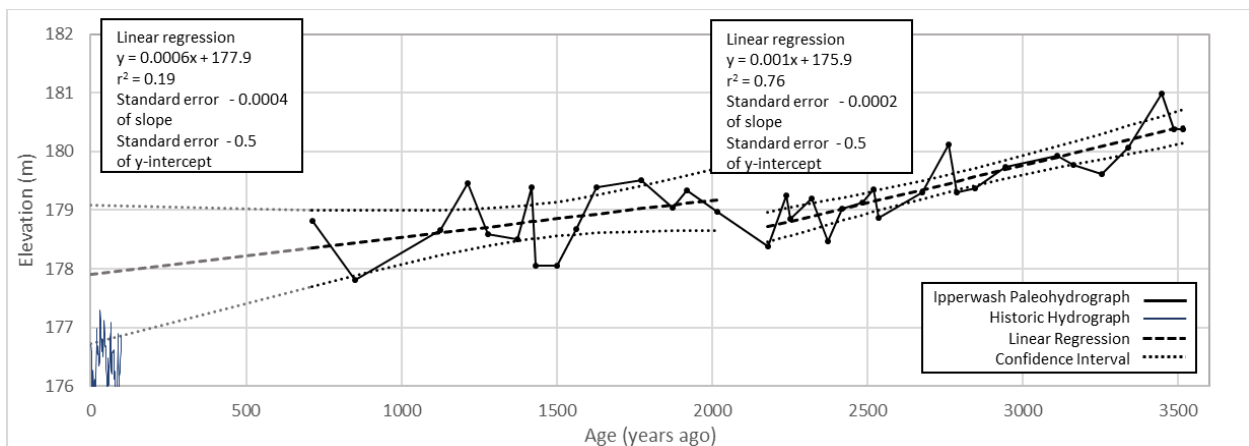


Figure 28: Ipperwash paleohydrograph with GLA removed and divided into two linear regressions which suggests two phases of lake level lowering. The two periods of lake level lowering are vertically offset by 0.5 m and a period of 160 years.

The millennial pattern in the Ipperwash paleohydrograph suggests two periods of oscillatory relative lake level fall separated by a 160 year period (between 2180 and 2020 years ago) showing a vertical offset of 0.5 m between the millennium trends. The oldest period lasted from 3520 to 2180 years ago and resulted in a mean net lake level fall of 1.7 m. The youngest period lasted from 2020 to 710 years ago and resulted in a mean net lake level fall of 0.8 m.



The millennial patterns compare with lake phases in the Lake Michigan paleohydrograph. The oldest millennium trend in the Ipperwash paleohydrograph roughly relates to the Algoma phase in Lake Michigan strandplain data using radiocarbon dates from 3400 to 2300 cal BP (Baedke and Thompson, 2000; Figure 26) and Lake Superior strandplain data using OSL dates from 2800 to 2000 cal years BP (Johnston et al., 2012). A vertical offset between the two millennium patterns in the Ipperwash paleohydrograph is observed over a period lasting from 2180 to 2020 years ago. This vertical offset between millennium trends at Ipperwash may relate to rising water levels during the transition from the Algoma phase to the 1700-high phase recorded in strandplain data of Lake Michigan (Baedke and Thompson, 2000; Figure 4) and the Algoma and Sault phases recorded in strandplain data of Lake Superior (Johnston et al., 2012). Farrand (1962) suggested Lake Superior separated from Lake Michigan-Huron at this time of low water level and Lake Superior became its own lake, as it is today elevated by a bedrock sill above Lake Michigan-Huron. But Johnston et al. (2012) suggests this time period only represented a short time period of separation and Lake Superior's final separation occurred closer to 1100 calendar years ago.

Extrapolating from published reports of a relationship between climate and lake level in geologic (Fraser et al., 1990; Lewis et al., 2008a) and historic (Argyilan Forman, 2003; Gronewold et al., 2016) times in the LGL, falls in lake level may be related to a relatively dry and warm climate and lake level rises may be related to wet and cool climate. To investigate this relation further the paleoclimate record for the LGL is examined. Shuman and Marsicek (2016) show mid-latitude North America experienced relatively dry and warm conditions from 2900 to 2100 cal BP and relatively wet and cool conditions from 2100 to 1800 cal BP with rapid changes occurring at 2100 cal BP. The period of the Ipperwash paleohydrograph lasting from 3520 to 2180 years ago is a period of lake level fall and corresponds with dry and warm conditions from 2900 to 2100 cal BP. Additionally, from 2180 to 2020 years ago the Ipperwash paleohydrograph records a relative lake level rise between the two millennium trends which corresponds with wet and cool conditions lasting from 2100 to 1800 cal BP. Since time periods of lake level falls and rises correspond with periods of dry and warm, and wet and cool climates respectively, climate is a possible dominant driver of millennium patterns in relative lake levels.

Alternatively, part of the two millennium trends may be a result of a long-term change in outlet conveyance that can be resolved through evaluation of rates of GIA between the study site and the

active outlet during certain time periods. A long-term lake level lowering in a paleohydrograph indicates the ground surface at the active outlet is not rising as fast as the study site. Using the pattern of GIA of Mainville and Craymer (2005), the long-term lowering would suggest that the Chicago outlet could be the dominate outlet when part of the Ipperwash strandplain formed. The rate of GIA at the Chicago outlet of Lake Michigan-Huron is falling at a rate of  $\sim 12$  cm/century relative to Ipperwash and the Port Huron/Sarnia outlet (Mainville and Craymer, 2005; Figure 2). This rate of GIA matches the long-term trend of the oldest millennium trend ( $10 \pm 2$  cm/century) which may indicate that the Chicago outlet regulated lake levels in Lake Michigan-Huron during the oldest millennium trend recorded in the Ipperwash paleohydrograph. Previous work also indicates the Chicago outlet of Lake Michigan-Huron was completely abandoned around 2400 cal BP (Chrzastowski and Thompson, 1992) which roughly corresponds with the end of the oldest millennial trend at Ipperwash, 2180 years ago.

The youngest millennium linear lowering trend in the Ipperwash paleohydrograph, lasting from 2020 to 710 years ago with a rate of  $6 \pm 4$  cm/century, also falls within the possible range of the rate of GIA between the Chicago outlet and Ipperwash. It is therefore possible that Chicago was also active during the most recent millennium trend in the Ipperwash paleohydrograph. This would suggest that the Chicago outlet remained the active outlet for Lake Michigan-Huron until at least 710 years ago, the youngest possible date for the final abandonment of the Chicago outlet.

Millennium trends can be explained by natural climate change and the abandonment of the Chicago outlet. Based on the interpretation of the Ipperwash paleohydrograph, the abandonment of the Chicago outlet is the most likely scenario responsible for the linear millennium trends within the Ipperwash paleohydrograph. Variations about this trend would then be related to climate. The active Chicago outlet most easily explains the millennium trend within the Ipperwash paleohydrograph and fits with previous interpretations of an active Chicago outlet during the Algoma lake phase interpreted from Lake Michigan strandplains (Chrzastowski and Thompson, 1992). However, the Ipperwash strandplain suggests the Chicago outlet remained active longer than previously thought, up to 710 years ago and during 1700-high lake phase in Lake Michigan. More detailed geologic information at the Chicago and Port Huron/Sarnia outlets are needed to determine the activation and abandonment of these outlets during geologic time and interpreted with strandplain data of Lake Michigan (Baedke and Thompson, 2000) and unpublished data of Lake Huron strandplains.

## 6.4 Centennial patterns

Groups of 3 to 7 ridges were identified based on cross-strandplain changes in foreshore thickness, mean grain size, beach ridge width and ridge height (Table 4; Figure 20). These groups are similar in length to beach ridges groups found in Lake Michigan (Baedke and Thompson, 2000) and Lake Superior (Johnston et al., 2007). At Ipperwash, a similar length oscillation is observed as rises and falls in lake level (basal foreshore) above and below the millennium trend lines (Figure 30). This pattern is best represented as oscillations about the millennium pattern because both patterns are interpreted to related to climate.

Rises and falls in lake levels about the millennium trends marks a centennial pattern in the Ipperwash strandplain and consists of groups of 3 to 5 ridges (Figure 30). Centennial patterns last an average of  $208 \pm 114$  years and have an amplitude of  $0.8 \pm 0.4$  m (Figure 30). Fraser et al. (1990) studied several Lake Michigan-Huron shorelines and observed a similar length cycle (lasting 100 to 150 years) based on radiocarbon dating of several high lake levels proxies (beach erosion, stream aggradation, marsh formation, and soil formation) and attributed the lake level cycle to natural climate change. This cycle was also observed in strandplains in Lake Michigan as a  $150 \pm 30$  year-long centennial lake level oscillations (Baedke and Thompson, 1997). A similarity in length to the centennial pattern observed in the Ipperwash paleohydrograph leads to the interpretation of the centennial pattern as a result of natural climate changes.

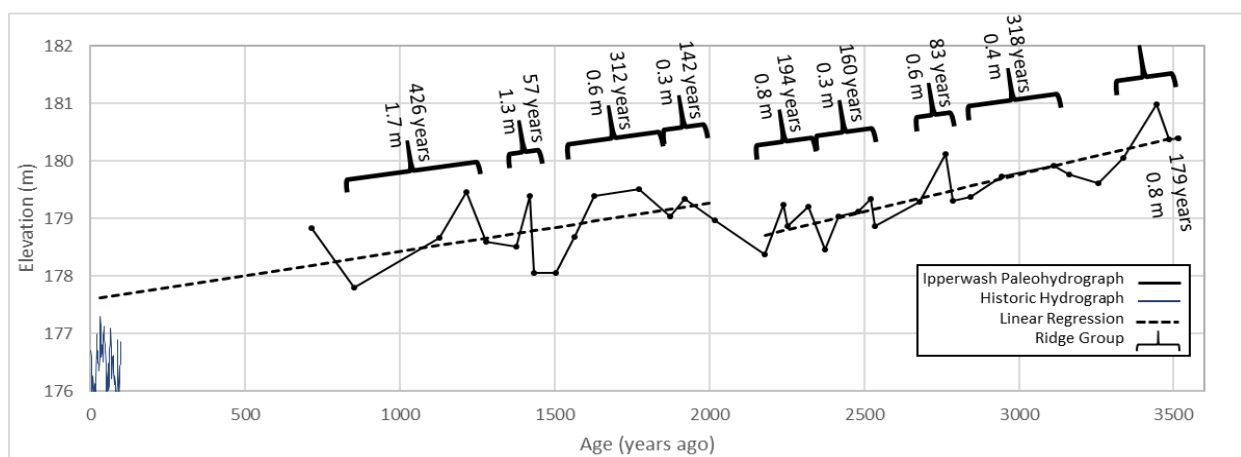


Figure 29: Ipperwash paleohydrograph divided into centennial oscillations as defined by lake level rises and falls about the millennium pattern lines. Centennial oscillations are represented by groups of 3 to 5 ridges. Length and amplitude of each oscillation is also labelled.

## **6.5 Multi-decadal patterns**

The multi-decadal pattern is represented by the average amount of time it takes for a single beach ridge to develop at Ipperwash for 2810 years (from 3520 to 710 years ago). The age model used to create the Ipperwash paleohydrograph assumes a constant rate of progradation (Figure 21). Using the linear model extending across 36 Ipperwash beach ridges indicates the average timing of beach ridge development at Ipperwash is  $73 \pm 35$  years. Since the Ipperwash strandplain beach ridges are variably spaced across the strandplain (Figure 18), the amount of time it takes for a single beach ridge to develop may vary.

Hanrahan et al., (2009) report an intermodulation of two near-decadal climate cycles linked with quasi-periodic beach ridge formation in Lake Michigan based on analysis of the historic water gauge record. Because Lake Michigan and Lake Huron occupy the same basin, the beach ridges at Ipperwash are interpreted to result from climate cycles.

Multi-decadal lake level oscillations in the Ipperwash paleohydrograph occur every  $73 \pm 35$  years and represent the average time it takes to form a single beach ridge. The interval of beach ridge development at Ipperwash overlaps with the range of beach ridge development in Lake Michigan (29-38 years; Beadke and Thompson, 2000) and Lake Superior (17-45 years; Johnston et al., 2012). Therefore, the multi-decadal oscillation in the Ipperwash paleohydrograph, Lake Michigan paleohydrograph, and Lake Superior paleohydrograph are interpreted to represent the natural rhythm in climate that has affected lake levels in Lakes Superior, Michigan and Huron over the late Holocene.

# Chapter 7

## Conclusion

The natural history of the LGL has been studied for over a century (Leverett and Taylor, 1915). Beach ridges record prehistoric lake levels (Thompson, 1992), and strandplains of beach ridges are used to reconstruct natural lake level fluctuations in the LGL (Johnston et al., 2014).

During the late Holocene, lake levels have naturally fluctuated in the LGL due to three dominate processes: GIA, outlet conveyance, and climate (Johnston et al., 2014). GIA is the rate of vertical ground movement in response to glacial advances and retreats. GIA occurs at different rates throughout the LGL as a result of the retreat of the Laurentide Ice Sheet causing lake levels to rise or fall at different relative rates within the same lake basin. Outlet conveyance is a change in the water carrying capacity of a lake's outflow channel(s) and causes lake levels to rise or fall at a universal rate within a single basin. Climate is a change in predominate regional weather patterns and cause lake levels to rise or fall within LGL basins.

The Ipperwash strandplain, southern Lake Huron, was studied to reconstruct past natural lake level changes in the Lake Huron basin and the Port Huron/Sarnia outlet during the late Holocene. The Port Huron/Sarnia outlet is the only remaining unregulated outlet (lacking any locks or dams) in the LGL and is therefore particularly susceptible to natural lake level changes. The Ipperwash strandplain offers a natural lake level record which mimics the lake level record of the Port Huron Sarnia outlet, because Ipperwash is the closest strandplain with the most beach ridges to the Port Huron/Sarnia outlet.

Elevation and age data were used to create the Ipperwash paleohydrograph. In order to obtain these data the lakeward margin of beach ridges were vibracored and analyzed to obtain prehistoric lake level elevations, and OSL ages were collected from beneath the crests of 10 beach ridges. OSL ages were then modelled using a linear regression to determine the age of individual beach ridges for the entire Ipperwash strandplain. The resultant Ipperwash paleohydrograph reconstructs a general cross-strandplain, linear, relative lake level lowering from a maximum elevation of 181.0 m to a minimum elevation of 177.8 m over a time period lasting from 3520 to 710 years ago.

Analysis of the Ipperwash paleohydrograph shows multi-millennium, millennium, centennial and multi-decadal patterns. GIA, outlet conveyance, and climate are the dominate drivers of lake level change in the LGL over historic (International Upper Great Lakes Study Board, 2009; 2012) and prehistoric times (Johnston et al., 2014) and used to interpret drivers of lake level patterns preserved within the Ipperwash paleohydrograph.

The multi-millennium pattern of the Ipperwash paleohydrograph shows a net lake level fall from 3520 to 710 years ago. This relative lake level fall is considered a record of GIA with a rate of 7 cm/century between Ipperwash and the ground surface at the Port Huron/Sarnia outlet, which currently regulates the water level in Lake Michigan-Huron.

Millennium patterns show two vertically offset periods of net lake level fall from 3520 to 2180 and 2020 to 710 years ago. These patterns correspond with the Algoma phase in lakes Superior, Michigan and Huron, the Sault phase in Lake Superior, or the 1700-high phase in Lake Michigan. The rate of lake level lowering from 3520 to 2180 in the Ipperwash paleohydrograph corresponds with the published rate of GIA between the Chicago outlet and Ipperwash. Therefore, the millennium pattern may be related to the dominance of the Chicago outlet from 3520 to 2180, and/or from 3520 to 710 years ago. However, regional climate variability also contributes to the lake level pattern preserved in the Ipperwash strandplain.

Centennial oscillations (lasting an average of 208 years) occur as groups of beach ridges at Ipperwash. Multi-decadal oscillations (lasting an average of 73 years) are represented as a single beach ridge at Ipperwash. Both centennial and multi-decadal oscillations are interpreted as a product of natural climate variability.

Interpretation of multi-millennium pattern within the Ipperwash paleohydrograph estimates the rate of GIA at Ipperwash to be 7 cm/century. However, estimates of GIA based on water gauge data suggest the rate of GIA at Ipperwash is 0 cm/century. This difference suggests an underestimation of GIA at Ipperwash based on water level gauge data due to insufficient nearby water level gauge data, or an outlet subsiding relative to the Ipperwash strandplain being dominate during the deposition of the Ipperwash strandplain. Interpretation of the millennium pattern of the Ipperwash paleohydrograph may suggest the Chicago outlet as the dominate outlet for Lake Michigan-Huron

from 3520 to 2180 years ago. However, variations in the millennium pattern may also be produced by climate variations. Based on interpretation of the Ipperwash paleohydrograph the Chicago outlet is presented as the dominate outlet from 3520 to 2180 years ago and may have remained the active outlet until as recently as 710 years ago. The dominance of the Chicago outlet affected the long-term rate of relative GIA across the entire Ipperwash paleohydrograph causing the rate of GIA to be higher than the hypothesized rate of GIA.

The Ipperwash paleohydrograph provides the natural record of lake level fluctuations at Ipperwash. The Ipperwash paleohydrograph shows a long-term relative lake level lowering driven by GIA. However, future lake level projections show lake levels in Lake Michigan-Huron will continue to fall over the next hundred years due to human caused climate change (Lofgren et al., 2002; 2011; Angel and Kunkel, 2010; Hayhoe et al., 2010; MacKay and Seglenieks, 2013). The long-term lowering driven by GIA will therefore likely be exacerbated by a lake level lowering driven by climate change. However, the Ipperwash paleohydrograph also shows centennial and multi-decadal lake level oscillations which will likely continue to affect lake levels at Ipperwash into the future. Researchers must be aware and account for the natural patterns shown in LGL paleohydrographs to more accurately predict future lake level changes.

Interpretation of the Ipperwash paleohydrograph suggests the Chicago outlet was the active outlet for Lake Michigan-Huron during the deposition of the Ipperwash strandplain, and potentially remained active until as recently as 710 years ago. By providing an alternative scenario for geologically recent outlet conveyance, this thesis provides new insights and theories into the history of outlet conveyance, GIA and climate in Lake Michigan-Huron. This reassessment of the natural history of Lake Michigan-Huron also shows the need to account for natural changes in outlet conveyance, GIA and climate when examining and interpreting instrumental records such as water level gauges. The Ipperwash paleohydrograph also shows coastal erosion and deposition at Ipperwash as a result of multi-decadal lake level rises and falls. This shows that the Ipperwash strandplain will continue to form new beach ridges into the future assuming sediment supply remains positive.

## Chapter 8

### Recommendations

Several recommendations for future studies, based on the results of this thesis, are presented that will further the understanding of the Ipperwash strandplain and the LGL.

- Compare and combine the Ipperwash paleohydrograph to four other unpublished Lake Huron strandplain paleohydrographs to create a single, Port Huron/Sarnia outlet reference paleohydrograph.
- Examine strandplain lake level records near the Chicago outlet and compare to other strandplain paleohydrographs in Lake Michigan-Huron to determine the timing of activation and abandonment of the Chicago outlet.
- Determine ages of the three spits located in the Port Huron/Sarnia outlet (Campbell, 2016), either by directly sampling sediment in each spit or by bracketing ages of each spit using archeology to determine the timing of spit formation and providing direct evidence for potential outlet conveyance due to sedimentation at the Port Huron/Sarnia outlet.
- Extract subsurface and age data from the shorelines located within the Thedford embayment associated with either Lake Nipissing and/or Algonquin (Cooper, 1974) and compare with peak Nipissing elevation data collected at the Port Huron/Sarnia outlet (Thompson et al., 2014).



## References

- Argyilan, E.P., Forman, S.L., Johnston, J.W., and Wilcox, D. A., 2005, Optically stimulated luminescence dating of late Holocene raised strandplain sequences adjacent to Lakes Michigan and Superior, Upper Peninsula, Michigan, USA: *Quaternary Research*, v. 63, p. 122–135, doi: 10.1016/j.yqres.2004.12.001.
- Argyilan, E.P., and Forman, S.L., Lake Level Response to Seasonal Climatic Variability in the Lake Michigan-Huron System from 1920 to 1995: *Journal of Great Lakes Research*, v. 29, p 488-500.
- Au-Sable-Bayfield Conservation Authority, 2000, Shoreline Management Plan: 2nd edition.
- Austin, J.A., and Colman, S.M., 2007, Lake Superior summer water temperatures are increasing more rapidly than regional air temperatures: A positive ice-albedo feedback: *Geophysical Research Letters*, v. 34, p. L06604, doi: 10.1029/2006GL029021.
- Baedke, S.J., and Thompson, T.A., 2000, A 4,700-Year Record of Lake Level and Isostasy for Lake Michigan: *Journal of Great Lakes Research*, v. 26, p. 416–426, doi: 10.1016/S0380-1330(00)70705-2.
- Baedke, S.J., Thompson, T.A., Johnston, J.W., and Wilcox, D.A., 2004, Reconstructing paleo lake levels from relict shorelines along the Upper Great Lakes: *Aquatic Ecosystem Health & Management*, v. 7, p. 435–449, doi: 10.1080/14634980490513274.
- Baird, W.F. and Associates, 2005, Regime Change (Man Made Intervention) and Ongoing Erosion in the St. Clair River and Impacts on Lake Michigan-Huron Lake Levels.
- BaMasoud, A., and Byrne, M.L., 2012, The impact of low ice cover on shoreline recession: A case study from Western Point Pelee, Canada: *Geomorphology*, v. 173-174, p. 141–148, doi: 10.1016/j.geomorph.2012.06.004.
- Blott, S.J. and Pye, K., 2001, GRADISTAT: a grain size distribution and statistics package for the analysis of unconsolidated sediments: *Earth Surface Processes and Landforms* v. 26, p. 1237-1248. <http://www.kpal.co.uk/gradistat.html>
- Bond, G., Showers, W., Cheseby, M., Lotti, R., Almasi, P., DeMenocal, P., Priore, P., Cullen, H., Hajda, I., and Bonani, G., 1997, A Pervasive Millennial-Scale Cycle in North Atlantic Holocene and Glacial Climates: *Science*, v. 278, p. 1257–1266.
- Booth, R.K., Jackson, S.T, and Thompson, T.A., 2002, Paleoecology of a Northern Michigan Lake and the Relationship among Climate, Vegetation, and Great Lakes Water Levels: *Quaternary Research*, v. 57, p. 120-130.

- Breckenridge, A., and Johnson, T.C., 2009, Paleohydrology of the upper Laurentian Great Lakes from the late glacial to early Holocene: *Quaternary Research*, v. 71, p. 397–408, doi:10.1016/j.yqres.2009.01.003.
- Chrzastowski, M.J. and Thompson, T.A., 1992, The late Wisconsinan and Holocene coastal evolution of the southern shore of Lake Michigan *in* *Quaternary Coastal of the United States: Marine and Lacustrine Systems*, Fletcher, C.H. and Wehmiller J.F. (eds), SEPM Special Publication 48, p. 397-413.
- Clark, J.A., Befus, K.M., and Sharman, G.R., 2012, A model of surface water hydrology of the Great Lakes, North America during the past 16,000years: *Physics and Chemistry of the Earth*, v. 53-54, p. 61–71, doi: 10.1016/j.pce.2010.12.005.
- Cohn, B., and Robinson, J.E., 1976, A Forecast Model for Great Lakes Water Levels: *The Journal of Geology*, v. 84, p. 455–465.
- Cooper, A.J., 1974, Quaternary geology of the Grand Bend-Parkhill area, southern Ontario: Ontario Geological Survey Report, v. 188.
- Curry, J.R., 1964, Transgressions and regressions, *in* Miller, R. ed., *Papers in Marine Geology*, New York, Macmillan, p. 175–203.
- Czuba, J. A., Best, J.L., Oberg, K. A., Parsons, D.R., Jackson, P.R., Garcia, M.H., and Ashmore, P., 2011, Bed morphology, flow structure, and sediment transport at the outlet of Lake Huron and in the upper St. Clair River: *Journal of Great Lakes Research*, v. 37, p. 480–493, doi: 10.1016/j.jglr.2011.05.011.
- Davis, J.C., 2002, *Statistics and Data Analysis in Geology* 3<sup>rd</sup> Edition, John Wiley & Sons Inc., New York, NY, p. 76.
- Desai, A.R., Austin, J. A., Bennington, V., and McKinley, G. A., 2009, Stronger winds over a large lake in response to weakening air-to-lake temperature gradient: *Nature Geoscience*, v. 2, p. 855–858, doi: 10.1038/ngeo693.
- Di Stefano, and Ferro, V., 2010, Comparison between grain-size analyses using laser diffraction and sedimentation methods diffraction and sedimentation methods: *Biosystems Engineering*, v. 106, p. 205–215, doi: 10.1016/j.biosystemseng.2010.03.013.
- Drzyzga, S. A., Shortridge, A.M., and Schaetzl, R.J., 2012, Mapping the phases of Glacial Lake Algonquin in the upper Great Lakes region, Canada and USA, using a geostatistical isostatic rebound model: *Journal of Paleolimnology*, v. 47, p. 357–371, doi: 10.1007/s10933-011-9550-9.

- Eyles, N., and Meulendyk, T., 2012, Ground-penetrating radar stratigraphy and depositional model for evolving Late Holocene aeolian dunes on the Lake Huron coast, Ontario: *Journal of Great Lakes Research*, v. 38, p. 708–719, doi: 10.1016/j.jglr.2012.09.003.
- Farrand, W.H., 1962, Postglacial uplift of North America: *American Journal of Science*, v. 200, p. 181-199.
- Fisher, T.G., and Whitman, R.L., 1999, Deglacial and Lake Level Fluctuation History Recorded in Cores, Beaver Lake, Upper Peninsula, Michigan: *Journal of Great Lakes Research*, v. 25, p. 263–274, doi: 10.1016/S0380-1330(99)70735-5.
- Folk, R.L. and Ward, W.C., 1957, Brazos River bar: a study in the significance of grain size parameters: *Journal of Sedimentary Petrology*, v. 27, p. 3-26.
- Fox, W.T., Ladd, J.W., and Martin, M.K., 1966, A profile of the four moments measures perpendicular to a shore line, South Haven, Michigan: *Journal of Sedimentary Petrology*, v. 36, i. 4, p. 1126–1130.
- Fraser, G. S., Larsen, C. E., and Hester, N. C., 1975, Climatically controlled high lake levels in Lake Michigan and Lake Huron basins: *Anais de Academia Brasileira de Ciencias*, Supplement 47, p. 51–66.
- Fraser, G. S., Larsen, C. E. & Hester, N. C., 1990, Climatic control of lake levels in the Lake Michigan and Lake Huron basins *in* Schneider, G. & Fraser, G. S. (eds) *Late Quaternary History of the Lake Michigan Basin: Geological Society of America Special Papers*, v. 251, p. 75–90.
- Fraser, G.S., Thompson, T.A., Kvale, E.P., Carlson, C.P., Fishbaugh, D.A., Gruver, B.L., Holbrook, J., Kairo, S., Kohler, C.S., Malone, A.E., Moore, C.H., Rachmanto, B., and Rhoades, L., 1991, Sediment and Sedimentary Structures of a Barred, Nontidal Coastline, Southern Shore of Lake Michigan: *Journal of Coastal Research*, v. 7, p. 1113–1124.
- Gao, C., 2011, Buried bedrock valleys and glacial and subglacial meltwater erosion in southern Ontario, Canada: *Canadian Journal of Earth Sciences*, v. 48, p. 801–818, doi: 10.1139/e10-104.
- Gilbert, G.K., 1898, Recent Earth Movements in the Great Lakes Region: *United States Geological Survey 18th Annual Report, Part 2*, p. 601–647.
- Goldthwait, J.W., 1908, A reconstruction of the water planes of the extinct glacial lakes in the Lake Michigan basin: *Journal of Geology*, v. 16, p. 459–476.

- Gronewold, A.D., Fortin, V., Lofgren, B., Clites, A., Stow, C.A., and Quinn, F., 2013b, Coasts, water levels, and climate change: A Great Lakes perspective: *Climatic Change*, v. 120, p. 697–711, doi: 10.1007/s10584-013-0840-2.
- Gronewold, A.D., Clites, A.H., Smith, J.P., Hunter, T.S., 2013a, A dynamic graphical interface for visualizing projected, measured, and reconstructed surface water elevations on the earth's largest lakes, *Environmental Modelling & Software*, v. 49, p. 34–39, <http://dx.doi.org/10.1016/j.envsoft.2013.07.003>
- Gronewold, A.D., and Stow, C.A., 2014, Water Loss from the Great Lakes: *Science*, v. 343, p. 1084–1085, doi: 10.1126/science.1249978.
- Gronewold, A.D., Clites, A.H., and Rear-McLaughlin, L., 2015, Great Lakes Water Levels: Monitoring Change in Earth's Largest Surface Freshwater System: *Clear Waters*, p. 16–18.
- Gronewold, A.D., Bruxer, J., Durnford, D., Smith, J.P., Clites, A.H., Seglenieks, F., Qian, S.S., Hunter, T.S., and Fortin, V., 2016, Hydrological driver of record-setting water level rise on Earth's largest lake system: *Water Resources Research*, v. 52, p. 1–20, doi: 10.1002/2014WR015716.
- Hanrahan, J.L., Kravtsov, S. V., and Roebber, P.J., 2010, Connecting past and present climate variability to the water levels of Lakes Michigan and Huron: *Geophysical Research Letters*, v. 37, p. n/a–n/a, doi: 10.1029/2009GL041707.
- Hanrahan, J.L., Kravtsov, S. V., and Roebber, P.J., 2009, Quasi-periodic decadal cycles in levels of lakes Michigan and Huron: *Journal of Great Lakes Research*, v. 35, p. 30–35, doi: 10.1016/j.jglr.2008.11.004.
- Hayhoe, K., VanDorn, J., Croley, T., Schlegel, N., and Wuebbles, D., 2010, Regional climate change projections for Chicago and the US Great Lakes: *Journal of Great Lakes Research*, v. 36, p. 7–21, doi: 10.1016/j.jglr.2010.03.012.
- Hesp, P.A., Dillenburg, S.R., Barboza, E.G., Tomazelli, L.J., Ayup-Zouain, R.N., Esteves, L.S., Gruber, N.L.S., Toldo, E.E., Tabajara, L.L.C.D. a, and Clerot, L.C.P., 2005, Beach ridges, foredunes or transgressive dunefields? Definitions and an examination of the Torres to Tramanda barrier system, Southern Brazil: *Anais da Academia Brasileira de Ciencias*, v. 77, p. 493–508, doi: 10.1590/S0001-37652005000300010.
- Hough, J.L., 1958, *Geology of the Great Lakes*: Urbana, IL, University of Illinois Press.
- Hough, J.L., 1962, Lake Stanley, a low stage of Lake Huron indicated by bottom sediments: *Geological Society of America Bulletin*, v. 73, p. 613–620.

- Hough, J.L., 1966, Correlation of Glacial Lake Stage in the Huron-Erie and Michigan Basins: The Journal of Geology, v. 74, p. 62–77.
- Howard, J.D., and Reineck, H.E., 1981, Depositional facies of high-energy beach-to-offshore sequence, Comparison with low-energy sequence: American Association of Petroleum Geologists Bulletin, v. 65, p. 807–830.
- Howard, J.L., 2015, Glaciolacustrine history of the Huron-Erie lowland in the southeastern Great Lakes region (USA) revisited: Journal of Great Lakes Research, v. 41, p. 965–972, doi: 10.1016/j.jglr.2015.07.012.
- International Upper Great Lakes Study Board, 2009, Impacts on Upper Great Lakes Water Levels: St. Clair River.
- International Upper Great Lakes Study Board, 2012, Lake Superior Regulation: Addressing Uncertainty in Upper Great Lakes Water Levels.
- Jalava, J.V., M. Kanter and S. Hodgkiss. 2015, Be Part of the Big Picture: Big Picture Report Card Discussion Paper: Carolinian Canada Coalition.
- Johnston, J.W., 1999, Sedimentology and Depositional History of the Wasaga Beach and Ipperwash Areas: University of Waterloo.
- Johnston, J.W., Thompson, T.A., and Baedke, S.J., 2007, Systematic pattern of beach-ridge development and preservation: Conceptual model and evidence from ground penetrating radar: The Geological Society of America Special Paper 432, p. 47–58, doi: 10.1130/2007.2432(04).
- Johnston, J.W., Argyle, E.P., Thompson, T. A., Baedke, S.J., Lepper, K., Wilcox, D.A., Forman, S.L., and Fisher, T.G., 2012, A Sault-outlet-referenced mid- to late-Holocene paleohydrograph for Lake Superior constructed from strandplains of beach ridges: Canadian Journal of Earth Sciences, v. 49, p. 1263–1279, doi: 10.1139/e2012-057.
- Johnston, J.W., Thompson, T.A., and Wilcox, D.A., 2014, Palaeohydrographic reconstructions from strandplains of beach ridges in the Laurentian Great Lakes: Geological Society, London, Special Publications, v. 388, p. 213–228, doi: 10.1144/SP388.22.
- Jol, H.M., and Bristow, C.S., 2003, GPR in sediments: advice on data collection, basic processing and interpretation, a good practice guide: Geological Society, London, Special Publications, v. 211, p. 9–27, doi: 10.1144/GSL.SP.2001.211.01.02.
- Karrow, P.F., and Calkin, P. (Eds.), 1985, Quaternary Evolution of the Great Lakes: St. Johns, Newfoundland, Geological Association of Canada, Special paper 30.

- Karrow, P.F., 1980, The Nipissing transgression around southern Lake Huron: *Canadian Journal of Earth Sciences*, v. 17.
- Karrow, P.F., and Lewis, C.F.M., 2007, Introduction to “The Greater and Lesser Great Lakes”: *Journal of Paleolimnology*, v. 37, p. 309–311, doi: 10.1007/s10933-006-9043-4.
- Kincare, K., and Larson, G.J., 2009, Evolution of the Great Lakes, *in* Schaetzl, R., Darden, J., and Brandt, D. eds., *Michigan Geography and Geology*, New York, Pearson, p. 174–190.
- Komar, P.D., 1998, *Beach Processes and Sedimentation*: New Jersey: Prentice-Hall, Inc.
- Larsen, C.E., 1985, A Stratigraphic Study of the Beach Features on the Southwestern Shore of Lake Michigan: New Evidence of Holocene Lake Level Fluctuations: *Environmental Geology Notes* 112, p. 31.
- Larson, G., and Schaetzl, R., 2001, Origin and Evolution of the Great Lakes: *Journal of Great Lakes Research*, v. 27, p. 518–546, doi: 10.1016/S0380-1330(01)70665-X.
- Lepper, K., Gorz, K., Fisher, T. and Lowell, T., 2011, Age Determinations for Lake Agassiz Shorelines West of Fargo, North Dakota, U.S.A.: *Canadian Journal of Earth Sciences*, v. 48: p. 1199-1207.
- Lepper, K., 2017, OSL dating results for sediment samples collected from the Ipperwash Strandplain of Lake Huron: Optical Dating and Dosimetry Lab North Dakota State University.
- Leverett, G., and Taylor, F.B., 1915, *The Pleistocene of Indiana Michigan and its history of the Great Lakes*: US Geological Survey Monographs, v. 53.
- Lewis, C.F.M., 1970, Recent uplift of Manitoulin Island, Ontario: *Canadian Journal of Earth Sciences*, v. 7, p. 665–675.
- Lewis, C.F.M., and Anderson, T.W., 1989, Oscillation of levels and cool phases of the Laurentian Great Lakes caused by inflows from glacial Lakes Agassiz and Barlow-Ojibway: *Journal of Paleolimnology*, v. 2, p. 99–146.
- Lewis, C.F.M., Blasco, S.M., and Gareau, P.L., 2005, Glacial Isostatic Adjustment of the Laurentian Great Lakes Basin: Using the Empirical Record of Strandline Deformation for Reconstruction of Early Holocene Paleo-Lakes and Discovery of a Hydrologically Closed Phase: *Géographie physique et Quaternaire*, v. 59, p. 187–210, doi: 10.7202/014754ar.
- Lewis, C.F.M., and Anderson, T.W., 2012, The sedimentary and palynological records of Serpent River Bog, and revised early Holocene lake-level changes in the Lake Huron and Georgian Bay region: *Journal of Paleolimnology*, v. 47, p. 391–410, doi: 10.1007/s10933-012-9595-4.

- Lewis, C.F.M., Blasco, S.M., King, J. W., Brooks, G.R., Coakley, J.P., Croley, T.E.I., Dettman, D.L., Edwards, T.W.D., Heil, C.W.J., Hubeny, J.B., Laird, K.R., McAndrews, J.H., McCarthy, F.M.G., Medioli, B.E., et al., 2008a, Dry Climate Disconnected the Laurentian Great Lakes: Eos, Transactions American Geophysical Union, v. 89, p. 541–542, doi: 10.1029/2008EO520001.
- Lewis, C.F.M., Karrow, P.F., Blasco, S.M., McCarthy, F.M.G., King, J.W., Moore, T.C., and Rea, D.K., 2008b, Evolution of lakes in the Huron basin: Deglaciation to present: Aquatic Ecosystem Health & Management, v. 11, p. 127–136, doi: 10.1080/14634980802095263.
- Lewis, C.F.M., and King, J.W., 2012, Introduction to “Holocene water levels and paleo-hydrology of the Laurentian Great Lakes”: Journal of Paleolimnology, v. 47, p. 293–297, doi: 10.1007/s10933-012-9597-2.
- Lofgren, B.M., Quinn, F.H., Clites, A.H., Assel, R. A., Eberhardt, A.J., and Luukkonen, C.L., 2002, Evaluation of Potential Impacts on Great Lakes Water Resources Based on Climate Scenarios of Two GCMs: Journal of Great Lakes Research, v. 28, p. 537–554, doi: 10.1016/S0380-1330(02)70604-7.
- Lofgren, B.M., Hunter, T.S., and Wilbarger, J., 2011, Effects of using air temperature as a proxy for potential evapotranspiration in climate change scenarios of Great Lakes basin hydrology: Journal of Great Lakes Research, v. 37, p. 744–752.
- MacKay, M., and Seglenieks, F., 2013, On the simulation of Laurentian Great Lakes water levels under projections of global climate change: Climatic Change, v. 117, p. 55–67, doi: 10.1007/s10584-012-0560-z.
- Magnuson, J.J., Robertson, D.M., Benson, B.J., Wynne, R.H., Livingstone, D.M., Arai, T., Assel, R., Barry, R.G., Card, V., and Kuusisto, E., 2000, Historical Trends in Lake and River Ice Cover in the Northern Hemisphere: Science, v. 289, p. 1743–1746, doi: 10.1126/science.289.5485.1743.
- Mainville, A., and Craymer, M.R., 2005, Present-day tilting of the Great Lakes region based on water level gauges: Geological Society of America Bulletin, v. 117, p. 1070, doi: 10.1130/B25392.1.
- Martin Associates, 2011, The Economic Impacts of the Great Lakes-St. Lawrence Seaway System.
- McCarthy, F., and McAndrews, J., 2012, Early Holocene drought in the Laurentian Great Lakes basin caused hydrologic closure of Georgian Bay: Journal of Paleolimnology, v. 47, p. 411–428, doi: 10.1007/s10933-010-9410-z.
- McCubbin, D.G., 1981, Barrier-Island and Strand-Plain Facies, *in* Scholle, P.A. and Spearing, D. eds., Sandstone Depositional Environments, AAPG Memoir 31, p. 247–280.

- Meadows, G.A., Meadows, L.A., Wood, W.L., Hubertz, J.M., and Perlin, M., 1997, The Relationship between Great Lakes Water Levels, Wave Energies, and Shoreline Damage: *Bulletin of the American Meteorological Society*, v. 78, p. 675–683.
- Mishra, V., Cherkauer, K. A., and Bowling, L.C., 2011, Changing thermal dynamics of lakes in the Great Lakes region: Role of ice cover feedbacks: *Global and Planetary Change*, v. 75, p. 155–172, doi: 10.1016/j.gloplachA.2010.11.003.
- Mitchum, R.M., Jr., Vail, P.R., and Sangree, J.B., 1977, Part six: stratigraphic interpretation of seismic reflection patterns in depositional sequences *in* Payton, C.E. (ed.), *Seismic stratigraphy – Applications to hydrocarbon exploration*. American Association of Petroleum Geologists, Tulsa, OK, *Memoirs*, v. 26, p. 117-133.
- Murray-Wallace, C. V., Banerjee, D., Bourman, R.P., Olley, J.M., and Brooke, B.P., 2002, Optically stimulated luminescence dating of Holocene relict foredunes, Guichen Bay, South Australia: *Quaternary Science Reviews*, v. 21, p. 1077–1086, doi: 10.1016/S0277-3791(01)00060-9.
- Otvos, E.G., 2000, Beach ridges - definitions and significance: *Geomorphology*, v. 32, p. 83–108, doi: 10.1016/S0169-555X(99)00075-6.
- Peltier, W.R., Argus, D.F. and Drummond, R., 2015, Space geodesy constrains ice-age terminal deglaciation: The global ICE-6G\_C (VM5a) model. *Journal of Geophysical Research Solid Earth*, v. 120, p. 450-487, doi:10.1002/2014JB011176..
- Pendleton, E.A., Thieler, E.R., Williams, S.J., Beach, W.P., Pendleton, E.A., Thieler, E.R., and Williams, S.J., 2010, Importance of Coastal Change Variables in Determining Vulnerability to Sea- and Lake-Level Change: *Journal of Coastal Research*, v. 26, p. 176–183, doi: 10.2112/08-1102.1.
- Polderman, N.J., and Pryor, S.C., 2004, Linking Synoptic-scale Climate Phenomena to Lake-Level Variability in the Lake Michigan-Huron Basin: *Journal of Great Lakes Research*, v. 30, p. 419–434, doi: 10.1016/S0380-1330(04)70359-7.
- Porter, D., 2015, Great Lakes-St. Lawrence Region, North American's Economic Engine: BMO Capital Markets Economic Research.
- Provincial Mapping Unit, 2016, Southwestern Ontario Orthophotography Project (SWOOP) 2015 Digital Elevation Model User Guide: Ministry of Natural Resources and Forestry.



- Quinn, F.H., and Sellinger, C.E., 2006, A reconstruction of Lake Michigan-Huron water levels derived from tree ring chronologies for the period 1600-1961: *Journal of Great Lakes Research*, v. 32, p. 29–39, doi: 10.3394/0380-1330(2006)32[29:AROLMW]2.0.CO;2.
- Rawling, J.E., III and Hanson, P.R., 2014, Dune formation on late Holocene sandy bay barriers along Lake Michigan's Door Peninsula: The importance of increased sediment supply following the Nipissing and Algoma high lake-level phases: *Papers in the Earth and Atmospheric Sciences*, P. 417.
- Reinders, F.J. and Associates, 1989, *Lake Huron Shoreline Processes Study*: Markham, ON, Reinders and Associates, 269 p.
- Saylor, J., Miller, G., and Marie, S., 1991, Current flow through the Straits of Mackinac: Great Lakes Environmental Research Laboratory.
- Saylor, J.H., and Sloss, P.W., 1976, Water Volume Transport and Oscillatory Current Flow through the Straits of Mackinac: *Journal of Physical Oceanography*, v. 6, p. 229–237, doi: 10.1175/1520-0485(1976)006<0229:WVTAOC>2.0.CO;2.
- Sellinger, C.E., and Quinn, F.H., 1999, Proceedings of the Great Lakes Paleo-Levels Workshop: The Last 4000 years: NOAA Technical Memorandum ERL GLERL-113, p. 1–43.
- Shuman, B.N., and Marsicek, J., 2016, The structure of Holocene climate change in mid-latitude North America: *Quaternary Science Reviews*, v. 141, p. 38–51, doi: 10.1016/j.quascirev.2016.03.009.
- Smith, D.G., and Jol, H.M., 1995, Ground penetrating radar: antenna frequencies and maximum probable depths of penetration in Quaternary sediments: *Journal of Applied Geophysics*, v. 33, p. 93-100.
- Sperazza, M., Moore, J.N., and Hendrix, M.S., 2004, High-resolution particle size analysis of naturally occurring very fine-grained sediment through laser diffractometry: *Journal of Sedimentary Research*, p. 736–743.
- Tamura, T., 2012, Beach ridges and prograded beach deposits as palaeoenvironment records: *Earth-Science Reviews*, v. 114, p. 279–297, doi: 10.1016/j.earscirev.2012.06.004.
- Taylor, M., and Stone, G.W., 1996, Beach-Ridges: A Review: *Journal of Coastal Research*, v. 12, p. 612–621.
- Teller, J.T., 1987, Proglacial lake and the southern margin of the Laurentide ice sheet, *in* Ruddiman, W.F. and Wright, H.E. eds., *North America and Adjacent Oceans during the Last Deglaciation*, Boulder, CO, Geological Society of America, p. 39–69.






- Thompson, T.A., Miller, C.S., Doss, P.K., Thompson, L.D.P., and Baedke, S.J. 1991. Land-based vibracoring and vibracore analysis: tips, tricks, and traps. Indiana Geological Survey Occasional Paper 58.
- Thompson, T.A., 1992, Beach-ridge development and lake-level variation in southern Lake Michigan: *Sedimentary Geology*, v. 80, p. 305–318, doi: 10.1016/0037-0738(92)90048-V.
- Thompson, T.A., and Baedke, S.J., 1995, Beach-ridge development in Lake Michigan: shoreline behavior in response to quasi-periodic lake-level events: *Marine Geology*, v. 129, p. 163–174, doi: 10.1016/0025-3227(95)00110-7.
- Thompson, T.A. and Baedke, S.J. 1997. Strand-plain evidence for late Holocene lake-level variations in Lake Michigan. *Geological Society of America Bulletin*, v. 109, i. 6, p. 666–682.
- Thompson, T.A., Johnston, J.W., and Lepper, K., 2014, The contemporary elevation of the peak Nipissing phase at outlets of the upper Great Lakes, *in* Fisher, T.G. and Hansen, E.C. eds., *Coastline and Dune Evolution along the Great Lakes: Geological Society of America Special Paper 508*, p. 15–29.
- Thompson, T. A., Lepper, K., Endres, A.L., Johnston, J.W., Baedke, S.J., Argyilan, E.P., Booth, R.K., and Wilcox, D.A., 2011, Mid Holocene lake level and shoreline behavior during the Nipissing phase of the upper Great Lakes at Alpena, Michigan, USA: *Journal of Great Lakes Research*, doi: 10.1016/j.jglr.2011.05.012.
- Van Heteren, S., Fitzgerald, D.M., Ckinlay, P.A.M., and Buynevich, V., 1998, Radar facies of paraglacial barrier systems: coastal New England, USA: *Sedimentology*, v. 45, p. 181–200.
- Viau, A.E., Gajewski, K., Fines, P., Atkinson, D.E., and Sawada, M.C., 2002, Widespread evidence of 1500 yr climate variability in North America during the past 14 000 yr: *Geology*, v. 30, p. 455, doi: 10.1130/0091-7613(2002)030<0455:WEOYCV>2.0.CO;2.
- Viau, A.E., Ladd, M., and Gajewski, K., 2012, The climate of North America during the past 2000 years reconstructed from pollen data: *Global and Planetary Change*, v. 84–85, p. 75–83, doi: 10.1016/j.gloplacha.2011.09.010.
- Watras, C.J., Read, J.S., Holman, K.D., Liu, Z., Song, Y.Y., Watras, A.J., Morgan, S., and Stanlet, E.H., 2014, Decadal oscillation of lakes and aquifers in the upper Great Lakes region of North America: Hydroclimatic implications: *Geophysical Research Letters*, v. 41, p. 1–7, doi: 10.1002/2013GL058507. Received.
- Wilcox, D., Thompson, T., Booth, R.K., and Nicholas, J.R., 2007, Lake-Level Variability and Water Availability in the Great Lakes: U.S. Geological Survey Circular, v. 1311, p. 25.

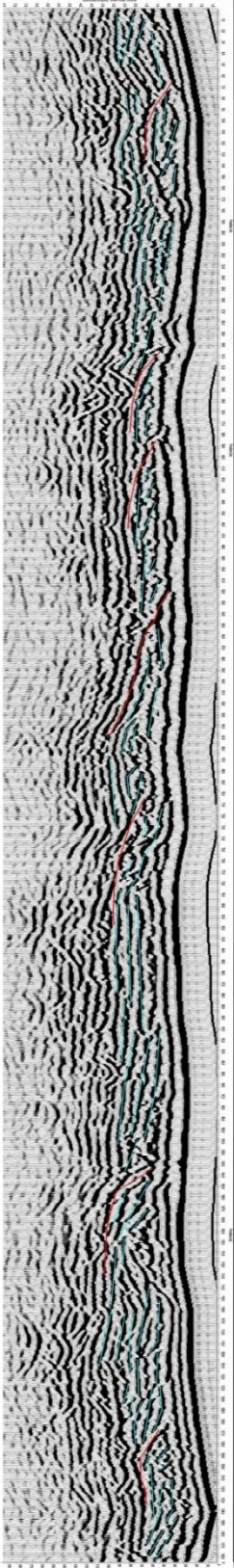
# Appendix A Ground Penetrating Radar Profiles

## GPR profiles location

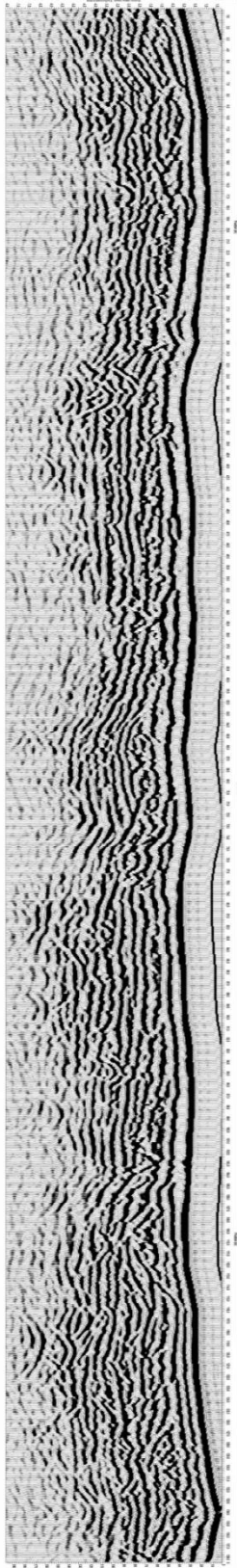


## Radar facie description and interpretation

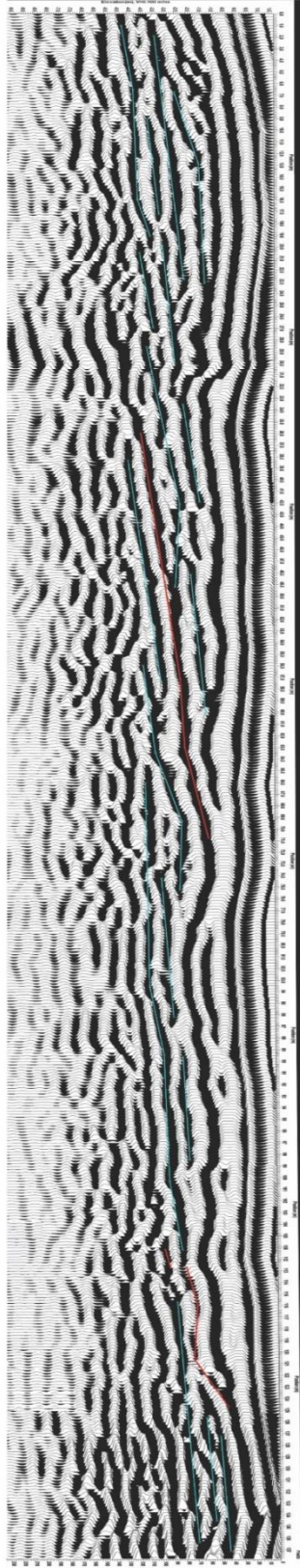
	Depth	Description	Interpretation
	2-0 m	Undulating to landward dipping semi-continuous reflections	Dune
	2-0 m	Lakeward dipping to landward dipping to horizontal continuous reflections	Disturbed Area
	0 m	Horizontal continuous reflection	Water Table
	0-9 m	Sigmoidal reflections which truncate other reflections	Ravinment surface
	5-9 m	Horizontal to lakeward dipping continuous reflections	Foreshore and shoreface



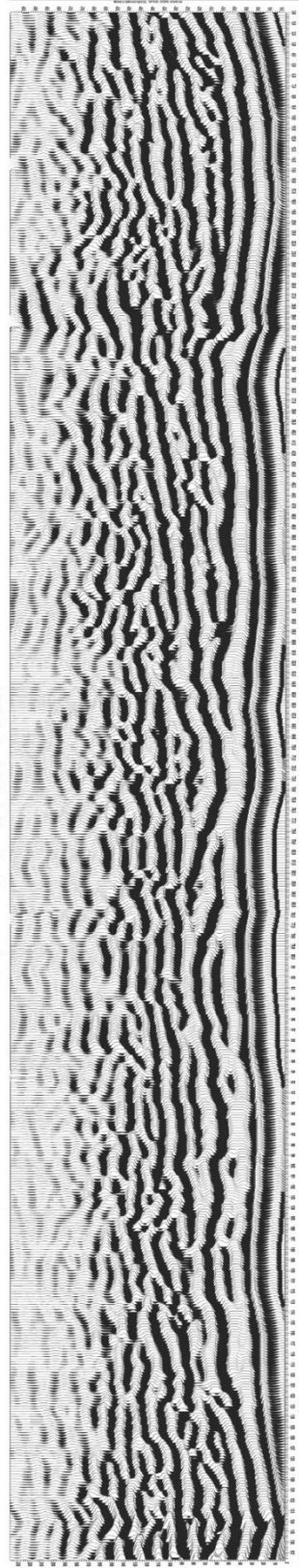
ATV-B 200 Mhz Lakeward →



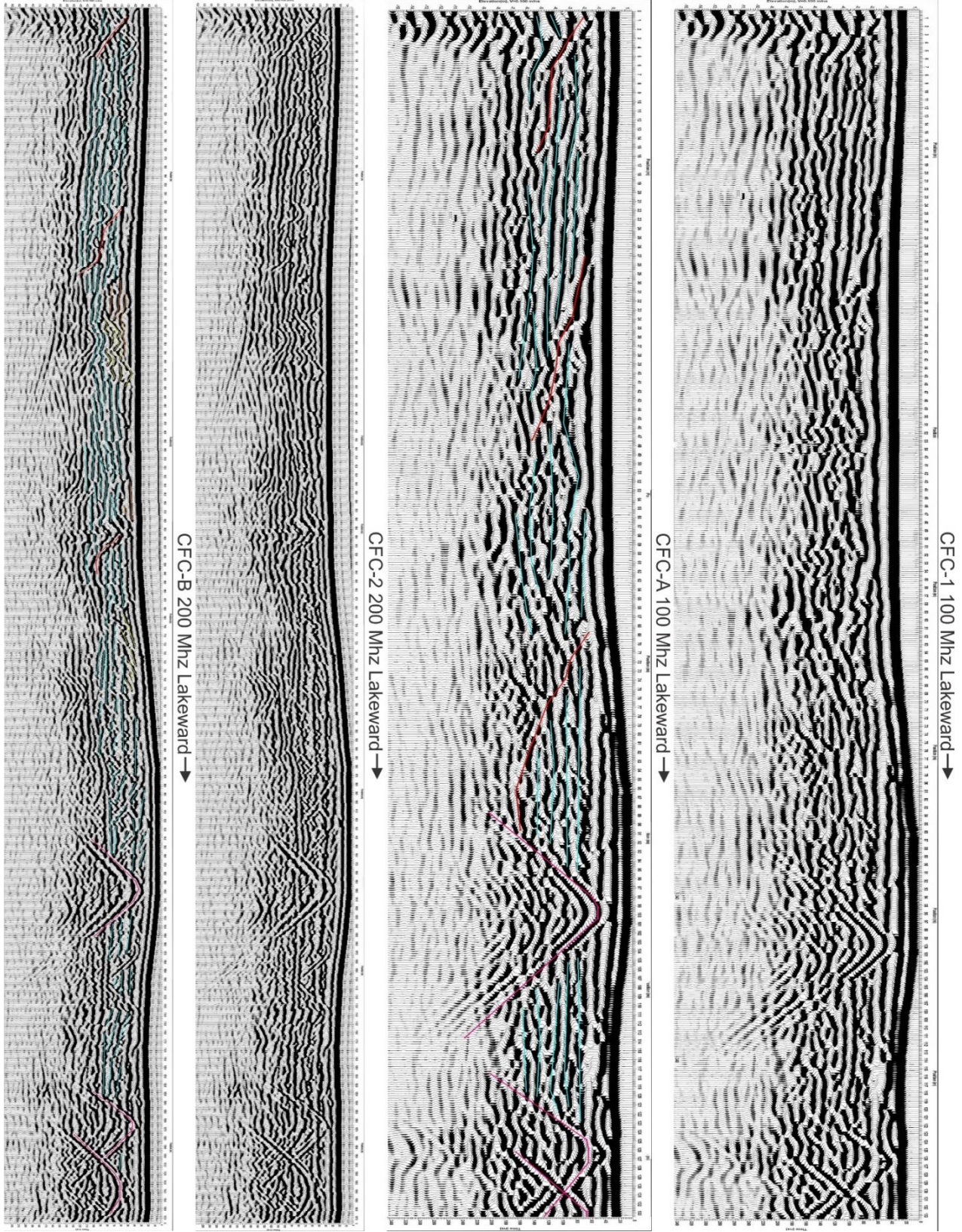
ATV-2 200 Mhz Lakeward →

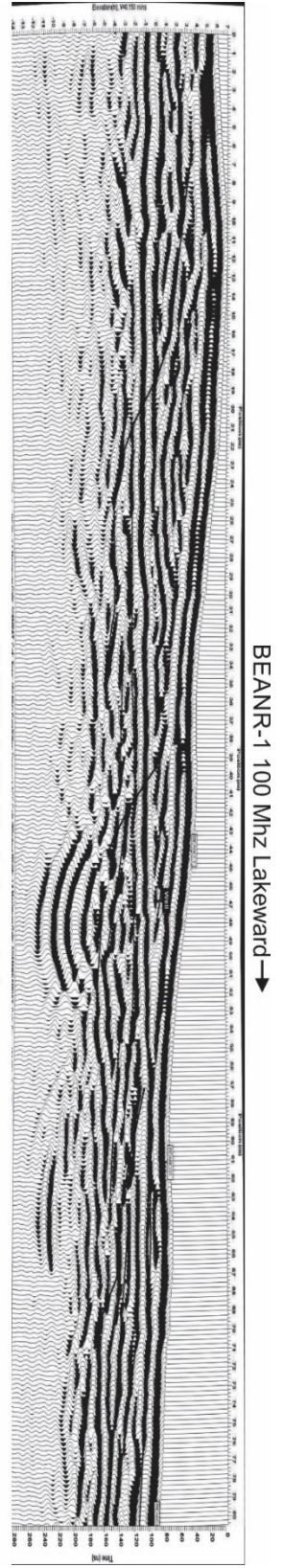


ATV-A 100 Mhz Lakeward →

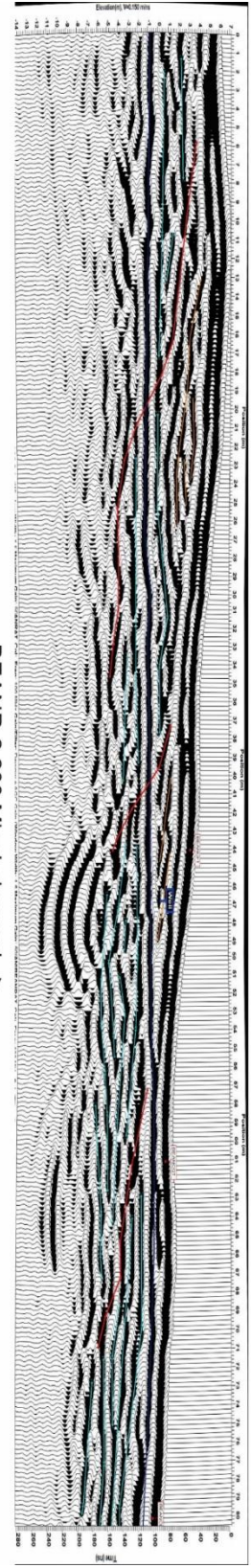


ATV-1 100 Mhz Lakeward →

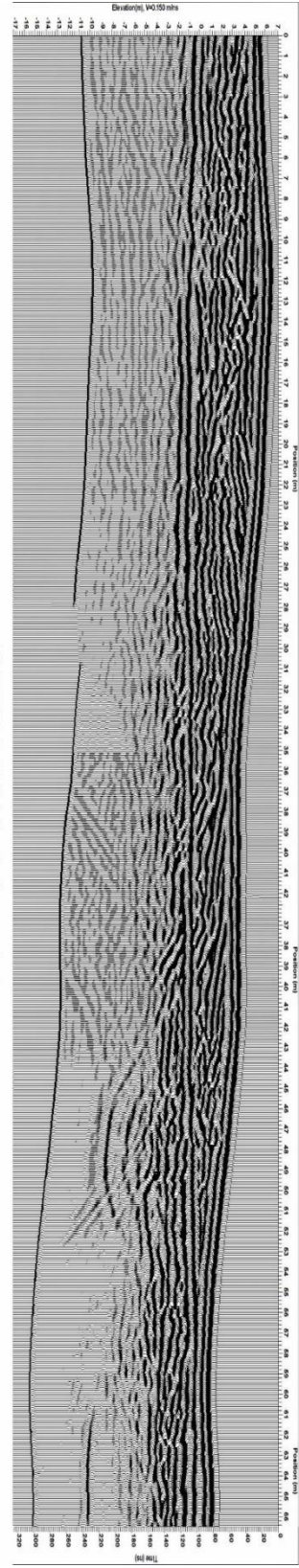




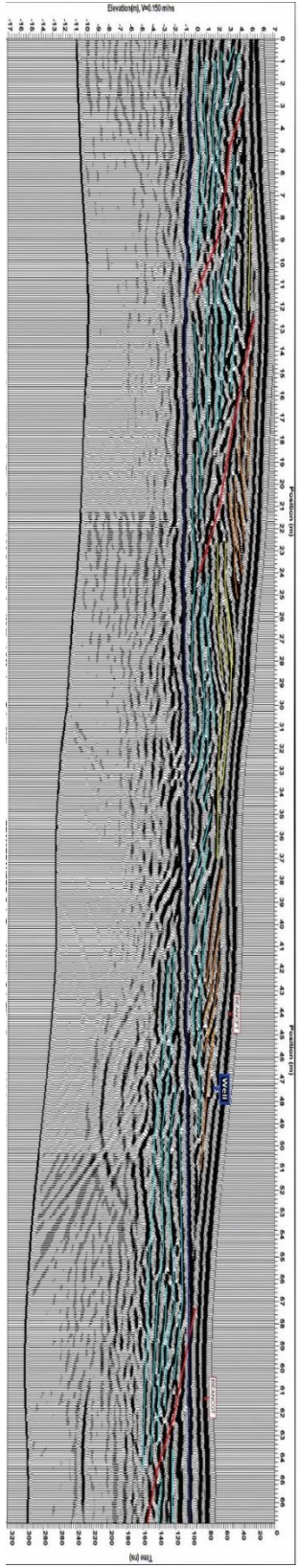
BEANR-1 100 Mhz Lakeward →



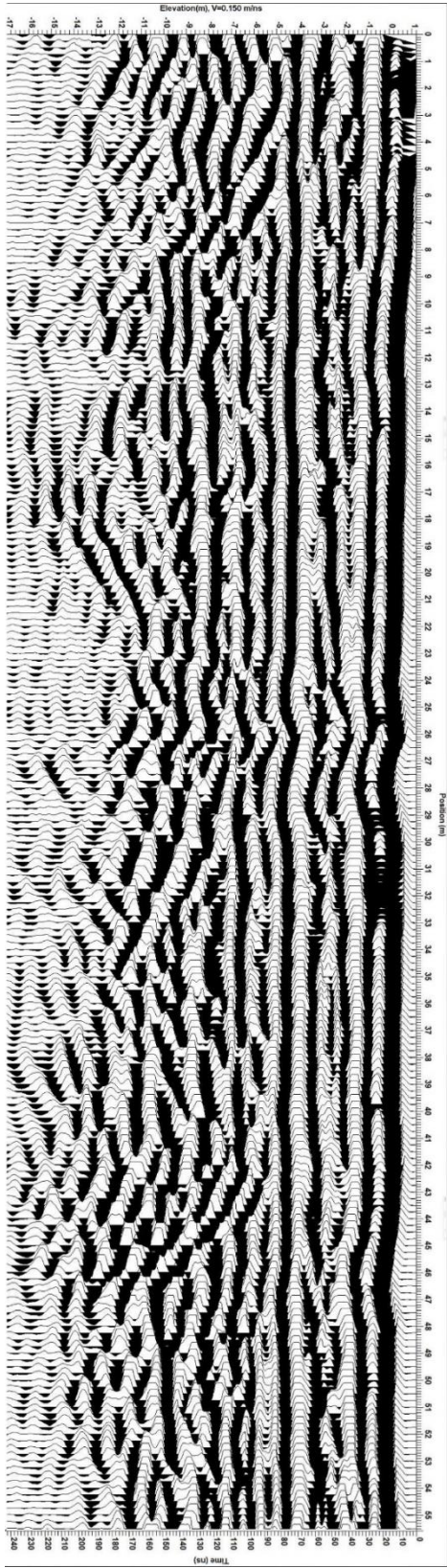
BEANR-2 200 Mhz Lakeward →



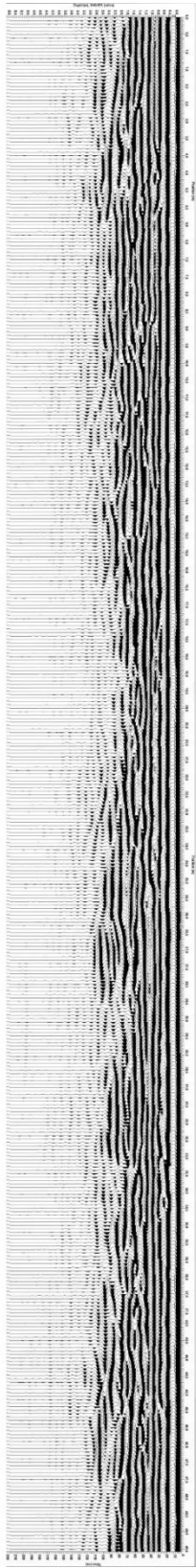
BEANR-B 200 Mhz Lakeward →



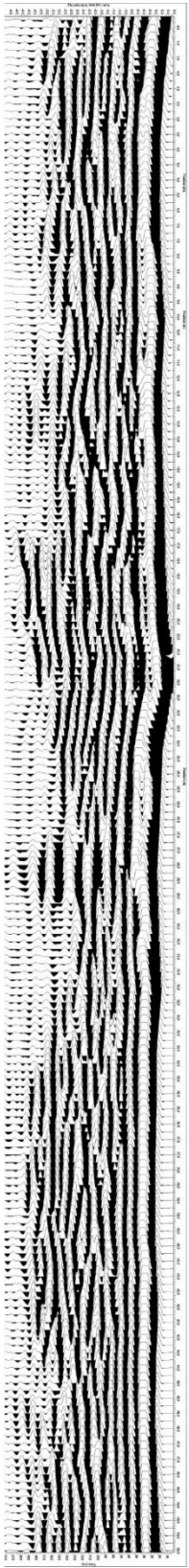
BEANR-A 100 Mhz Lakeward →



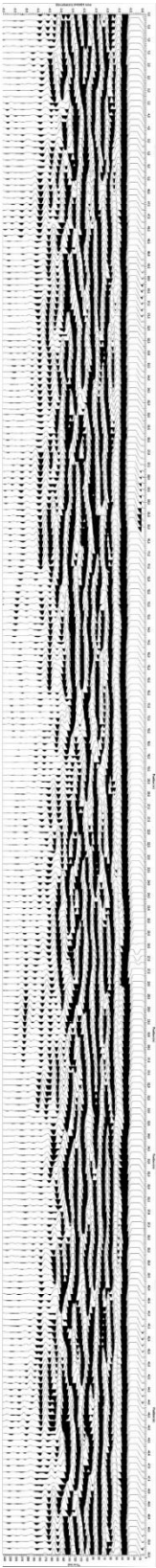
BEANC-2 100 Mhz



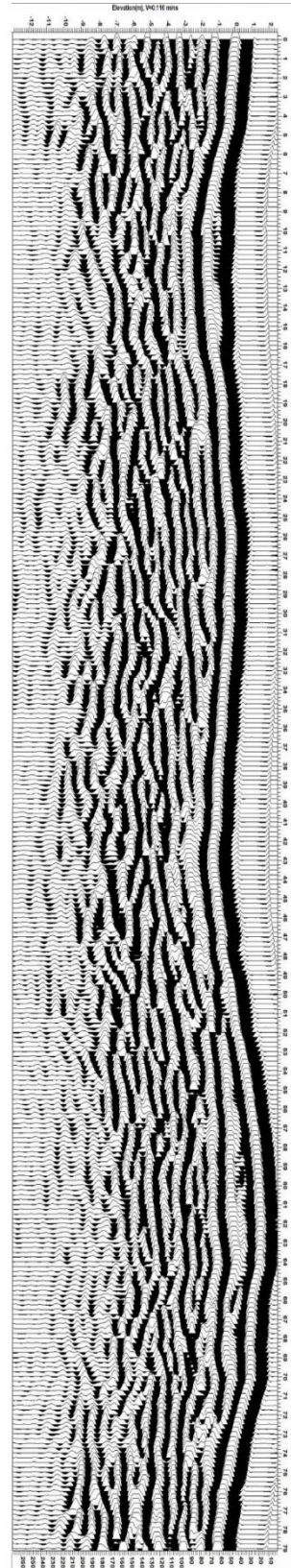
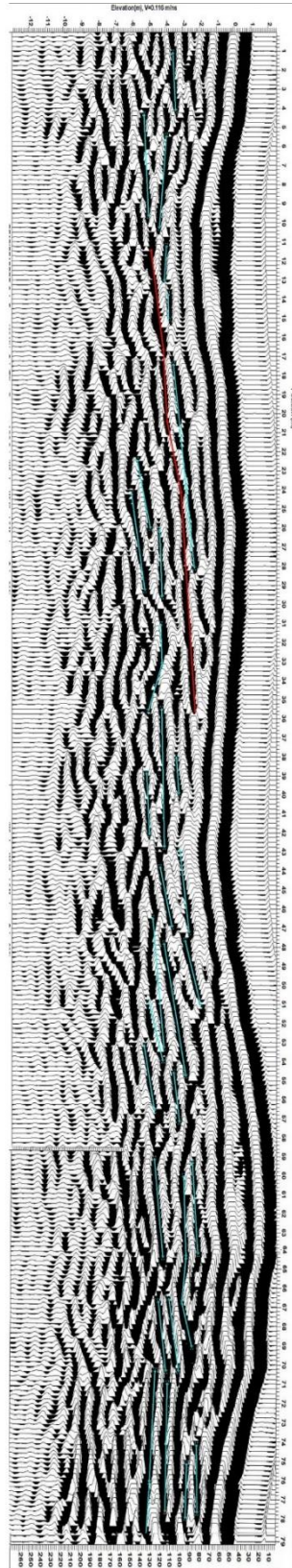
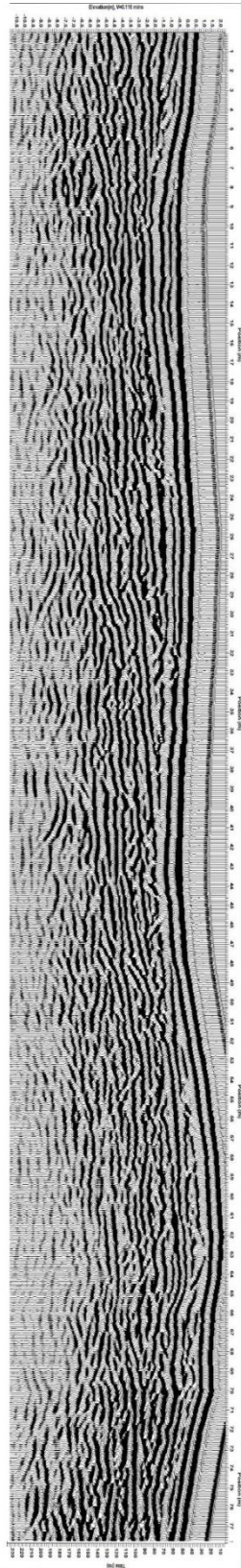
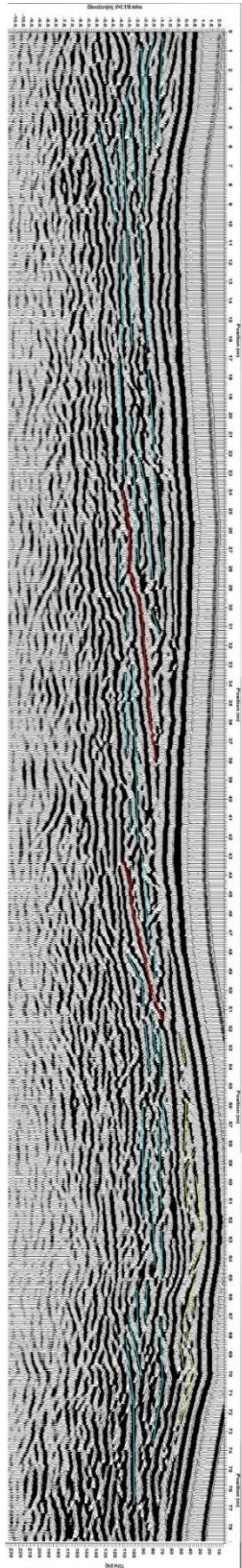
BEANC-2 200 Mhz



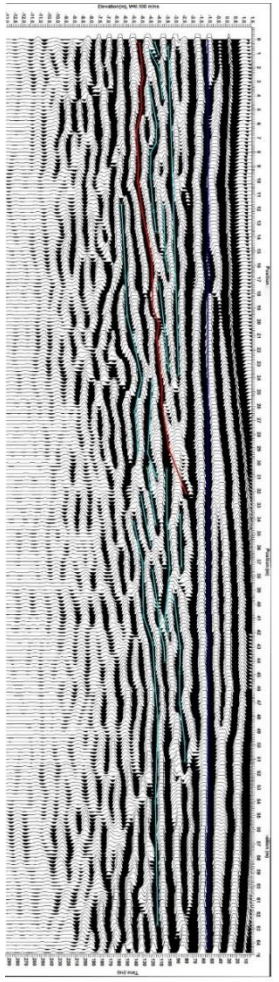
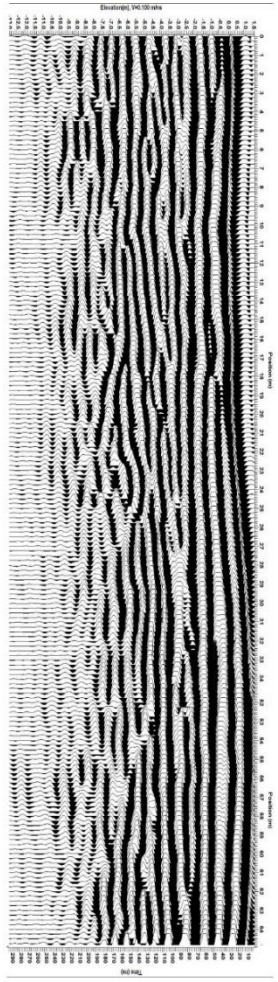
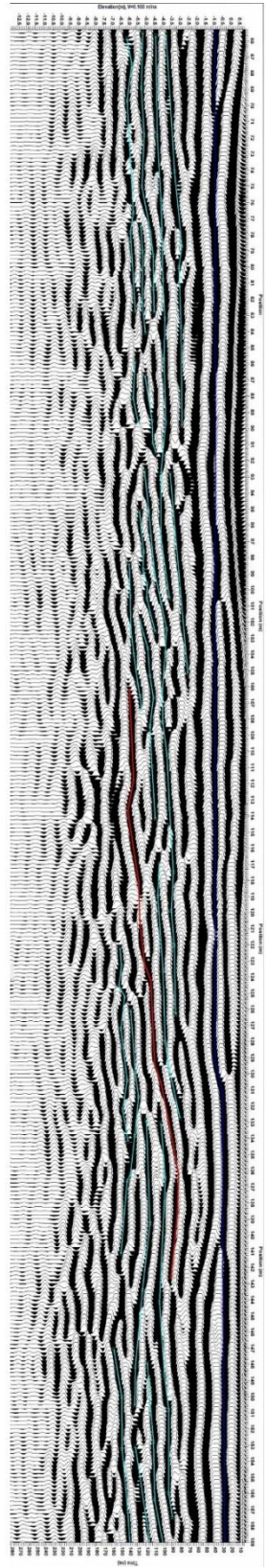
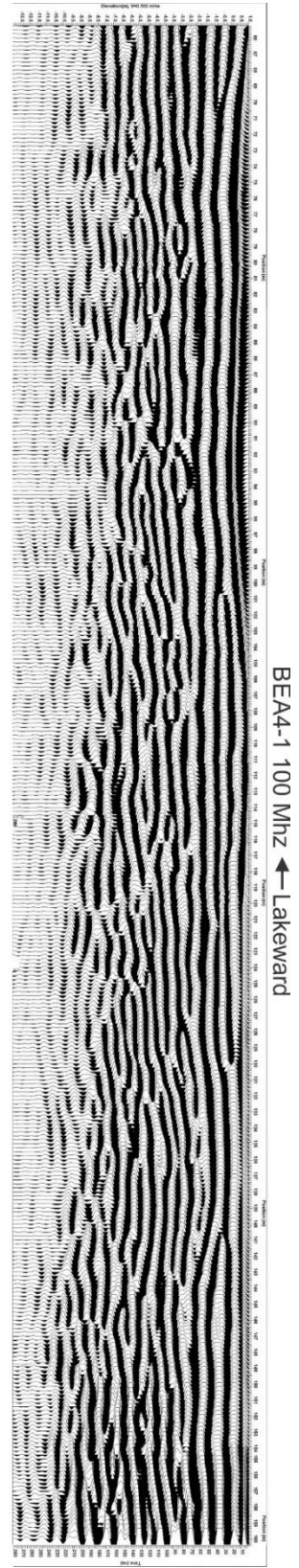
BEANC-7 200 Mhz

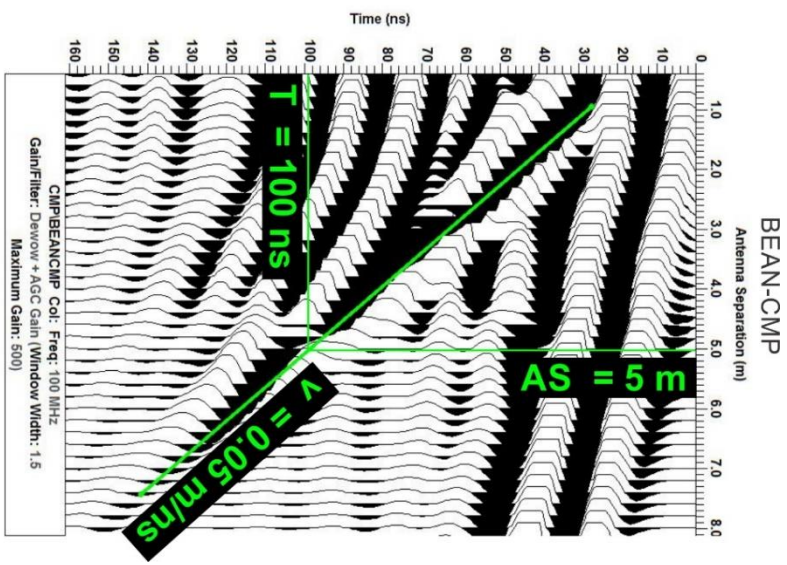
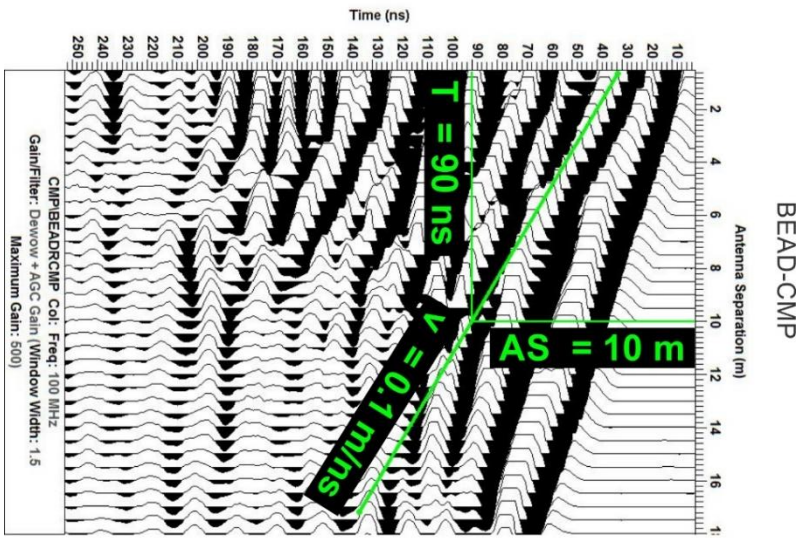
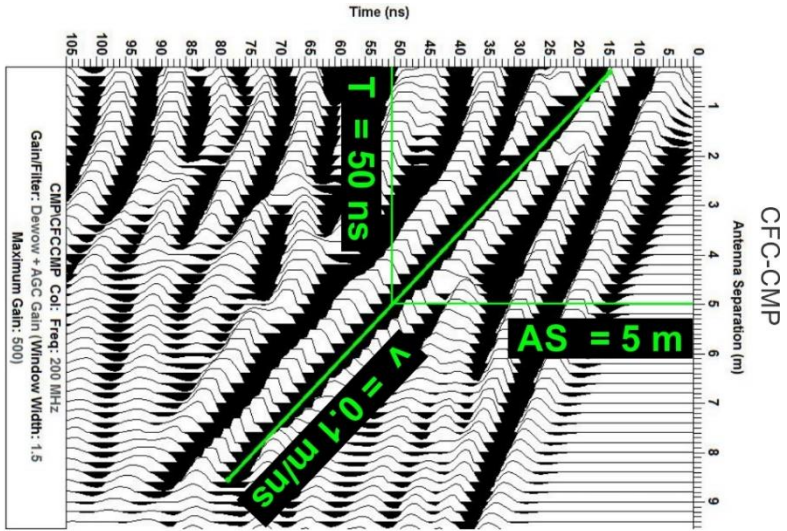


BEANC-1 200 Mhz









## Appendix B Modern Beach Survey and Elevation Calibration

Station	Instrument Height	Front Shot	Elevation (m)	Distance	Comments
Grand Bend					
Water	179.98	3.82 3.56 3.3	176.42	5.2	Water level=0.425 Water Elevation=176.845
Geodetic Marker 72U083	179.98	2 1.81 1.62	178.17	3.8	Elevation=178.89 NAV88 Elevation=178.17 IGLD85
Ipperwash					
1	179.975	0.57 0.49 0.41	179.485	1.6	Top of washroom sign
2	179.975	0.85 0.71 0.56	179.265	2.9	Break in slope Sample 01
3	179.975	2.2 2.13 2.06	177.845	1.4	Trough in dune sample 02
4	179.975	1.63 1.625 1.61	178.35	0.2	top of scarp
5	179.975	2.56 2.58 2.16	177.395	0.04	Base of scarp
6	179.975	3.11 3.06 3.03	176.915	0.8	top of waves sample 03
7	179.975	3.53 3.48 3.44	176.495	0.9	sample 04 Water level=0.35
7	178.835	2.37 2.34 2.31	176.495	0.6	Reshoot 7
8	178.835	2.53 2.45 2.36	176.385	1.7	sample 05
9	178.835	2.52 2.4 2.26	176.435	2.6	sample 06

Water elevation  
at Goderich 176.905

## Appendix C Cross Strandplain Topographic Survey

Station	Horizontal Distance	Vertical Distance	Prism Height	Orientation	Comments	VD-PH	IGLD Elevation	Height of Instrument
1	31.729	-4.146	1.52	174° 54' 05"	Top of Washroom sign BA4	-5.666	179.485	185.151
2	17.172	-3.857	1.52	174° 13' 20"	Bottom of lakeward rail	-5.377	179.774	185.151
3	46.548	-5.17	2.52	154° 01' 55"	edge of wave scarp	-7.69	177.461	185.151
4	17.732	-3.625	2.32	159° 56' 45"	break of slope in foredune	-5.945	179.206	185.151
5	17.796	1.332	1.64	262° 40' 55"	dune crest	-0.308	184.843	185.151
6	75.604	-1.846	1.72	326° 00' 35"	southwest corner of restroom	-3.566	181.585	185.151
7	111.237	-3.401	1.96	341° 27' 20"	edge of parkinglot and parkway drive	-5.361	179.79	185.151
8	119.992	-3.346	1.96	341° 28' 45"	edge of road	-5.306	179.845	185.151
9	136.904	-2.26	1.52	341° 57' 00"	dune crest	-3.78	181.371	185.151
9	37.757	0.976	2.5	285° 35' 40"	reshoot	-1.524	181.371	182.895
10	9.898	-1.553	2.5	025° 17' 10"	edge of swamp/water surface	-4.053	178.842	182.895
11	28.367	-1.536	2.5	033° 26' 20"	south edge of swamp	-4.036	178.859	182.895
11	49.996	-2.608	2.5	297° 13' 30"	reshoot	-5.108	178.859	183.967
12	44.596	-2.165	2.5	297° 51' 10"	core 2001	-4.665	179.302	183.967
13	40.761	-1.492	2.5	300° 31' 20"	OSL 2001	-3.992	179.975	183.967
14	29.949	-1.385	2.5	304° 29' 30"	path/ dune crest	-3.885	180.082	183.967
15	23.425	-1.616	2.5	302° 33' 45"	Break in slope	-4.116	179.851	183.967
16	16.783	-1.397	2.5	301° 47' 40"	core 2002	-3.897	180.07	183.967
17	9.874	-0.518	1.83	188° 28' 10"	crest 2002	-2.348	181.619	183.967
17	36.895	1.211	1.83	212° 03' 30"	reshoot	-0.619	181.619	182.238
18	5.98	-0.673	1.52	255° 38' 55"	break in slope	-2.193	180.045	182.238
19	17.943	-1.159	1.52	052° 25' 10"	core 2003	-2.679	179.559	182.238
20	18.943	-0.157	1.52	046° 25' 35"	nail lower	-1.677	180.561	182.238
21	19.071	-0.063	1.52	046° 25' 05"	nail upper	-1.583	180.655	182.238
22	47.303	-0.89	1.52	069° 03' 15"	next day nail lower	-2.41	180.561	182.971
23	47.288	-0.782	1.52	069° 05' 00"	next day nail upper	-2.302	180.655	182.957
24	40.989	0.066	1.52	056° 31' 35"	crest 2002	-1.454	181.503	182.957
25	11.528	-1.124	1.52	049° 59' 55"	swale	-2.644	180.313	182.957
25	15.22	-1.855	1.85	043° 22' 35"	core 2004	-3.705	179.252	182.957
26	8.269	0.049	1.79	184° 14' 25"	crest	-1.741	181.216	182.957
27	20.912	-1.017	2	273° 49' 50"	swale	-3.017	179.94	182.957
27	18.809	-0.97	2	331° 40' 25"	reshoot	-2.97	179.94	182.91
28	19.355	0	1.85	054° 39' 45"	crest	-1.85	181.06	182.91

29	24.45	-0.959	2.6	052° 27' 30"	swale	-3.559	179.351	182.91
30	25.227	-0.965	2.6	052° 22' 00"	water table	-3.565	179.345	182.91
31	21.748	-0.858	1.65	051° 44' 05"	core 2005	-2.508	180.402	182.91
31	8.813	-0.506	1.65	330° 22' 30"	reshoot	-2.156	180.402	182.558
32	6.917	-0.306	1.52	349° 24' 10"	OSL 2005	-1.826	180.732	182.558
33	3.625	-0.241	1.52	178° 32' 35"	crest	-1.761	180.797	182.558
34	9.973	-0.846	1.8	149° 11' 25"	edge of swale/water table	-2.646	179.912	182.558
35	23.092	0.727	2.6	088° 53' 25"	reshoot	-1.873	179.912	181.785
36	15.408	0.014	1.85	215° 37' 30"	south edge of swamp	-1.836	179.949	181.785
36	18.316	-1.114	1.85	223° 25' 30"	reshoot	-2.964	179.949	182.913
37	11.508	-0.903	1.63	165° 19' 15"	core 2006	-2.533	180.38	182.913
38	6.423	0.155	1.63	073° 56' 55"	crest	-1.475	181.438	182.913
39	13.899	-1.06	1.72	024° 56' 00"	water table/ edge of swale	-2.78	180.133	182.913
39	14.15	0.11	2.6	231° 28' 45"	reshoot	-2.49	180.133	182.623
40	13.315	-0.592	1.7	230° 40' 20"	swamp through vegetation	-2.292	180.331	182.623
41	2.04	0.059	1.52	004° 14' 15"	core 2007	-1.461	181.162	182.623
42	10.881	1.424	1.52	016° 29' 40"	crest	-0.096	182.527	182.623
43	23.696	0.434	2.6	038° 36' 35"	swamp/water table	-2.166	180.457	182.623
43	8.496	-0.032	2.2	342° 31' 45"	reshoot	-2.232	180.457	182.689
44	2.6	-0.367	1.61	334° 30' 40"	core 2008	-1.977	180.712	182.689
45	16.64	0.732	1.85	172° 46' 20"	crest	-1.118	181.571	182.689
45	45.561	0.548	1.85	002° 45' 30"	reshoot	-1.302	181.571	182.873
46	37.173	0.074	1.79	001° 34' 40"	path	-1.716	181.157	182.873
47	11.8	-1.03	1.74	357° 16' 50"	swale	-2.77	180.103	182.873
48	5.77	-0.634	1.9	355° 42' 15"	core 2009	-2.534	180.339	182.873
49	1.732	0.032	1.8	059° 08' 45"	OSL 2009	-1.768	181.105	182.873
50	26.055	-0.384	2	186° 00' 55"	core 2010	-2.384	181.105	183.489
50	13.731	-1.877	2	058° 41' 30"	reshoot	-3.877	181.105	184.982
51	3.234	-0.159	1.52	122° 18' 00"	crest	-1.679	183.303	184.982
52	9.537	-0.05	1.52	187° 49' 55"	nail upper	-1.57	183.412	184.982
53	9.608	-0.298	1.52	187° 57' 45"	nail lower	-1.818	183.164	184.982
54	12.911	-1.063	2	218° 53' 15"	core 2011	-3.063	181.919	184.982
54	20.717	0.2	2	243° 57' 00"	reshoot	-1.8	181.919	183.719
55	17.177	0.202	1.8	216° 26' 20"	crest/edge of ditch	-1.598	182.121	183.719
56	4.311	-0.526	2	216° 57' 30"	bottom of ditch	-2.526	181.193	183.719
57	2.297	-0.543	2	275° 30' 45"	ditch water table	-2.543	181.176	183.719
58	1.069	0.017	1.7	280° 19' 05"	edge of ditch	-1.683	182.036	183.719
59	15.812	0.064	1.7	038° 00' 35"	core 2012	-1.636	182.083	183.719

60	29.242	1.678	1.75	038° 31' 10"	crest	-0.072	183.647	183.719
60	36.617	-0.409	1.75	016° 31' 05"	reshoot	-2.159	183.647	185.806
61	11.361	-1.413	1.75	007° 11' 05"	core 2013 bench	-3.163	182.643	185.806
62	3.873	-0.072	1.52	133° 58' 10"	crest	-1.592	184.214	185.806
63	22.362	-0.751	1.99	202° 01' 25"	swale	-2.741	183.065	185.806
63	21.891	0.989	2	235° 20' 20"	reshoot	-1.011	183.065	184.076
64	3.259	-0.151	1.7	046° 07' 00"	water table	-1.851	182.225	184.076
65	27.482	0.337	1.8	055° 36' 30"	core 2014	-1.463	182.613	184.076
65	13.08	-2.72	1.8	252° 23' 20"	reshoot	-4.52	182.613	187.133
66	17.308	0.024	1.8	194° 41' 35"	OSL 2014/crest	-1.776	185.357	187.133
67	12.136	-1.689	1.8	160° 55' 40"	break in slope	-3.489	183.644	187.133
68	25.444	-2.232	1.8	127° 39' 45"	core 2015	-4.032	183.101	187.133
69	34.129	-2.914	1.8	120° 39' 45"	water table	-4.714	182.419	187.133
69	58.056	-1.194	2.6	208° 59' 10"	reshoot	-3.794	182.419	186.213
70	52.576	-1.466	2.6	191° 16' 20"	swale bottom	-4.066	182.147	186.213
71	26.78	-1.309	2.25	164° 17' 30"	core 2016	-3.559	182.654	186.213
72	13.343	0.225	1.55	112° 22' 05"	crest	-1.325	184.888	186.213
73	15.572	-1.925	1.7	020° 22' 20"	water table/edge of swale	-3.625	182.588	186.213
74	40.517	-1.557	1.83	037° 04' 40"	core 2017	-3.387	182.826	186.213
75	48.654	-0.675	1.83	037° 05' 10"	crest	-2.505	183.708	186.213
75	53.651	0.783	2.6	067° 05' 10"	reshoot	-1.817	183.708	185.525
76	22.848	0.152	1.52	202° 50' 00"	southern side of cement well	-1.368	184.157	185.525
77	22.918	0.063	1.52	202° 42' 50"	well south side ground surface	-1.457	184.068	185.525
78	31.855	-0.107	2.6	292° 37' 55"	swale	-2.707	182.818	185.525
79	35.157	-0.103	2.6	295° 35' 35"	core 2018	-2.703	182.822	185.525
80	36.94	-0.601	1.63	296° 01' 55"	OSL 2018	-2.231	183.294	185.525
80	64.864	-2.463	1.52	169° 51' 05"	reshoot	-3.983	183.294	187.277
81	48.014	-3.306	1.52	169° 48' 35"	swale	-4.826	182.451	187.277
82	33.857	-2.992	1.52	176° 38' 05"	water table/ edge swale	-4.512	182.765	187.277
83	37.082	-3.073	1.52	144° 48' 30"	core 2019	-4.593	182.684	187.277
84	33.039	-2.295	1.52	146° 02' 40"	crest	-3.815	183.462	187.277
85	13.725	-2.676	1.52	159° 36' 25"	core 2020	-4.196	183.081	187.277
86	3.672	-0.232	1.52	194° 13' 45"	crest	-1.752	185.525	187.277
87	14.036	-2.869	1.52	325° 30' 00"	break in slope/water table	-4.389	182.888	187.277
88	16.791	-3.161	1.52	356° 42' 10"	swale	-4.681	182.596	187.277
89	35.135	-2.383	2.15	050° 10' 40"	core 2021	-4.533	182.744	187.277
90	41.681	-1.296	2.15	044° 34' 10"	crest	-3.446	183.831	187.277

90	28.471	0.414	2.15	278° 39' 00"	reshoot	-1.736	183.831	185.567
91	9.785	-0.489	2.15	289° 39' 00"	swale	-2.639	182.928	185.567
92	6.479	-0.336	2.15	276° 48' 55"	core 2022/water table	-2.486	183.081	185.567
93	2.72	0.055	1.52	240° 20' 45"	OSL 2022/crest	-1.465	184.102	185.567
94	3.723	-1.057	1.52	096° 36' 25"	water table/swamp edge	-2.577	182.99	185.567
95	10.269	-0.67	1.95	111° 02' 20"	swale	-2.62	182.947	185.567
96	18.068	-0.486	1.95	107° 16' 15"	core 2023	-2.436	183.131	185.567
97	24.755	0.361	1.95	102° 09' 30"	crest	-1.589	183.978	185.567
98	37.363	-0.454	1.95	114° 27' 30"	swale	-2.404	183.163	185.567
99	48.292	-0.694	1.52	116° 00' 25"	core 2024	-2.214	183.353	185.567
100	57.937	0.59	1.7	111° 59' 15"	crest	-1.11	184.457	185.567
100	34.018	-0.508	1.72	174° 29' 05"	reshoot	-2.228	184.457	186.685
101	26.984	-1.827	1.72	172° 45' 45"	water table/edge of swale	-3.547	183.138	186.685
102	22.002	-1.727	1.82	173° 22' 15"	middle of swamp	-3.547	183.138	186.685
103	11.163	0.007	1.52	301° 26' 45"	east gate post	-1.513	185.172	186.685
104	8.08	0.064	1.52	316° 00' 20"	west gate post/end of day	-1.456	185.229	186.685
105	10.327	0.02	1.52	011° 36' 25"	east gate post	-1.5	185.172	186.672
106	7.451	0.096	1.52	025° 05' 55"	west gate post	-1.424	185.248	186.672
106	18.852	-1.715	1.75	243° 04' 35"	core 2025	-3.465	183.207	186.672
107	12.001	-0.453	1.7	241° 05' 50"	crest	-2.153	184.519	186.672
108	15.767	-0.721	1.65	212° 15' 10"	OSL 2025	-2.371	184.301	186.672
109	11.931	-0.648	2.25	179° 27' 10"	core 2026	-2.898	183.774	186.672
110	3.78	-0.304	1.52	144° 49' 45"	crest	-1.824	184.848	186.672
111	8.84	-1.94	1.52	086° 12' 05"	water table/edge of swale	-3.46	183.212	186.672
112	34.976	-1.587	1.65	022° 34' 20"	road intersection	-3.237	183.435	186.672
112	50.302	-1.166	1.65	064° 58' 20"	reshoot	-2.816	183.435	186.251
113	22.127	-1.081	2.25	071° 45' 55"	mid swale	-3.331	182.92	186.251
114	10.914	-1.311	1.52	087° 11' 30"	core 2027	-2.831	183.42	186.251
115	10.212	0.819	1.75	187° 57' 15"	crest	-0.931	185.32	186.251
116	14.429	-1.049	1.75	224° 29' 25"	water table/edge of swale	-2.799	183.452	186.251
117	21.225	-1.341	2	239° 28' 25"	mid swale	-3.341	182.91	186.251
118	40.294	-0.551	2	266° 45' 00"	core 2028	-2.551	183.7	186.251
119	46.806	-0.081	2	267° 05' 30"	crest	-2.081	184.17	186.251
119	24.645	0.339	2	068° 19' 35"	reshoot	-1.661	184.17	185.831
120	17.662	0.045	1.75	033° 42' 10"	core 2029	-1.705	184.126	185.831
121	13.629	1.386	1.75	346° 55' 40"	crest	-0.364	185.467	185.831
122	16.259	-0.544	1.75	315° 57' 05"	water table/edge of swale	-2.294	183.537	185.831
123	19.015	-0.619	1.75	313° 04' 35"	mid swale	-2.369	183.462	185.831
124	19.158	-0.526	1.6	288° 07' 20"	core 2030	-2.126	183.705	185.831

125	27.538	-0.059	1.6	303° 09' 10"	OSL 2030/crest	-1.659	184.172	185.831
126	39.082	-0.643	1.7	269° 42' 45"	water table/edge of swale	-2.343	183.488	185.831
127	46.353	-0.273	2.5	271° 46' 45"	mid swale	-2.773	183.058	185.831
128	76.673	0.543	2.6	267° 37' 35"	core 2031	-2.057	183.774	185.831
129	83.855	1.075	2.6	267° 35' 25"	crest	-1.525	184.306	185.831
129	46.657	0.891	2.6	082° 07' 40"	reshoot	-1.709	184.306	186.015
130	38.135	0.234	2.6	079° 07' 40"	water table at edge of swale	-2.366	183.649	186.015
131	31.463	-0.85	1.52	074° 38' 30"	mid swale	-2.37	183.645	186.015
132	22.197	-0.768	1.52	065° 30' 25"	core 2032	-2.288	183.727	186.015
133	17.914	0.864	1.52	029° 51' 30"	crest	-0.656	185.359	186.015
134	16.696	-0.53	1.52	335° 46' 35"	water table/edge of swale	-2.05	183.965	186.015
135	26.842	-0.712	1.52	311° 04' 40"	mid swale	-2.232	183.783	186.015
136	35.861	-0.149	1.52	288° 55' 55"	core 2033	-1.669	184.346	186.015
137	40.847	0.552	1.52	289° 02' 30"	crest	-0.968	185.047	186.015
138	51.543	-0.352	1.52	269° 56' 10"	water table/edge of swale	-1.872	184.143	186.015
139	56.508	-0.508	1.52	269° 01' 15"	mid swale	-2.028	183.987	186.015
140	67.889	0.37	1.9	261° 16' 05"	core 2034	-1.53	184.485	186.015
141	72.914	1.165	1.76	261° 35' 20"	OSL 2034	-0.595	185.42	186.015
141	50.72	0.149	1.76	248° 20' 40"	reshoot	-1.611	185.42	187.031
142	40.672	0.408	1.76	238° 43' 25"	nails in tree at curve in logging road(lower)	-1.352	185.679	187.031
143	40.644	0.659	1.76	238° 49' 10"	upper	-1.101	185.93	187.031
144	23.776	-0.883	1.8	241° 49' 40"	water table/edge of swale	-2.683	184.348	187.031
145	16.498	-1.111	2	238° 41' 30"	mid swale	-3.111	183.92	187.031
146	6.559	-0.559	2	230° 27' 30"	core 2035	-2.559	184.472	187.031
147	3.277	0.209	1.82	167° 55' 15"	crest	-1.611	185.42	187.031
148	18.374	-1.101	1.52	061° 56' 10"	water table/edge of swale	-2.621	184.41	187.031
149	21.377	-1.183	1.52	064° 33' 40"	mid swale	-2.703	184.328	187.031
150	28.022	-0.837	1.52	061° 42' 00"	crest uncored ridge	-2.357	184.674	187.031
151	39.635	-1.323	1.65	061° 36' 28"	mid swale	-2.973	184.058	187.031
152	48.115	-0.436	1.89	061° 36' 25"	core 2036	-2.326	184.705	187.031
153	57.06	1.108	1.89	063° 16' 25"	crest	-0.782	186.249	187.031
153	29.162	1.116	2.35	356° 03' 25"	reshoot	-1.234	186.249	187.483
154	8.838	-0.551	1.52	021° 58' 05"	swale edge	-2.071	185.412	187.483
154	4.438	-0.728	1.52	066° 59' 25"	core 2037	-2.248	185.235	187.483
155	2.949	0.104	1.75	323° 56' 20"	crest	-1.646	185.837	187.483
156	14.976	-1.247	1.7	285° 55' 20"	water table/edge of swale	-2.947	184.536	187.483
157	15.987	-1.413	1.7	285° 04' 35"	mid swale	-3.113	184.37	187.483
158	36.721	-0.491	2	257° 01' 10"	core 2038	-2.491	184.992	187.483



159	42.812	0.737	1.77	253° 00' 10"	OSL 2038/crest	-1.033	186.45	187.483
159	44.626	-0.024	1.6	175° 35' 45"	reshoot	-1.624	186.45	188.074
160	20.247	-2.024	1.52	301° 53' 05"	water edge/wetland/swale	-3.544	184.53	188.074
161	46.334	-0.94	2.45	331° 27' 05"	core 2039	-3.39	184.684	188.074
161	30.023	-1.594	2.25	243° 07' 00"	reshoot	-3.844	184.684	188.528
162	19.083	-1.135	1.7	242° 34' 15"	crest	-2.835	185.693	188.528
163	11.004	-2.246	1.68	228° 56' 05"	water table/edge of swale	-3.926	184.602	188.528
164	8.31	-2.347	1.52	204° 38' 55"	core 2040	-3.867	184.661	188.528
165	4.04	-0.177	1.52	088° 58' 50"	crest	-1.697	186.831	188.528
166	5.033	-0.819	1.52	212° 06' 50"	nails in large birch directly in front of core 2040 (upper)	-2.339	186.189	188.528
167	5.059	-1.082	1.52	211° 52' 05"	lower	-2.602	185.926	188.528

## Appendix D Modern Beach Sample Statistics

Sample	Distance Landward (m)	Sediment Name:									
1	3.8	Very Coarse Silty Medium Sand									
	<b>Mean (Φ)</b>	<b>Mean</b>	<b>Sorting (Φ)</b>	<b>Sorting</b>	<b>Skewness (Φ)</b>	<b>Skewness</b>	<b>Kurtosis (Φ)</b>	<b>Kurtosis</b>	<b>D10 (Φ)</b>	<b>D90 (Φ)</b>	
	2.688	Fine Sand	1.006	Poorly Sorted	0.551	Very Fine Skewed	0.538	Very Platykurtic	1.623	4.190	
2	2.3	Very Coarse Silty Medium Sand									
	2.652	Fine Sand	1.009	Poorly Sorted	0.560	Very Fine Skewed	0.543	Very Platykurtic	1.595	4.170	
3	0.1	Moderately Sorted Coarse Sand									
	1.168	Medium Sand	0.875	Moderately Sorted	0.152	Fine Skewed	0.998	Mesokurtic	0.203	2.225	
4	0.0	Very Coarse Silty Medium Sand									
	2.425	Fine Sand	1.190	Poorly Sorted	0.454	Very Fine Skewed	0.552	Very Platykurtic	1.111	4.154	
5	-1.1	Very Coarse Silty Medium Sand									
	2.509	Fine Sand	1.072	Poorly Sorted	0.562	Very Fine Skewed	1.079	Mesokurtic	1.454	4.125	
6	-2.0	Very Coarse Silty Medium Sand									
	2.505	Fine Sand	1.077	Poorly Sorted	0.557	Very Fine Skewed	1.094	Mesokurtic	1.445	4.124	

# Appendix E Core Statistics

Core Number	Ridge #	Core GID85	Crest GID85	Swale GID85	Crest Distance (m)	Swale Distance (m)	Core Distance (m)	Total Penetration	Recovery (m)	Rodding + Compaction	Foreshore Top Depth	Foreshore Base Depth	Foreshore Top Elev.	Foreshore Base Elev.	Base of Recovery	Foreshore Thickness	OSL Age	Ridge Height	Ridge Width	
2001	3	179.347	180.127	179.896	215.8155	229.0525	209.197	1.918	1.7	0.218	0.72	1.36	178.657	177.647			650±20	1.574	64.17275	
2002	4	180.115	181.664	180.09	254.85575	293.22525	235.671	2.185	1.37	0.815	0.36	1.29	179.755	178.825	178.745	0.93		1.574	64.17275	
2003	5	179.604	181.548	180.358	323.01825	344.23475	312.41	3.435	2.92	0.515	1.43	1.8	178.044	177.804	176.684	0.24		1.19	51.0095	
2004	6	179.297	181.261	179.985	369.283	398.163	354.843	1.927	1.51	0.417	0.59	1	178.707	177.787			860±40	1.276	53.92825	
2005	8	180.447	180.842	179.957	425.661	451.777	412.603	3.1	2.41	0.69	1.02	2.15	179.427	178.037				0.885	53.614	
2006	9	180.425	181.483	180.376	476.9665	501.2295	464.835	2.73	2.265	0.465	0.42	1.77	179.305	178.655	178.16	0.65		1.107	49.4525	
2007	10	181.207	182.572	180.502	522.285	540.133	513.361	2.595	1.855	0.74	1.06	1.75	180.147	179.457	179.351	0.69		2.07	38.9035	
2008	11	180.757	181.616	180.148	562.437	589.197	549.057	2.62	2.25	0.37	0.48	2.16	180.127	178.447	178.506	1.68		1.468	49.064	
2009	12	180.384	181.15	180.384	608.65925	620.82375	602.577	2.375	1.98	0.395	1.07	1.88	179.314	178.474	178.403	0.84	1120±40	0.766	31.62675	
2010	13	181.15	183.348	181.15	636.70125	656.29175	626.906	2.775	2.305	0.47	0.7	1.76	180.49	179.39	178.228	1.1		2.198	35.468	
2011	14	181.964	182.166	181.238	674.5055	691.3425	666.087	2.14	1.92	0.22	0.97	1.41	180.994	180.554	179.427	0.44		0.928	35.05075	
2012	15	182.128	183.692	182.128	708.974	727.4	699.761	2.555	2.2	0.355	0.85	1.57	181.228	181.028	179.311	0.2		1.564	36.0575	
2013	16	182.688	184.259	183.11	756.683	796.823	736.613	2.145	1.79	0.355	0.92	1.51	181.678	181.178	180.281	0.5		1.149	69.423	
2014	17	182.658	185.402	183.689	830.9725	859.1315	816.893	2.619	2.224	0.395	0.56	0.77	182.098	181.888	179.817	0.21	1410±60	1.713	62.3085	
2015	18	183.146	183.146	182.192	879.3775	891.7105	873.211	2.305	1.73	0.575	0.83	1.14	182.286	182.006	180.799	0.28		0.954	32.579	
2016	19	182.699	184.933	182.633	911.29	938.116	897.877	3.485	3.17	0.315	0.84	1.16	181.599	181.37	178.912	0.169		2.3	46.4055	
2017	20	182.871	183.753	182.863	974.2905	1019.8135	951.529	2.754	2.4	0.354	0.72	1.03	181.981	181.841	179.854	0.14		0.89	81.6975	
2018	21	182.867	183.399	182.496	1050.70775	1066.97325	1042.575	2.71	2.27	0.44	0.43	1.4	182.437	181.467	179.98	0.97	1860±60	0.843	47.15975	
2019	22	182.729	183.507	182.729	1077.24825	1081.53275	1075.106	3.6	3.17	0.43	0.89	1.85	181.719	181.089	178.942	0.63		0.778	41.5595	
2020	23	183.126	183.507	182.641	1092.99775	1111.64325	1083.675	2.67	2.38	0.29	0.54	1.38	182.536	181.746	180.129	0.79		0.866	30.1105	
2021	24	182.789	185.57	182.973	1128.491	1143.541	1120.966	3.59	3.36	0.23	0.8	1.43	181.889	181.359	178.812	0.53		2.597	31.89775	
2022	25	183.126	183.876	182.992	1156.837	1168.379	1151.066	2.12	2.08	0.04	0.49	1.42	182.106	181.706	180.429	0.4	2180±80	0.884	24.838	
2023	26	183.176	184.147	183.208	1183.2425	1201.4275	1174.15	3.385	3	0.385	0.97	2.21	181.956	180.966	179.559	0.99		0.939	33.0485	
2024	27	183.398	184.023	183.183	1215.954	1226.822	1210.52	2.66	2.2	0.46	0.81	1.87	182.328	181.528	180.581	0.8		0.84	25.3945	
2025	28	183.252	184.502	183.252	1234.12	1237.848	1232.256	3.325	2.74	0.585	1.01	1.63	182.062	181.622	179.856	0.44	2300±80	1.25	11.026	
2026	29	183.819	184.564	182.965	1259.621	1299.939	1239.712	2.73	2.2	0.53	1.04	1.97	182.449	181.849	180.963	0.6		1.599	61.591	
2027	30	183.465	184.893	182.955	1330.9485	1354.1495	1319.348	3.34	2.8	0.54	1	2.09	182.395	181.375	180.009	1.02		1.938	54.7105	
2028	31	183.745	185.365	183.745	1369.1335	1375.9005	1365.75	3.015	2.65	0.365	1.39	1.95	182.305	181.795	180.439	0.51		1.62	21.751	
2029	32	184.171	184.215	183.507	1387.468	1403.836	1379.284	2.63	1.83	0.8	0.84	1.55	183.261	182.621	181.685	0.64		0.708	27.9355	
2030	33	183.75	185.512	183.103	1425.7955	1453.2385	1412.02	2.635	2.17	0.465	0.78	1.94	182.94	181.81	180.924	1.13	2650±90	2.409	49.4025	
2031	34	183.819	184.217	183.69	1476.89525	1496.72975	1466.978	3.5	2.95	0.55	1.12	1.94	182.519	181.909	179.792	0.61		0.527	43.49125	
2032	35	183.772	185.404	183.828	1519.9745	1546.6295	1506.647	2.77	2.51	0.26	0.39	1.54	183.292	182.232	180.653	1.06		1.576	49.89975	
2033	36	184.391	185.404	184.032	1566.88175	1580.73125	1559.957	3.36	2.97	0.39	0.66	1.97	183.621	182.421	180.146	1.2		1.372	34.10175	
2034	37	184.53	185.092	183.965	1600.69925	1626.78575	1587.656	3.27	2.78	0.49	0.58	2.26	183.91	182.27	180.955	1.64	2780±100	1.127	46.0545	
2035	38	184.517	185.465	184.103	1651.47	1674.752	1639.829	3.3	2.95	0.35	0.4	2.41	183.977	182.857	180.924	1.12		1.362	47.96625	
2036	40	184.75	185.465	185.457	1696.4665	1716.6135	1686.393	2.76	2.33	0.43	0.84	2.19	183.81	182.56	181.764	1.25		0.008	41.8615	
2037	41	185.28	186.294	184.415	1731.60475	1741.44025	1726.687	2.31	1.84	0.47	0.76	N/A	184.52	182.784				1.879	24.82675	
2038	42	185.037	185.882	184.575	1751.57975	1762.02325	1746.358	3.39	2.93	0.46	1.25	1.55	183.807	183.487	181.451	0.32	3490±110	1.307	20.583	
2039	43	184.729	186.495	184.647	1771.79275	1780.88825	1767.245	2.61	2.04	0.57	0.42	1.85	183.829	182.879	182.033	0.95		1.848	18.865	
2040	44	184.706	185.738	183.57			1785.436	3.46	2.64	0.82	1.02	1.82	183.686	182.886	181.41	0.8				

## Appendix F Core Sediment Sample Statistics

Core:	Depth (cm):	Sediment Name:	Mean	Sorting	Skewness (Φ)	Kurtosis (Φ)	D10 (Φ)	D99 (Φ)
2001	10	Well Sorted Fine Sand						
	<b>Mean (Φ)</b>	<b>Mean</b>	<b>Sorting (Φ)</b>	<b>Sorting</b>	<b>Skewness (Φ)</b>	<b>Skewness</b>	<b>Kurtosis (Φ)</b>	<b>Kurtosis</b>
	2.62713	Fine Sand	0.46101	Well Sorted	0.04694	Symmetrical	1.02209	Mesokurtic
2001	65	Well Sorted Fine Sand						
	2.47766	Fine Sand	0.41557	Well Sorted	-0.00382	Symmetrical	0.96049	Mesokurtic
2001	85	Well Sorted Fine Sand						
	2.58819	Fine Sand	0.38548	Well Sorted	-0.01601	Symmetrical	0.96495	Mesokurtic
2001	125	Well Sorted Fine Sand						
	2.49264	Fine Sand	0.40345	Well Sorted	-0.00302	Symmetrical	0.96191	Mesokurtic
2001	150	Well Sorted Fine Sand						
	2.32955	Fine Sand	0.45391	Well Sorted	-0.00989	Symmetrical	0.95538	Mesokurtic
2002	30	Well Sorted Fine Sand						
	2.54014	Fine Sand	0.39440	Well Sorted	-0.01049	Symmetrical	0.96152	Mesokurtic
2002	45	Well Sorted Fine Sand						
	2.44508	Fine Sand	0.40628	Well Sorted	-0.00117	Symmetrical	0.95979	Mesokurtic
2002	70	Well Sorted Fine Sand						
	2.44918	Fine Sand	0.43081	Well Sorted	-0.00612	Symmetrical	0.95501	Mesokurtic
2002	90	Well Sorted Fine Sand						
	2.49240	Fine Sand	0.41249	Well Sorted	-0.00749	Symmetrical	0.96104	Mesokurtic
2002	125	Well Sorted Fine Sand						
	2.26445	Fine Sand	0.44172	Well Sorted	-0.01261	Symmetrical	0.94333	Mesokurtic
2002	133	Well Sorted Fine Sand						
	2.43973	Fine Sand	0.40716	Well Sorted	-0.00120	Symmetrical	0.95948	Mesokurtic
2003	60	Well Sorted Fine Sand						
	2.53805	Fine Sand	0.43464	Well Sorted	0.00846	Symmetrical	0.98089	Mesokurtic
2003	130	Well Sorted Fine Sand						
	2.41506	Fine Sand	0.41951	Well Sorted	-0.00201	Symmetrical	0.95485	Mesokurtic
2003	155	Well Sorted Fine Sand						
	2.33854	Fine Sand	0.43634	Well Sorted	-0.00867	Symmetrical	0.95706	Mesokurtic
2003	178	Moderately Well Sorted Slightly Gravelly Sand						
	2.03448	Fine Sand	0.64345	Moderately Well Sorted	-0.11654	Coarse Skewed	1.03276	Mesokurtic
2003	190	Well Sorted Fine Sand						
	2.45800	Fine Sand	0.39533	Well Sorted	0.00303	Symmetrical	0.96067	Mesokurtic

<b>Core:</b>	<b>Depth (cm):</b>	<b>Sediment Name:</b>																	
2003	285	Well Sorted Fine Sand																	
	<b>Mean (Φ)</b>	<b>Mean</b>	<b>Sorting (Φ)</b>	<b>Sorting</b>	<b>Skewness (Φ)</b>	<b>Skewness</b>	<b>Kurtosis (Φ)</b>	<b>Kurtosis</b>	<b>D10 (Φ)</b>	<b>D99 (Φ)</b>									
	2.55594	Fine Sand	0.43225	Well Sorted	-0.00868	Symmetrical	0.96003	Mesokurtic	1.99384	1.60384									
2004	55	Well Sorted Fine Sand																	
	2.52672	Fine Sand	0.46139	Well Sorted	0.01440	Symmetrical	0.98097	Mesokurtic	1.93690	1.54372									
2004	70	Well Sorted Fine Sand																	
	2.51131	Fine Sand	0.42958	Well Sorted	-0.00555	Symmetrical	0.96365	Mesokurtic	1.95228	1.56918									
2004	125	Well Sorted Fine Sand																	
	2.53684	Fine Sand	0.42197	Well Sorted	-0.00709	Symmetrical	0.96305	Mesokurtic	1.98767	1.60823									
2004	145	Well Sorted Fine Sand																	
	2.52638	Fine Sand	0.41324	Well Sorted	-0.00696	Symmetrical	0.96415	Mesokurtic	1.98714	1.61264									
2005	70	Well Sorted Fine Sand																	
	2.61134	Fine Sand	0.42027	Well Sorted	-0.01107	Symmetrical	0.95930	Mesokurtic	2.07228	1.70369									
2005	105	Well Sorted Fine Sand																	
	2.55837	Fine Sand	0.46247	Well Sorted	0.02997	Symmetrical	0.99667	Mesokurtic	1.97202	1.57777									
2005	120	Well Sorted Fine Sand																	
	2.56407	Fine Sand	0.40120	Well Sorted	-0.01355	Symmetrical	0.96248	Mesokurtic	2.05273	1.69900									
2005	195	Well Sorted Fine Sand																	
	2.59423	Fine Sand	0.40680	Well Sorted	-0.01381	Symmetrical	0.96379	Mesokurtic	2.07341	1.70840									
2005	205	Well Sorted Fine Sand																	
	2.51826	Fine Sand	0.45719	Well Sorted	-0.01755	Symmetrical	0.96209	Mesokurtic	1.92295	1.51870									
2005	220	Well Sorted Fine Sand																	
	2.56620	Fine Sand	0.42696	Well Sorted	-0.00825	Symmetrical	0.95512	Mesokurtic	2.01168	1.62593									
2006	50	Well Sorted Fine Sand																	
	2.55957	Fine Sand	0.44032	Well Sorted	-0.00919	Symmetrical	0.96058	Mesokurtic	1.98664	1.59074									
2006	105	Well Sorted Fine Sand																	
	2.51911	Fine Sand	0.40260	Well Sorted	-0.00769	Symmetrical	0.96240	Mesokurtic	1.99182	1.62593									
2006	120	Well Sorted Fine Sand																	
	2.42736	Fine Sand	0.44676	Well Sorted	-0.00831	Symmetrical	0.94814	Mesokurtic	1.85123	1.43831									
2006	140	Well Sorted Fine Sand																	
	2.63328	Fine Sand	0.38980	Well Sorted	-0.00603	Symmetrical	0.96571	Mesokurtic	2.12219	1.76121									
2006	175	Well Sorted Fine Sand																	
	2.53185	Fine Sand	0.49966	Well Sorted	-0.02063	Symmetrical	0.94815	Mesokurtic	1.88547	1.41889									

Core:	Depth (cm):	Sediment Name:												
2006	185	Well Sorted Fine Sand												
	<b>Mean (Φ)</b>	<b>Mean</b>	<b>Sorting (Φ)</b>	<b>Sorting</b>	<b>Skewness (Φ)</b>	<b>Skewness</b>	<b>Kurtosis (Φ)</b>	<b>Kurtosis</b>	<b>D10 (Φ)</b>	<b>D99 (Φ)</b>				
	2.54028	Fine Sand	0.43115	Well Sorted	-0.01576	Symmetrical	0.96845	Mesokurtic	1.97796	1.58208				
2006	210	Well Sorted Fine Sand												
	2.52972	Fine Sand	0.44245	Well Sorted	-0.01577	Symmetrical	0.96657	Mesokurtic	1.95297	1.55216				
2007	40	Well Sorted Fine Sand												
	2.62522	Fine Sand	0.46793	Well Sorted	0.03306	Symmetrical	0.99645	Mesokurtic	2.03929	1.64386				
2007	100	Well Sorted Fine Sand												
	2.60838	Fine Sand	0.43475	Well Sorted	0.00296	Symmetrical	0.96544	Mesokurtic	2.05717	1.68501				
2007	115	Well Sorted Fine Sand												
	2.71452	Fine Sand	0.41022	Well Sorted	-0.00231	Symmetrical	0.95912	Mesokurtic	2.17842	1.81097				
2007	150	Well Sorted Fine Sand												
	2.63783	Fine Sand	0.41887	Well Sorted	-0.01124	Symmetrical	0.96074	Mesokurtic	2.09397	1.71786				
2007	175	Moderately Well Sorted Slightly Gravelly Sand												
	2.17373	Fine Sand	0.76606	Moderately Sorted	-0.23694	Coarse Skewed	1.21504	Leptokurtic	1.06772	-0.49570				
2007	183	Well Sorted Fine Sand												
	2.52792	Fine Sand	0.40276	Well Sorted	-0.00891	Symmetrical	0.95935	Mesokurtic	2.00103	1.63039				
2008	45	Well Sorted Fine Sand												
	2.71393	Fine Sand	0.45837	Well Sorted	0.03924	Symmetrical	1.00494	Mesokurtic	2.13414	1.74662				
2008	85	Well Sorted Fine Sand												
	2.60569	Fine Sand	0.42091	Well Sorted	-0.01102	Symmetrical	0.95946	Mesokurtic	2.06707	1.69900				
2008	105	Well Sorted Fine Sand												
	2.65149	Fine Sand	0.41064	Well Sorted	-0.00538	Symmetrical	0.96165	Mesokurtic	2.11419	1.74662				
2008	115	Well Sorted Fine Sand												
	2.61389	Fine Sand	0.41956	Well Sorted	-0.01190	Symmetrical	0.96084	Mesokurtic	2.07489	1.70369				
2008	223	Well Sorted Fine Sand												
	2.53042	Fine Sand	0.44625	Well Sorted	-0.01566	Symmetrical	0.96630	Mesokurtic	1.94908	1.54793				
2008	230	Well Sorted Fine Sand												
	2.48670	Fine Sand	0.47115	Well Sorted	-0.01947	Symmetrical	0.95597	Mesokurtic	1.88220	1.44222				
2008	235	Well Sorted Fine Sand												
	2.71324	Fine Sand	0.40941	Well Sorted	-0.00155	Symmetrical	0.95938	Mesokurtic	2.17822	1.81097				
2009	60	Well Sorted Fine Sand												
	2.73779	Fine Sand	0.47814	Well Sorted	0.09415	Symmetrical	1.07360	Mesokurtic	2.16103	1.81097				

Core:	Depth (cm):	Sediment Name:																
2009	100	Well Sorted Fine Sand																
	<b>Mean (Φ)</b>	<b>Mean</b>	<b>Sorting (Φ)</b>	<b>Sorting</b>	<b>Skewness (Φ)</b>	<b>Skewness</b>	<b>Kurtosis (Φ)</b>	<b>Kurtosis</b>	<b>D10 (Φ)</b>	<b>D99 (Φ)</b>								
	2.54603	Fine Sand	0.41337	Well Sorted	-0.00691	Symmetrical	0.95810	Mesokurtic	2.00935	1.63935								
2009	110	Well Sorted Fine Sand																
	2.51991	Fine Sand	0.42675	Well Sorted	-0.01100	Symmetrical	0.96611	Mesokurtic	1.96317	1.57347								
2009	190	Moderately Well Sorted Fine Sand																
	2.61014	Fine Sand	0.50525	Moderately Well Sorted	-0.07230	Symmetrical	1.01354	Mesokurtic	1.93723	0.15361								
2009	180	Well Sorted Fine Sand																
	2.70694	Fine Sand	0.40373	Well Sorted	-0.00695	Symmetrical	0.96046	Mesokurtic	2.17693	1.81097								
2009	195	Well Sorted Fine Sand																
	2.71329	Fine Sand	0.43389	Well Sorted	-0.00570	Symmetrical	0.96360	Mesokurtic	2.14609	1.75633								
2010	60	Well Sorted Fine Sand																
	2.48255	Fine Sand	0.46474	Well Sorted	0.02647	Symmetrical	0.99950	Mesokurtic	1.90173	1.51457								
2010	80	Well Sorted Fine Sand																
	2.72098	Fine Sand	0.43049	Well Sorted	0.01207	Symmetrical	0.97353	Mesokurtic	2.16525	1.79086								
2010	160	Well Sorted Fine Sand																
	2.62057	Fine Sand	0.42477	Well Sorted	-0.01593	Symmetrical	0.95943	Mesokurtic	2.07308	1.69900								
2010	170	Well Sorted Fine Sand																
	2.59669	Fine Sand	0.47028	Well Sorted	-0.02481	Symmetrical	0.95500	Mesokurtic	1.97888	1.55216								
2010	180	Well Sorted Fine Sand																
	2.71649	Fine Sand	0.40307	Well Sorted	-0.00488	Symmetrical	0.95822	Mesokurtic	2.19063	1.83136								
2010	225	Well Sorted Fine Sand																
	2.67420	Fine Sand	0.41891	Well Sorted	-0.00802	Symmetrical	0.96006	Mesokurtic	2.12270	1.74178								
2011	90	Well Sorted Fine Sand																
	2.56046	Fine Sand	0.44711	Well Sorted	-0.00821	Symmetrical	0.95989	Mesokurtic	1.97875	1.58208								
2011	110	Well Sorted Fine Sand																
	2.67699	Fine Sand	0.43018	Well Sorted	-0.00930	Symmetrical	0.95965	Mesokurtic	2.11177	1.72738								
2011	135	Well Sorted Fine Sand																
	2.69084	Fine Sand	0.42700	Well Sorted	-0.00752	Symmetrical	0.96497	Mesokurtic	2.12999	1.74662								
2011	139	Well Sorted Fine Sand																
	2.60858	Fine Sand	0.45272	Well Sorted	-0.01275	Symmetrical	0.94449	Mesokurtic	2.01726	1.60823								
2011	145	Well Sorted Fine Sand																
	2.69314	Fine Sand	0.40332	Well Sorted	-0.00623	Symmetrical	0.96258	Mesokurtic	2.16353	1.79586								

Core:	Depth (cm):	Sediment Name:																			
2011	180	Moderately Well Sorted Slightly Gravelly Sand																			
	<b>Mean (Φ)</b>	<b>Mean</b>	<b>Sorting (Φ)</b>	<b>Sorting</b>	<b>Skewness (Φ)</b>	<b>Skewness</b>	<b>Kurtosis (Φ)</b>	<b>Kurtosis</b>	<b>D10 (Φ)</b>	<b>D99 (Φ)</b>											
	2.71548	Fine Sand	0.51233	Moderately Well Sorted	-0.13091	Coarse Skewed	1.19061	Leptokurtic	2.07315	-0.49570											
2012	50	Well Sorted Fine Sand																			
	2.73218	Fine Sand	0.39026	Well Sorted	-0.00833	Symmetrical	0.96066	Mesokurtic	2.23441	1.88364											
2012	85	Well Sorted Fine Sand																			
	2.60687	Fine Sand	0.41856	Well Sorted	-0.01326	Symmetrical	0.96065	Mesokurtic	2.07011	1.70369											
2012	105	Well Sorted Fine Sand																			
	2.60428	Fine Sand	0.42278	Well Sorted	-0.01321	Symmetrical	0.95925	Mesokurtic	2.06327	1.69432											
2012	110	Well Sorted Fine Sand																			
	2.62086	Fine Sand	0.44206	Well Sorted	-0.01590	Symmetrical	0.95041	Mesokurtic	2.04997	1.65290											
2012	115	Well Sorted Fine Sand																			
	2.65558	Fine Sand	0.41718	Well Sorted	-0.01065	Symmetrical	0.96174	Mesokurtic	2.10896	1.73216											
2012	145	Well Sorted Fine Sand																			
	2.59546	Fine Sand	0.45943	Well Sorted	-0.01830	Symmetrical	0.95360	Mesokurtic	1.99405	1.57347											
2012	155	Well Sorted Fine Sand																			
	2.68058	Fine Sand	0.42140	Well Sorted	-0.01189	Symmetrical	0.95987	Mesokurtic	2.12475	1.74178											
2012	165	Well Sorted Fine Sand																			
	2.76127	Fine Sand	0.45654	Well Sorted	-0.00097	Symmetrical	0.94876	Mesokurtic	2.16699	1.76121											
2012	215	Well Sorted Fine Sand																			
	2.71547	Fine Sand	0.41468	Well Sorted	-0.00218	Symmetrical	0.96082	Mesokurtic	2.17391	1.80088											
2013	40	Well Sorted Fine Sand																			
	2.69396	Fine Sand	0.47383	Well Sorted	0.04806	Symmetrical	1.01672	Mesokurtic	2.10172	1.71786											
2013	90	Well Sorted Fine Sand																			
	2.52674	Fine Sand	0.47276	Well Sorted	-0.01852	Symmetrical	0.95691	Mesokurtic	1.91216	1.49411											
2013	110	Well Sorted Fine Sand																			
	2.61026	Fine Sand	0.41529	Well Sorted	-0.01341	Symmetrical	0.96129	Mesokurtic	2.07642	1.70840											
2013	130	Moderately Well Sorted Slightly Gravelly Sand																			
	2.43721	Fine Sand	0.53267	Moderately Well Sorted	-0.05884	Symmetrical	0.99935	Mesokurtic	1.72721	-0.07039											
2013	149	Moderately Well Sorted Slightly Gravelly Sand																			
	2.48280	Fine Sand	0.59338	Moderately Well Sorted	-0.15688	Coarse Skewed	1.19637	Leptokurtic	1.73212	-0.62293											
2013	155	Well Sorted Fine Sand																			
	2.65701	Fine Sand	0.41650	Well Sorted	-0.00967	Symmetrical	0.96138	Mesokurtic	2.11097	1.73216											



Core:	Depth (cm):	Sediment Name:																
2013	175	Well Sorted Fine Sand																
	<b>Mean (Φ)</b>	<b>Mean</b>	<b>Sorting (Φ)</b>	<b>Sorting</b>	<b>Skewness (Φ)</b>	<b>Skewness</b>	<b>Kurtosis (Φ)</b>	<b>Kurtosis</b>	<b>D10 (Φ)</b>	<b>D99 (Φ)</b>								
	2.64889	Fine Sand	0.41887	Well Sorted	-0.01325	Symmetrical	0.96167	Mesokurtic	2.10158	1.72261								
2014	50	Well Sorted Fine Sand																
	2.53712	Fine Sand	0.42068	Well Sorted	0.00371	Symmetrical	0.95679	Mesokurtic	1.99195	1.64837								
2014	65	Moderately Well Sorted Fine Sand																
	2.47868	Fine Sand	0.51017	Moderately Well Sorted	-0.02972	Symmetrical	0.95674	Mesokurtic	1.81055	1.34373								
2014	75	Moderately Well Sorted Slightly Gravelly Sand																
	2.24145	Fine Sand	0.64607	Moderately Well Sorted	-0.07033	Symmetrical	0.99370	Mesokurtic	1.37816	0.40354								
2014	80	Well Sorted Fine Sand																
	2.65823	Fine Sand	0.48242	Well Sorted	0.00316	Symmetrical	0.96577	Mesokurtic	2.03920	1.61264								
2014	160	Well Sorted Fine Sand																
	2.75969	Fine Sand	0.43047	Well Sorted	0.00070	Symmetrical	0.95008	Mesokurtic	2.20370	1.82113								
2014	210	Well Sorted Fine Sand																
	2.79513	Fine Sand	0.43333	Well Sorted	-0.00192	Symmetrical	0.94890	Mesokurtic	2.24441	1.86250								
2015	90	Well Sorted Fine Sand																
	2.72847	Fine Sand	0.42208	Well Sorted	-0.00037	Symmetrical	0.95619	Mesokurtic	2.17916	1.80088								
2015	105	Well Sorted Fine Sand																
	2.70574	Fine Sand	0.42275	Well Sorted	-0.00459	Symmetrical	0.96207	Mesokurtic	2.15237	1.77596								
2015	113	Well Sorted Fine Sand																
	2.68682	Fine Sand	0.43451	Well Sorted	-0.00796	Symmetrical	0.96354	Mesokurtic	2.11581	1.72738								
2015	120	Well Sorted Fine Sand																
	2.75005	Fine Sand	0.40176	Well Sorted	-0.00483	Symmetrical	0.96000	Mesokurtic	2.24120	1.88364								
2015	160	Well Sorted Fine Sand																
	2.71968	Fine Sand	0.40326	Well Sorted	-0.00471	Symmetrical	0.95886	Mesokurtic	2.19483	1.83650								
2016	80	Well Sorted Fine Sand																
	2.57623	Fine Sand	0.41834	Well Sorted	-0.01176	Symmetrical	0.95911	Mesokurtic	2.03846	1.66658								
2016	100	Well Sorted Fine Sand																
	2.54868	Fine Sand	0.47917	Well Sorted	-0.01881	Symmetrical	0.95742	Mesokurtic	1.92200	1.49818								
2016	120	Well Sorted Fine Sand																
	2.63724	Fine Sand	0.43317	Well Sorted	-0.01646	Symmetrical	0.95573	Mesokurtic	2.07628	1.69900								
2016	160	Well Sorted Fine Sand																
	2.75104	Fine Sand	0.42408	Well Sorted	-0.00137	Symmetrical	0.95180	Mesokurtic	2.20307	1.82623								

Core:	Depth (cm):	Sediment Name:																
2016	180	Well Sorted Fine Sand																
	<b>Mean (<math>\Phi</math>)</b>	<b>Mean</b>	<b>Sorting (<math>\Phi</math>)</b>	<b>Sorting</b>	<b>Skewness (<math>\Phi</math>)</b>	<b>Skewness</b>	<b>Kurtosis (<math>\Phi</math>)</b>	<b>Kurtosis</b>	<b>D10 (<math>\Phi</math>)</b>	<b>D99 (<math>\Phi</math>)</b>								
	2.80459	Fine Sand	0.40687	Well Sorted	0.00139	Symmetrical	0.95911	Mesokurtic	2.28126	1.91594								
2016	290	Well Sorted Fine Sand																
	2.88670	Fine Sand	0.48439	Well Sorted	-0.00614	Symmetrical	0.94535	Mesokurtic	2.26238	1.83136								
2017	50	Well Sorted Fine Sand																
	2.66015	Fine Sand	0.48078	Well Sorted	0.02566	Symmetrical	0.99476	Mesokurtic	2.05828	1.64837								
2017	90	Well Sorted Fine Sand																
	2.56315	Fine Sand	0.42342	Well Sorted	-0.00833	Symmetrical	0.95615	Mesokurtic	2.01414	1.63487								
2017	100	Moderately Well Sorted Fine Sand																
	2.48909	Fine Sand	0.53816	Moderately Well Sorted	-0.05675	Symmetrical	0.98391	Mesokurtic	1.77408	0.12343								
2017	110	Well Sorted Fine Sand																
	2.59733	Fine Sand	0.46419	Well Sorted	-0.01858	Symmetrical	0.95406	Mesokurtic	1.98954	1.56918								
2017	230	Well Sorted Fine Sand																
	2.81056	Fine Sand	0.41761	Well Sorted	0.00014	Symmetrical	0.95508	Mesokurtic	2.27426	1.90509								
2018	40	Well Sorted Fine Sand																
	2.82071	Fine Sand	0.44133	Well Sorted	0.02822	Symmetrical	0.97706	Mesokurtic	2.26662	1.89432								
2018	90	Well Sorted Fine Sand																
	2.83398	Fine Sand	0.42575	Well Sorted	-0.00036	Symmetrical	0.94932	Mesokurtic	2.28335	1.90509								
2018	130	Well Sorted Fine Sand																
	2.72629	Fine Sand	0.42052	Well Sorted	-0.00202	Symmetrical	0.95857	Mesokurtic	2.17845	1.80088								
2018	138	Moderately Well Sorted Slightly Gravelly Sand																
	2.14581	Fine Sand	0.81556	Moderately Sorted	-0.23257	Coarse Skewed	1.24365	Leptokurtic	0.97578	-0.69599								
2018	150	Well Sorted Fine Sand																
	2.70008	Fine Sand	0.44172	Well Sorted	-0.00848	Symmetrical	0.96176	Mesokurtic	2.12067	1.72738								
2018	220	Well Sorted Fine Sand																
	2.74248	Fine Sand	0.43310	Well Sorted	-0.00269	Symmetrical	0.95554	Mesokurtic	2.17908	1.78588								
2019	50	Well Sorted Fine Sand																
	2.62627	Fine Sand	0.47354	Well Sorted	0.01583	Symmetrical	0.97492	Mesokurtic	2.02100	1.60823								
2019	90	Well Sorted Fine Sand																
	2.66406	Fine Sand	0.41678	Well Sorted	-0.00791	Symmetrical	0.96111	Mesokurtic	2.11620	1.73697								
2019	150	Well Sorted Fine Sand																
	2.68886	Fine Sand	0.42826	Well Sorted	-0.00977	Symmetrical	0.96467	Mesokurtic	2.12550	1.73697								

Core:	Depth (cm):	Sediment Name:																
2019	165	Moderately Well Sorted Slightly Gravelly Sand																
	<b>Mean (Φ)</b>	<b>Mean</b>	<b>Sorting (Φ)</b>	<b>Sorting</b>	<b>Skewness (Φ)</b>	<b>Skewness</b>	<b>Kurtosis (Φ)</b>	<b>Kurtosis</b>	<b>D10 (Φ)</b>	<b>D99 (Φ)</b>								
	2.06412	Fine Sand	1.20863	Poorly Sorted	-0.56125	Very Coarse Skewed	1.82668	Very Leptokurtic	-0.07291	-1.33342								
2019	190	Well Sorted Fine Sand																
	2.79040	Fine Sand	0.41918	Well Sorted	-0.00061	Symmetrical	0.95539	Mesokurtic	2.25684	1.88897								
2019	310	Well Sorted Fine Sand																
	2.90655	Fine Sand	0.41062	Well Sorted	0.00581	Symmetrical	0.95136	Mesokurtic	2.37212	2.00578								
2020	50	Well Sorted Fine Sand																
	2.74799	Fine Sand	0.44475	Well Sorted	0.00797	Symmetrical	0.94611	Mesokurtic	2.17129	1.81097								
2020	60	Well Sorted Fine Sand																
	2.58996	Fine Sand	0.47005	Well Sorted	-0.00342	Symmetrical	0.96113	Mesokurtic	1.97970	1.56490								
2020	70	Well Sorted Fine Sand																
	2.65412	Fine Sand	0.43644	Well Sorted	-0.01438	Symmetrical	0.95345	Mesokurtic	2.08618	1.70369								
2020	130	Well Sorted Fine Sand																
	2.63775	Fine Sand	0.43474	Well Sorted	-0.01446	Symmetrical	0.95475	Mesokurtic	2.07548	1.69900								
2020	135	Moderately Well Sorted Fine Sand																
	2.36836	Fine Sand	0.50242	Moderately Well Sorted	-0.01073	Symmetrical	0.94370	Mesokurtic	1.71204	1.25843								
2020	140	Well Sorted Fine Sand																
	2.70554	Fine Sand	0.40529	Well Sorted	-0.00661	Symmetrical	0.96115	Mesokurtic	2.17357	1.80591								
2020	220	Well Sorted Fine Sand																
	2.67266	Fine Sand	0.41250	Well Sorted	-0.00899	Symmetrical	0.96266	Mesokurtic	2.12961	1.75147								
2021	50	Moderately Sorted Fine Sand																
	2.74242	Fine Sand	0.72817	Moderately Sorted	0.26694	Fine Skewed	1.77758	Very Leptokurtic	2.09187	1.68501								
2021	90	Well Sorted Fine Sand																
	2.72725	Fine Sand	0.42598	Well Sorted	-0.00145	Symmetrical	0.95885	Mesokurtic	2.17261	1.79086								
2021	130	Moderately Well Sorted Fine Sand																
	2.51652	Fine Sand	0.56625	Moderately Well Sorted	-0.06692	Symmetrical	0.98605	Mesokurtic	1.75788	0.27579								
2021	140	Moderately Well Sorted Slightly Gravelly Sand																
	2.50647	Fine Sand	0.65142	Moderately Well Sorted	-0.19259	Coarse Skewed	1.28750	Leptokurtic	1.70865	-0.28688								
2021	150	Well Sorted Fine Sand																
	2.65369	Fine Sand	0.41060	Well Sorted	-0.00858	Symmetrical	0.96388	Mesokurtic	2.11496	1.74178								
2021	250	Well Sorted Fine Sand																
	2.83644	Fine Sand	0.39043	Well Sorted	0.01000	Symmetrical	0.95887	Mesokurtic	2.32666	1.97143								

Core:	Depth (cm):	Sediment Name:																
2021	330	Well Sorted Fine Sand																
	<b>Mean (Φ)</b>	<b>Mean</b>	<b>Sorting (Φ)</b>	<b>Sorting</b>	<b>Skewness (Φ)</b>	<b>Skewness</b>	<b>Kurtosis (Φ)</b>	<b>Kurtosis</b>	<b>D10 (Φ)</b>	<b>D99 (Φ)</b>								
	2.88992	Fine Sand	0.43714	Well Sorted	0.00175	Symmetrical	0.95691	Mesokurtic	2.32136	1.93236								
2022	45	Well Sorted Fine Sand																
	2.78454	Fine Sand	0.49734	Well Sorted	0.05603	Symmetrical	1.00714	Mesokurtic	2.16496	1.76121								
2022	80	Well Sorted Fine Sand																
	2.78967	Fine Sand	0.43828	Well Sorted	0.00121	Symmetrical	0.94530	Mesokurtic	2.22911	1.84166								
2022	110	Well Sorted Fine Sand																
	2.68613	Fine Sand	0.40423	Well Sorted	-0.00630	Symmetrical	0.96298	Mesokurtic	2.15515	1.78588								
2022	140	Moderately Well Sorted Fine Sand																
	2.53092	Fine Sand	0.51945	Moderately Well Sorted	-0.03160	Symmetrical	0.94611	Mesokurtic	1.85097	1.36216								
2022	150	Well Sorted Fine Sand																
	2.62945	Fine Sand	0.41886	Well Sorted	-0.01404	Symmetrical	0.96119	Mesokurtic	2.08692	1.71312								
2022	195	Well Sorted Fine Sand																
	2.80304	Fine Sand	0.43062	Well Sorted	-0.00104	Symmetrical	0.94972	Mesokurtic	2.25403	1.87832								
2023	80	Well Sorted Fine Sand																
	2.68701	Fine Sand	0.43746	Well Sorted	-0.00841	Symmetrical	0.96360	Mesokurtic	2.11249	1.72261								
2023	110	Well Sorted Fine Sand																
	2.70787	Fine Sand	0.39254	Well Sorted	-0.00438	Symmetrical	0.96722	Mesokurtic	2.19796	1.85204								
2023	200	Well Sorted Fine Sand																
	2.60882	Fine Sand	0.41797	Well Sorted	-0.01219	Symmetrical	0.96065	Mesokurtic	2.07266	1.70369								
2023	220	Moderately Well Sorted Slightly Gravely Sand																
	2.58046	Fine Sand	0.51441	Moderately Well Sorted	-0.11630	Coarse Skewed	1.12531	Leptokurtic	1.91687	-0.86394								
2023	225	Well Sorted Fine Sand																
	2.76966	Fine Sand	0.40501	Well Sorted	-0.00306	Symmetrical	0.95996	Mesokurtic	2.25560	1.89432								
2023	295	Well Sorted Fine Sand																
	2.85674	Fine Sand	0.44287	Well Sorted	-0.00172	Symmetrical	0.95099	Mesokurtic	2.28354	1.89970								
2024	70	Well Sorted Fine Sand																
	2.81257	Fine Sand	0.43858	Well Sorted	-0.00153	Symmetrical	0.94431	Mesokurtic	2.25271	1.87832								
2024	110	Well Sorted Fine Sand																
	2.63413	Fine Sand	0.40471	Well Sorted	-0.01079	Symmetrical	0.96488	Mesokurtic	2.10645	1.73697								
2024	150	Well Sorted Fine Sand																
	2.60989	Fine Sand	0.43245	Well Sorted	-0.01149	Symmetrical	0.95535	Mesokurtic	2.05594	1.67577								

Core:	Depth (cm):	Sediment Name:																		
2024	180	Moderately Well Sorted Fine Sand																		
	<b>Mean (Φ)</b>	<b>Mean</b>	<b>Sorting (Φ)</b>	<b>Sorting</b>	<b>Skewness (Φ)</b>	<b>Skewness</b>	<b>Kurtosis (Φ)</b>	<b>Kurtosis</b>	<b>D10 (Φ)</b>	<b>D99 (Φ)</b>										
	2.52797	Fine Sand	0.59846	Moderately Well Sorted	-0.10879	Coarse Skewed	1.04835	Mesokurtic	1.72580	0.09696										
2024	190	Well Sorted Fine Sand																		
	2.72089	Fine Sand	0.40492	Well Sorted	-0.00452	Symmetrical	0.95801	Mesokurtic	2.19378	1.83136										
2024	210	Well Sorted Fine Sand																		
	2.73924	Fine Sand	0.42059	Well Sorted	0.00004	Symmetrical	0.95454	Mesokurtic	2.19444	1.82113										
2025	90	Well Sorted Fine Sand																		
	2.75051	Fine Sand	0.43454	Well Sorted	0.01379	Symmetrical	0.95493	Mesokurtic	2.19103	1.82113										
2025	130	Well Sorted Fine Sand																		
	2.54214	Fine Sand	0.46256	Well Sorted	-0.01882	Symmetrical	0.96275	Mesokurtic	1.93774	1.52284										
2025	160	Moderately Well Sorted Slightly Gravelly Sand																		
	2.19253	Fine Sand	0.88490	Moderately Sorted	-0.25973	Coarse Skewed	1.07990	Mesokurtic	0.85988	-0.56560										
2025	165	Well Sorted Fine Sand																		
	2.76932	Fine Sand	0.40513	Well Sorted	-0.00404	Symmetrical	0.95962	Mesokurtic	2.25495	1.89432										
2025	210	Well Sorted Fine Sand																		
	2.76311	Fine Sand	0.45414	Well Sorted	-0.00187	Symmetrical	0.94851	Mesokurtic	2.17189	1.76611										
2025	270	Well Sorted Fine Sand																		
	2.72973	Fine Sand	0.44210	Well Sorted	-0.00413	Symmetrical	0.95984	Mesokurtic	2.15323	1.75633										
2026	90	Well Sorted Fine Sand																		
	2.72289	Fine Sand	0.46260	Well Sorted	0.03048	Symmetrical	0.98633	Mesokurtic	2.13286	1.74178										
2026	130	Well Sorted Fine Sand																		
	2.86329	Fine Sand	0.41297	Well Sorted	0.00154	Symmetrical	0.95230	Mesokurtic	2.32275	1.94898										
2026	150	Well Sorted Fine Sand																		
	2.82171	Fine Sand	0.43086	Well Sorted	-0.00204	Symmetrical	0.94870	Mesokurtic	2.26819	1.88897										
2026	185	Moderately Well Sorted Fine Sand																		
	2.56592	Fine Sand	0.55382	Moderately Well Sorted	-0.07032	Symmetrical	1.00127	Mesokurtic	1.83248	0.12658										
2026	195	Moderately Sorted Slightly Gravelly Sand																		
	2.11487	Fine Sand	0.98293	Moderately Sorted	-0.33959	Very Coarse Skewed	1.11284	Leptokurtic	0.55082	-0.53605										
2026	205	Well Sorted Fine Sand																		
	2.63988	Fine Sand	0.46224	Well Sorted	-0.01700	Symmetrical	0.94805	Mesokurtic	2.03833	1.62149										
2027	90	Well Sorted Fine Sand																		
	2.59874	Fine Sand	0.42272	Well Sorted	-0.01430	Symmetrical	0.95907	Mesokurtic	2.05828	1.68501										

Core:	Depth (cm):	Sediment Name:																		
2027	110	Well Sorted Fine Sand																		
	<b>Mean (Φ)</b>	<b>Mean</b>	<b>Sorting (Φ)</b>	<b>Sorting</b>	<b>Skewness (Φ)</b>	<b>Skewness</b>	<b>Kurtosis (Φ)</b>	<b>Kurtosis</b>	<b>D10 (Φ)</b>	<b>D99 (Φ)</b>										
	2.73287	Fine Sand	0.41303	Well Sorted	-0.00300	Symmetrical	0.95551	Mesokurtic	2.19721	1.82623										
2027	170	Well Sorted Fine Sand																		
	2.76592	Fine Sand	0.41820	Well Sorted	0.00085	Symmetrical	0.95576	Mesokurtic	2.23485	1.87303										
2027	207	Well Sorted Slightly Gravelly Sand																		
	2.72029	Fine Sand	0.45985	Well Sorted	-0.01909	Symmetrical	0.96877	Mesokurtic	2.11572	1.51870										
2027	220	Well Sorted Fine Sand																		
	2.76193	Fine Sand	0.41608	Well Sorted	-0.00175	Symmetrical	0.95612	Mesokurtic	2.23226	1.87303										
2027	260	Well Sorted Fine Sand																		
	2.65706	Fine Sand	0.44620	Well Sorted	-0.01490	Symmetrical	0.95510	Mesokurtic	2.07796	1.69432										
2028	130	Well Sorted Fine Sand																		
	2.62211	Fine Sand	0.42048	Well Sorted	-0.01417	Symmetrical	0.96074	Mesokurtic	2.07954	1.70840										
2028	150	Well Sorted Fine Sand																		
	2.58239	Fine Sand	0.46387	Well Sorted	-0.02020	Symmetrical	0.95843	Mesokurtic	1.97476	1.55639										
2028	193	Well Sorted Slightly Gravelly Sand																		
	2.61224	Fine Sand	0.47315	Well Sorted	-0.09218	Symmetrical	1.05985	Mesokurtic	1.98912	-0.18903										
2028	200	Well Sorted Fine Sand																		
	2.73329	Fine Sand	0.42842	Well Sorted	-0.00379	Symmetrical	0.95743	Mesokurtic	2.17536	1.79086										
2028	220	Well Sorted Fine Sand																		
	2.72785	Fine Sand	0.44097	Well Sorted	-0.00888	Symmetrical	0.96076	Mesokurtic	2.15140	1.75147										
2028	260	Well Sorted Fine Sand																		
	2.80957	Fine Sand	0.44247	Well Sorted	-0.00273	Symmetrical	0.94286	Mesokurtic	2.24559	1.85726										
2029	130	Well Sorted Fine Sand																		
	2.62550	Fine Sand	0.41839	Well Sorted	-0.01434	Symmetrical	0.96164	Mesokurtic	2.08439	1.70840										
2029	145	Moderately Sorted Slightly Gravelly Sand																		
	2.14444	Fine Sand	0.92146	Moderately Sorted	-0.31608	Very Coarse Skewed	1.27936	Leptokurtic	0.63925	-0.97085										
2029	155	Moderately Sorted Slightly Gravelly Sand																		
	2.44659	Fine Sand	0.78471	Moderately Sorted	-0.28119	Coarse Skewed	1.56047	Very Leptokurtic	1.45408	-0.75702										
2029	160	Well Sorted Fine Sand																		
	2.65643	Fine Sand	0.41807	Well Sorted	-0.01139	Symmetrical	0.96159	Mesokurtic	2.10848	1.72738										
2030	70	Well Sorted Fine Sand																		
	2.69957	Fine Sand	0.46085	Well Sorted	-0.00775	Symmetrical	0.95422	Mesokurtic	2.09873	1.70369										

Core:	Depth (cm):	Sediment Name:																
2030	90	Moderately Well Sorted Fine Sand																
	<b>Mean (Φ)</b>	<b>Mean</b>	<b>Sorting (Φ)</b>	<b>Sorting</b>	<b>Skewness (Φ)</b>	<b>Skewness</b>	<b>Kurtosis (Φ)</b>	<b>Kurtosis</b>	<b>D10 (Φ)</b>	<b>D99 (Φ)</b>								
	2.63480	Fine Sand	0.51660	Moderately Well Sorted	0.02096	Symmetrical	1.00268	Mesokurtic	1.97901	1.54372								
2030	150	Well Sorted Fine Sand																
	2.82615	Fine Sand	0.39784	Well Sorted	0.00603	Symmetrical	0.96023	Mesokurtic	2.30704	1.94342								
2030	191	Poorly Sorted Slightly Gravelly Sand																
	2.10355	Fine Sand	1.21641	Poorly Sorted	-0.46450	Very Coarse Skewed	1.37003	Leptokurtic	0.06369	-1.31034								
2030	200	Well Sorted Fine Sand																
	2.78766	Fine Sand	0.43780	Well Sorted	-0.00137	Symmetrical	0.94640	Mesokurtic	2.22616	1.83650								
2031	90	Well Sorted Fine Sand																
	2.82557	Fine Sand	0.41640	Well Sorted	0.00542	Symmetrical	0.95299	Mesokurtic	2.28818	1.92139								
2031	130	Well Sorted Slightly Gravelly Sand																
	2.75003	Fine Sand	0.47454	Well Sorted	-0.03327	Symmetrical	0.98794	Mesokurtic	2.12448	-0.31034								
2031	180	Well Sorted Fine Sand																
	2.74120	Fine Sand	0.41515	Well Sorted	-0.00120	Symmetrical	0.95616	Mesokurtic	2.20595	1.83650								
2031	190	Moderately Sorted Slightly Gravelly Sand																
	2.44496	Fine Sand	0.80066	Moderately Sorted	-0.24666	Coarse Skewed	1.42291	Leptokurtic	1.37443	-0.73118								
2031	200	Well Sorted Fine Sand																
	2.70692	Fine Sand	0.41477	Well Sorted	-0.00658	Symmetrical	0.96305	Mesokurtic	2.16325	1.78588								
2031	290	Well Sorted Fine Sand																
	2.66717	Fine Sand	0.42928	Well Sorted	-0.01202	Symmetrical	0.95599	Mesokurtic	2.10436	1.72261								
2032	70	Well Sorted Fine Sand																
	2.73006	Fine Sand	0.43856	Well Sorted	-0.00218	Symmetrical	0.95917	Mesokurtic	2.15890	1.77103								
2032	130	Well Sorted Fine Sand																
	2.59735	Fine Sand	0.41871	Well Sorted	-0.01343	Symmetrical	0.96052	Mesokurtic	2.06231	1.69432								
2032	152	Moderately Sorted Slightly Gravelly Sand																
	2.47923	Fine Sand	0.82743	Moderately Sorted	-0.27976	Coarse Skewed	1.98997	Leptokurtic	1.67798	-1.31615								
2032	152	Moderately Well Sorted Slightly Gravelly Sand																
	2.54194	Fine Sand	0.56903	Moderately Well Sorted	-0.14905	Coarse Skewed	1.18425	Leptokurtic	1.82049	-0.64155								
2032	160	Well Sorted Fine Sand																
	2.67247	Fine Sand	0.42627	Well Sorted	-0.01070	Symmetrical	0.95724	Mesokurtic	2.11180	1.72738								
2032	230	Well Sorted Fine Sand																
	2.67966	Fine Sand	0.42989	Well Sorted	-0.01126	Symmetrical	0.96134	Mesokurtic	2.11347	1.72738								

Core:	Depth (cm):	Sediment Name:	Mean	Sorting (Φ)	Sorting	Skewness (Φ)	Skewness	Kurtosis (Φ)	Kurtosis	D10 (Φ)	D99 (Φ)	
2033	60	Well Sorted Fine Sand										
			Mean (Φ)	Mean	Sorting (Φ)	Sorting	Skewness (Φ)	Skewness	Kurtosis (Φ)	Kurtosis	D10 (Φ)	D99 (Φ)
	2.69191	Fine Sand	0.45966	Well Sorted	Well Sorted	0.01953	Symmetrical	0.98764	Mesokurtic	2.10359	1.71312	
2033	110	Well Sorted Fine Sand										
	2.68394	Fine Sand	0.41380	Well Sorted	Well Sorted	-0.00739	Symmetrical	0.96068	Mesokurtic	2.13970	1.76611	
2033	180	Well Sorted Fine Sand										
	2.52576	Fine Sand	0.47637	Well Sorted	Well Sorted	-0.01706	Symmetrical	0.95479	Mesokurtic	1.90797	1.48600	
2033	195	Well Sorted Slightly Gravelly Sand										
	2.64774	Fine Sand	0.44645	Well Sorted	Well Sorted	-0.03258	Symmetrical	0.96723	Mesokurtic	2.06617	0.16650	
2033	200	Well Sorted Fine Sand										
	2.62038	Fine Sand	0.43919	Well Sorted	Well Sorted	-0.01420	Symmetrical	0.95219	Mesokurtic	2.05555	1.66200	
2033	280	Well Sorted Fine Sand										
	2.63412	Fine Sand	0.40693	Well Sorted	Well Sorted	-0.00846	Symmetrical	0.96450	Mesokurtic	2.10467	1.73697	
2034	50	Well Sorted Fine Sand										
	2.67228	Fine Sand	0.46884	Well Sorted	Well Sorted	0.03506	Symmetrical	1.01026	Mesokurtic	2.08482	1.70369	
2034	70	Well Sorted Fine Sand										
	2.62069	Fine Sand	0.44382	Well Sorted	Well Sorted	-0.00916	Symmetrical	0.94756	Mesokurtic	2.04954	1.67116	
2034	160	Well Sorted Fine Sand										
	2.67176	Fine Sand	0.39007	Well Sorted	Well Sorted	-0.00145	Symmetrical	0.96342	Mesokurtic	2.16058	1.81097	
2034	210	Well Sorted Slightly Gravelly Sand										
	2.62822	Fine Sand	0.47562	Well Sorted	Well Sorted	-0.04816	Symmetrical	0.98560	Mesokurtic	2.00189	0.11247	
2034	225	Poorly Sorted Slightly Gravelly Sand										
	2.05783	Fine Sand	1.09112	Poorly Sorted	Poorly Sorted	-0.44860	Very Coarse Skewed	1.39310	Leptokurtic	0.19860	-1.00000	
2034	230	Well Sorted Fine Sand										
	2.58749	Fine Sand	0.43979	Well Sorted	Well Sorted	-0.00782	Symmetrical	0.95029	Mesokurtic	2.01569	1.62149	
2035	60	Well Sorted Fine Sand										
	2.58236	Fine Sand	0.43048	Well Sorted	Well Sorted	-0.00537	Symmetrical	0.95229	Mesokurtic	2.02662	1.66200	
2035	160	Well Sorted Fine Sand										
	2.67991	Fine Sand	0.40227	Well Sorted	Well Sorted	-0.00488	Symmetrical	0.96315	Mesokurtic	2.15179	1.78588	
2035	170	Well Sorted Fine Sand										
	2.63529	Fine Sand	0.41762	Well Sorted	Well Sorted	-0.01184	Symmetrical	0.96123	Mesokurtic	2.09326	1.71786	
2035	190	Well Sorted Fine Sand										
	2.59021	Fine Sand	0.43835	Well Sorted	Well Sorted	-0.01146	Symmetrical	0.95144	Mesokurtic	2.02010	1.62149	



Core:	Depth (cm):	Sediment Name:																		
2035	238	Well Sorted Fine Sand																		
	<b>Mean (Φ)</b>	<b>Mean</b>	<b>Sorting (Φ)</b>	<b>Sorting</b>	<b>Skewness (Φ)</b>	<b>Skewness</b>	<b>Kurtosis (Φ)</b>	<b>Kurtosis</b>	<b>D10 (Φ)</b>	<b>D99 (Φ)</b>										
	2.66618	Fine Sand	0.45165	Well Sorted	-0.01220	Symmetrical	0.95876	Mesokurtic	2.08039	1.69432										
2035	245	Well Sorted Fine Sand																		
	2.66355	Fine Sand	0.44153	Well Sorted	-0.01326	Symmetrical	0.95700	Mesokurtic	2.08859	1.70369										
2035	280	Moderately Well Sorted Slightly Gravelly Sand																		
	2.69083	Fine Sand	0.50796	Moderately Well Sorted	-0.03281	Symmetrical	0.99224	Mesokurtic	2.03137	-0.02857										
2036	80	Moderately Well Sorted Fine Sand																		
	2.55049	Fine Sand	0.52505	Moderately Well Sorted	0.05635	Symmetrical	1.03382	Mesokurtic	1.90567	1.47794										
2036	100	Well Sorted Fine Sand																		
	2.68748	Fine Sand	0.42634	Well Sorted	-0.00811	Symmetrical	0.96330	Mesokurtic	2.12697	1.74178										
2036	160	Well Sorted Fine Sand																		
	2.66111	Fine Sand	0.42529	Well Sorted	-0.01023	Symmetrical	0.95742	Mesokurtic	2.10458	1.72738										
2036	200	Well Sorted Fine Sand																		
	2.67572	Fine Sand	0.41637	Well Sorted	-0.00757	Symmetrical	0.96061	Mesokurtic	2.12784	1.75147										
2036	215	Well Sorted Slightly Gravelly Sand																		
	2.57721	Fine Sand	0.46855	Well Sorted	-0.03181	Symmetrical	0.97744	Mesokurtic	1.96197	1.14242										
2036	230	Well Sorted Fine Sand																		
	2.71357	Fine Sand	0.44174	Well Sorted	-0.00976	Symmetrical	0.96129	Mesokurtic	2.13478	1.73697										
2037	70	Well Sorted Fine Sand																		
	2.74428	Fine Sand	0.46489	Well Sorted	0.03105	Symmetrical	0.98241	Mesokurtic	2.15154	1.75633										
2037	90	Well Sorted Fine Sand																		
	2.69716	Fine Sand	0.44800	Well Sorted	0.00870	Symmetrical	0.97374	Mesokurtic	2.11615	1.72738										
2037	130	Well Sorted Fine Sand																		
	2.69099	Fine Sand	0.44757	Well Sorted	0.00971	Symmetrical	0.97819	Mesokurtic	2.11148	1.72261										
2037	170	Well Sorted Fine Sand																		
	2.67006	Fine Sand	0.48060	Well Sorted	0.00464	Symmetrical	0.96805	Mesokurtic	2.05817	1.63487										
2038	120	Well Sorted Fine Sand																		
	2.59561	Fine Sand	0.41438	Well Sorted	-0.01316	Symmetrical	0.96114	Mesokurtic	2.06604	1.69900										
2038	140	Well Sorted Fine Sand																		
	2.50894	Fine Sand	0.47438	Well Sorted	-0.02073	Symmetrical	0.95667	Mesokurtic	1.89640	1.46196										
2038	152	Moderately Sorted Fine Sand																		
	2.23692	Fine Sand	0.70582	Moderately Sorted	-0.13308	Coarse Skewed	1.02965	Mesokurtic	1.26141	-0.01436										



## Appendix G Reasoning for Facies Differentiation

	<b>2001</b>	<b>S-F Contact</b>	<b>Explanation</b>	<b>F-D Contact</b>	<b>Explanation</b>
Mean					
D(99)					
Skewness				X	coarser → less coarse
Sorting					
X-plots					
Visual				X	laminae → no laminae
Photo				X	brown → light brown
Peel				X	laminae → no laminae
<b>2002</b>		<b>S-F Contact</b>	<b>Explanation</b>	<b>F-D Contact</b>	<b>Explanation</b>
Mean					
D(99)					
Skewness					
Sorting					
X-plots					
Visual				X	laminae → no laminae
Photo				X	laminae → no laminae
Peel				X	laminae → no laminae
<b>2003</b>		<b>S-F Contact</b>	<b>Explanation</b>	<b>F-D Contact</b>	<b>Explanation</b>
Mean		X	fine → normally graded	X	normally graded → fine
D(99)		X	fine → normally graded	X	normally graded → fine
Skewness		X	fine → normally graded	X	normally graded → fine
Sorting		X	well sorted → moderately well sorted to well sorted	X	less well sorted → well sorted
X-plots		X	grouping in Sorting vs Mean graph	X	
Visual		X	abrupt layer of shell fragments above contact, consistently spaced laminae → inconsistently spaced laminae	X	laminae → no laminae
Photo		X	abrupt layer of shell fragments above contact, consistently spaced laminae → inconsistently spaced laminae, brown → grey	X	laminae → no laminae
Peel		X	abrupt layer of shell fragments above contact, consistently spaced laminae → inconsistently spaced laminae	X	laminae → no laminae
<b>2004</b>		<b>S-F Contact</b>	<b>Explanation</b>	<b>F-D Contact</b>	<b>Explanation</b>
Mean					
D(99)					
Skewness					
Sorting					
X-plots					

Visual			x	laminae → no laminae
Photo			x	laminae → no laminae, light brown → brown
Peel			x	laminae → no laminae
<b>2005</b>	<b>S-F Contact</b>	<b>Explanation</b>	<b>F-D Contact</b>	<b>Explanation</b>
Mean	x	fine → normally graded		normally graded → fine
D(99)	x	fine → normally graded		normally graded → fine
Skewness	x	fine → normally graded	x	normally graded → fine
Sorting	x	well sorted → moderately well sorted to well sorted		less well sorted → well sorted
X-plots				
Visual	x	abrupt layer of shell fragments above contact, consistently spaced laminae → inconsistently spaced laminae	x	laminae → no laminae
Photo	x	abrupt layer of shell fragments above contact, consistently spaced laminae → inconsistently spaced laminae, brown → grey	x	laminae → no laminae, brown → light brown
Peel	x	abrupt layer of shell fragments above contact, consistently spaced laminae → inconsistently spaced laminae	x	laminae → no laminae
<b>2007</b>	<b>S-F Contact</b>	<b>Explanation</b>	<b>F-D Contact</b>	<b>Explanation</b>
Mean	x	fine → normally graded	x	normally graded → fine
D(99)	x	fine → normally graded	x	normally graded → fine
Skewness	x	fine → normally graded	x	normally graded → fine
Sorting	x	well sorted → moderately well sorted to well sorted	x	less well sorted → well sorted
X-plots				
Visual	x	abrupt layer of shell fragments above contact, consistently spaced laminae → inconsistently spaced laminae	x	laminae → no laminae
Photo	x	abrupt layer of shell fragments above contact, consistently spaced laminae → inconsistently spaced laminae, brown → grey	x	laminae → no laminae, brown → light brown
Peel	x	abrupt layer of shell fragments above contact, consistently spaced laminae → inconsistently spaced laminae	x	laminae → no laminae
<b>2007</b>	<b>S-F Contact</b>	<b>Explanation</b>	<b>F-D Contact</b>	<b>Explanation</b>
Mean	x	fine → normally graded	x	normally graded → fine
D(99)	x	fine → normally graded	x	normally graded → fine
Skewness	x	fine → normally graded	x	normally graded → fine
Sorting	x	well sorted → moderately well sorted to well sorted	x	less well sorted → well sorted
X-plots				
Visual	x	abrupt layer of shell fragments above contact, consistently spaced laminae → inconsistently spaced laminae	x	laminae → no laminae
Photo	x	abrupt layer of shell fragments above contact, consistently spaced laminae → inconsistently spaced laminae, brown → grey	x	laminae → no laminae, brown → light brown
Peel	x	abrupt layer of shell fragments above contact, consistently spaced laminae → inconsistently spaced laminae	x	laminae → no laminae

2008	S-F Contact	Explanation	F-D Contact	Explanation
Mean	x	fine → normally graded	x	normally graded → fine
D(99)	x	fine → normally graded	x	normally graded → fine
Skewness	x	fine → normally graded	x	normally graded → fine
Sorting	x	well sorted → less well sorted to well sorted	x	less well sorted → well sorted
X-plots				
Visual	x	abrupt layer of shell fragments above contact, brown → grey	x	laminae → no laminae
Photo	x	abrupt layer of shell fragments above contact, brown → grey	x	laminae → no laminae, brown → light brown
Peel	x	abrupt layer of shell fragments above contact, brown → grey	x	laminae → no laminae
<b>2009</b>	<b>S-F Contact</b>	<b>Explanation</b>	<b>F-D Contact</b>	<b>Explanation</b>
Mean	x	fine → normally graded	x	normally graded → fine
D(99)	x	fine → normally graded	x	normally graded → fine
Skewness	x	fine → normally graded	x	normally graded → fine
Sorting	x	well sorted → less well sorted to well sorted	x	less well sorted → well sorted
X-plots			x	grouping in Skewness vs Mean graph
Visual	x	abrupt layer of shell fragments above contact, brown → grey	x	laminae → no laminae
Photo	x	abrupt layer of shell fragments above contact, brown → grey	x	laminae → no laminae, brown → light brown
Peel	x	abrupt layer of shell fragments above contact, brown → grey	x	laminae → no laminae
<b>2010</b>	<b>S-F Contact</b>	<b>Explanation</b>	<b>F-D Contact</b>	<b>Explanation</b>
Mean	x	fine → normally graded	x	normally graded → fine
D(99)	x	fine → normally graded	x	normally graded → fine
Skewness	x	fine → normally graded	x	normally graded → fine
Sorting	x	well sorted → moderately well sorted to well sorted	x	less well sorted → well sorted
X-plots			x	grouping in Skewness vs Mean graph
Visual	x	abrupt layer of shell fragments above contact, consistently spaced laminae → consistently spaced laminae to inconsistently spaced laminae	x	laminae → no laminae
Photo	x	abrupt layer of shell fragments above contact, consistently spaced laminae → consistently spaced laminae to inconsistently spaced laminae, brown → grey	x	laminae → no laminae, brown → light brown
Peel	x	abrupt layer of shell fragments above contact, consistently spaced laminae → consistently spaced laminae to inconsistently spaced laminae	x	laminae → no laminae
<b>2011</b>	<b>S-F Contact</b>	<b>Explanation</b>	<b>F-D Contact</b>	<b>Explanation</b>
Mean	x	fine → normally graded	x	normally graded → fine
D(99)			x	normally graded → fine



Skewness	x	fine → normally graded	x	normally graded → fine
Sorting	x	well sorted → moderately well sorted to well sorted	x	less well sorted → well sorted
X-Plots			x	grouping in all graphs
Visual	x	abrupt layer of shell fragments above contact	x	laminæ → no laminæ
Photo	x	abrupt layer of shell fragments above contact, brown → grey	x	laminæ → no laminæ, brown → light brown
Peel	x	abrupt layer of shell fragments above contact	x	laminæ → no laminæ
<b>2015</b>	<b>S-F Contact</b>	<b>Explanation</b>	<b>F-D Contact</b>	<b>Explanation</b>
Mean	x	fine → normally graded	x	normally graded → fine
D(99)	x	fine → normally graded	x	normally graded → fine
Skewness	x	fine → normally graded	x	normally graded → fine
Sorting	x	well sorted → moderately well sorted to well sorted	x	less well sorted → well sorted
X-Plots				
Visual	x	abrupt layer of shell fragments above contact, horizontal laminæ → lakeward dipping laminæ	x	laminæ → no laminæ
Photo	x	abrupt layer of shell fragments above contact, horizontal laminæ → lakeward dipping laminæ, grey → brown	x	laminæ → no laminæ
Peel	x	abrupt layer of shell fragments above contact, horizontal laminæ → lakeward dipping laminæ	x	laminæ → no laminæ
<b>2016</b>	<b>S-F Contact</b>	<b>Explanation</b>	<b>F-D Contact</b>	<b>Explanation</b>
Mean				
D(99)				
Skewness				
Sorting				
X-Plots				
Visual	x	abrupt layer of shell fragments above contact	x	laminæ → no laminæ, imbricated wood detritus (storm line)
Photo	x	abrupt layer of shell fragments above contact, brown → grey	x	laminæ → no laminæ, brown → light brown
Peel	x	abrupt layer of shell fragments above contact	x	laminæ → no laminæ
<b>2017</b>	<b>S-F Contact</b>	<b>Explanation</b>	<b>F-D Contact</b>	<b>Explanation</b>
Mean	x	fine → normally graded	x	normally graded → fine
D(99)	x	fine → normally graded	x	normally graded → fine
Skewness	x	fine → normally graded	x	normally graded → fine
Sorting	x	well sorted → moderately well sorted to well sorted	x	less well sorted → well sorted
X-Plots			x	grouping in Skewness vs Mean graph
Visual	x	abrupt layer of shell fragments above contact, consistently spaced laminæ → inconsistently spaced laminæ	x	laminæ → no laminæ

Photo	x	abrupt layer of shell fragments above contact, consistently spaced laminae → Inconsistently spaced laminae, brown → grey	x	laminae → no laminae, brown → light brown
Peel	x	abrupt layer of shell fragments above contact, consistently spaced laminae → inconsistently spaced laminae	x	laminae → no laminae
<b>2018</b>	<b>S-F Contact</b>	<b>Explanation</b>	<b>F-D Contact</b>	<b>Explanation</b>
Mean	x	fine → normally graded	x	normally graded → fine
D(99)	x	fine → normally graded	x	normally graded → fine
Skewness	x	fine → normally graded	x	normally graded → fine
Sorting	x	well sorted → moderately well sorted to well sorted	x	less well sorted → well sorted
X-plots	x	grouping in all graphs	x	grouping in all graphs
Visual	x	abrupt layer of shell fragments above contact, inconsistently spaced horizontal laminae → consistently spaced lakeward dipping laminae	x	laminae → no laminae
Photo	x	abrupt layer of shell fragments above contact, inconsistently spaced horizontal laminae → consistently spaced lakeward dipping laminae, grey → brown	x	laminae → no laminae, brown → light brown
Peel	x	abrupt layer of shell fragments above contact, inconsistently spaced horizontal laminae → consistently spaced lakeward dipping laminae	x	laminae → no laminae
<b>2019</b>	<b>S-F Contact</b>	<b>Explanation</b>	<b>F-D Contact</b>	<b>Explanation</b>
Mean	x	fine → normally graded	x	normally graded → fine
D(99)	x	fine → normally graded	x	normally graded → fine
Skewness	x	fine → normally graded	x	normally graded → fine
Sorting	x	well sorted → moderately well sorted to well sorted	x	less well sorted → well sorted
X-plots	x	grouping in Mean vs Sorting		
Visual	x	abrupt layer of shell fragments above contact, consistently spaced, horizontal laminae and ripple marks → inconsistently spaced, lakeward dipping laminae	x	laminae → no laminae
Photo	x	abrupt layer of shell fragments above contact, consistently spaced, horizontal laminae, ripples marked → inconsistently spaced, lakeward dipping laminae, brown → grey	x	laminae → no laminae, brown → light brown
Peel	x	abrupt layer of shell fragments above contact, consistently spaced, horizontal laminae and ripple marks → inconsistently spaced, lakeward dipping laminae	x	laminae → no laminae
<b>2020</b>	<b>S-F Contact</b>	<b>Explanation</b>	<b>F-D Contact</b>	<b>Explanation</b>
Mean	x	fine → normally graded	x	normally graded → fine
D(99)	x	fine → normally graded	x	normally graded → fine
Skewness	x	fine → more coarse	x	normally graded → fine
Sorting	x	well sorted → moderately well sorted to well sorted	x	less well sorted → well sorted
X-plots				



Visual	x	abrupt layer of shell fragments above contact, consistently spaced laminae → inconsistently spaced laminae	x	laminae → no laminae
Photo	x	abrupt layer of shell fragments above contact, consistently spaced laminae → inconsistently spaced laminae, brown → grey	x	laminae → no laminae
Peel	x	abrupt layer of shell fragments above contact, consistently spaced laminae → inconsistently spaced laminae	x	laminae → no laminae
<b>2021</b>	<b>S-F Contact</b>	<b>Explanation</b>	<b>F-D Contact</b>	<b>Explanation</b>
Mean	x	fine → normally graded	x	normally graded → fine
D(99)	x	fine → normally graded	x	normally graded → fine
Skewness	x	fine → normally graded	x	
Sorting	x	well sorted → moderately well sorted to well sorted	x	
X-plots				
Visual	x	abrupt layer of shell fragments above contact, consistently spaced laminae → inconsistently spaced laminae	x	laminae → no laminae
Photo	x	abrupt layer of shell fragments above contact, consistently spaced laminae → inconsistently spaced laminae, brown → grey	x	laminae → no laminae, brown → light brown
Peel	x	abrupt layer of shell fragments above contact, laminae	x	laminae → no laminae
<b>2022</b>	<b>S-F Contact</b>	<b>Explanation</b>	<b>F-D Contact</b>	<b>Explanation</b>
Mean	x	fine → normally graded	x	normally graded → fine
D(99)	x	fine → normally graded	x	normally graded → fine
Skewness	x	fine → normally graded	x	
Sorting	x	well sorted → moderately well sorted to well sorted	x	less well sorted → well sorted
X-plots				
Visual	x	abrupt layer of shell fragments above contact	x	laminae → no laminae
Photo	x	abrupt layer of shell fragments above contact, brown → grey	x	laminae → no laminae, brown → light brown
Peel	x	abrupt layer of shell fragments above contact, laminae	x	laminae → no laminae
<b>2023</b>	<b>S-F Contact</b>	<b>Explanation</b>	<b>F-D Contact</b>	<b>Explanation</b>
Mean	x	fine → normally graded	x	normally graded → fine
D(99)	x	fine → normally graded	x	normally graded → fine
Skewness	x	fine → normally graded	x	normally graded → fine
Sorting	x	well sorted → moderately well sorted to well sorted	x	less well sorted → well sorted
X-plots				
Visual	x	abrupt layer of shell fragments above contact, consistently spaced laminae → inconsistently spaced laminae	x	laminae → no laminae
Photo	x	abrupt layer of shell fragments above contact, consistently spaced laminae → inconsistently spaced laminae, brown → grey	x	laminae → no laminae

Peel	x	abrupt layer of shell fragments above contact, consistently spaced laminae → inconsistently spaced laminae	x	laminae → no laminae
<b>2024</b>	<b>S-F Contact</b>	<b>Explanation</b>	<b>F-D Contact</b>	<b>Explanation</b>
Mean	x	fine → normally graded	x	normally graded → fine
D(99)	x	fine → normally graded	x	normally graded → fine
Skewness	x	fine → normally graded	x	normally graded → fine
Sorting	x	well sorted → moderately well sorted to well sorted	x	less well sorted → well sorted
X-plots				
Visual	x	abrupt layer of shell fragments above contact, consistently spaced laminae → inconsistently spaced laminae	x	laminae → no laminae
Photo	x	abrupt layer of shell fragments above contact, consistently spaced laminae → inconsistently spaced laminae, brown → grey	x	laminae → no laminae, brown → light brown
Peel	x	abrupt layer of shell fragments above contact, consistently spaced laminae → inconsistently spaced laminae	x	laminae → no laminae
<b>2025</b>	<b>S-F Contact</b>	<b>Explanation</b>	<b>F-D Contact</b>	<b>Explanation</b>
Mean	x	fine → normally graded	x	normally graded → fine
D(99)	x	fine → normally graded	x	normally graded → fine
Skewness	x	fine → normally graded	x	normally graded → fine
Sorting	x	well sorted → moderately well sorted to well sorted	x	less well sorted → well sorted
X-plots	x	groupings in all graphs	x	grouping in Skewness vs Mean graph
Visual	x	abrupt layer of shell fragments above contact, consistently spaced, horizontal laminae → inconsistently spaced, lakeward dipping laminae	x	laminae → no laminae
Photo	x	abrupt layer of shell fragments above contact, consistently spaced, horizontal laminae → inconsistently spaced, lakeward dipping laminae, grey → brown	x	laminae → no laminae, brown → light brown
Peel	x	abrupt layer of shell fragments above contact, consistently spaced, horizontal laminae → inconsistently spaced, lakeward dipping laminae	x	laminae → no laminae
<b>2026</b>	<b>S-F Contact</b>	<b>Explanation</b>	<b>F-D Contact</b>	<b>Explanation</b>
Mean	x	fine → normally graded	x	normally graded → fine
D(99)	x	fine → normally graded	x	normally graded → fine
Skewness	x	fine → normally graded	x	normally graded → fine
Sorting	x	well sorted → moderately well sorted to well sorted	x	less well sorted → well sorted
X-plots			x	grouping in all graphs
Visual	x	abrupt layer of shell fragments above contact	x	laminae → no laminae
Photo	x	abrupt layer of shell fragments above contact, brown → grey	x	laminae → no laminae, brown → light brown
Peel	x	abrupt layer of shell fragments above contact	x	laminae → no laminae

2027	S-F Contact	Explanation	F-D Contact	Explanation
Mean	x	fine → normally graded	x	normally graded → fine
D(99)	x	fine → normally graded	x	normally graded → fine
Skewness			x	normally graded → fine
Sorting	x	well sorted → moderately well sorted to well sorted	x	less well sorted → well sorted
X-Plots				
Visual	x	abrupt layer of shell fragments above contact	x	laminae → no laminae
Photo	x	abrupt layer of shell fragments above contact, brown → grey	x	laminae → no laminae, brown → light brown
Peel	x	abrupt layer of shell fragments above contact	x	laminae → no laminae
2030	S-F Contact	Explanation	F-D Contact	Explanation
Mean	x	fine → normally graded	x	normally graded → fine
D(99)	x	fine → normally graded	x	normally graded → fine
Skewness	x	fine → normally graded	x	normally graded → fine
Sorting	x	well sorted → moderately well sorted to well sorted	x	less well sorted → well sorted
X-Plots				
Visual	x	abrupt layer of shell fragments above contact	x	laminae → no laminae
Photo	x	abrupt layer of shell fragments above contact, brown → grey	x	laminae → no laminae, brown → light brown
Peel	x	abrupt layer of shell fragments above contact	x	laminae → no laminae
2028	S-F Contact	Explanation	F-D Contact	Explanation
Mean	x	fine → normally graded	x	normally graded → fine
D(99)	x	fine → normally graded	x	normally graded → fine
Skewness	x	fine → normally graded	x	normally graded → fine
Sorting	x	well sorted → moderately well sorted to well sorted	x	less well sorted → well sorted
X-Plots	x	groupings in Sorting, Skewness and D(99) vs Mean		
Visual	x	abrupt layer of shell fragments above contact	x	laminae → no laminae
Photo	x	abrupt layer of shell fragments above contact, brown → grey	x	laminae → no laminae, brown → light brown
Peel	x	abrupt layer of shell fragments above contact	x	laminae → no laminae
2027	S-F Contact	Explanation	F-D Contact	Explanation
Mean	x	fine → normally graded	x	normally graded → fine
D(99)	x	fine → normally graded	x	normally graded → fine
Skewness			x	normally graded → fine
Sorting	x	well sorted → moderately well sorted to well sorted	x	less well sorted → well sorted
X-Plots				
Visual	x	abrupt layer of shell fragments above contact, consistently spaced, rippled laminae → inconsistently spaced, lakeward dipping laminae	x	laminae → no laminae
Photo	x	abrupt layer of shell fragments above contact, consistently spaced, rippled laminae → inconsistently spaced, lakeward dipping laminae, grey → brown	x	laminae → no laminae, brown → light brown
Peel	x	abrupt layer of shell fragments above contact, consistently spaced, rippled laminae → inconsistently spaced, lakeward dipping laminae	x	laminae → no laminae
2029	S-F Contact	Explanation	F-D Contact	Explanation
Mean	x	fine → normally graded	x	normally graded → fine
D(99)	x	fine → normally graded	x	normally graded → fine
Skewness	x	fine → normally graded	x	normally graded → fine
Sorting	x	well sorted → moderately well sorted to well sorted	x	less well sorted → well sorted
X-Plots				
Visual	x	abrupt layer of shell fragments above contact	x	laminae → no laminae
Photo	x	abrupt layer of shell fragments above contact, brown → grey	x	laminae → no laminae, brown → light brown
Peel	x	abrupt layer of shell fragments above contact	x	laminae → no laminae
2030	S-F Contact	Explanation	F-D Contact	Explanation
Mean	x	fine → normally graded	x	normally graded → fine

D(99)	x	fine → normally graded	x	normally graded → fine
Skewness	x	fine → normally graded	x	normally graded → fine
Sorting	x	well sorted → moderately well sorted to well sorted	x	less well sorted → well sorted
X-plots			x	grouping in Skewness vs Mean graph
Visual	x	abrupt layer of shell fragments above contact, consistently spaced laminae → inconsistently spaced laminae	x	laminae → no laminae
Photo	x	abrupt layer of shell fragments above contact, consistently spaced laminae → inconsistently spaced laminae, brown → grey	x	laminae → no laminae, brown → light brown
Peel	x	abrupt layer of shell fragments above contact, consistently spaced laminae → inconsistently spaced laminae	x	laminae → no laminae
<b>2031</b>	<b>S-F Contact</b>	<b>Explanation</b>	<b>F-D Contact</b>	<b>Explanation</b>
Mean	x	fine → normally graded	x	normally graded → fine
D(99)	x	fine → normally graded		
Skewness	x	fine → normally graded		
Sorting	x	well sorted → moderately well sorted to well sorted	x	less well sorted → well sorted
X-plots			x	groupings in Sorting, Skewness and D(99) vs Mean graphs
Visual	x	abrupt layer of shell fragments above contact, consistently spaced laminae → inconsistently spaced, lakeward dipping laminae	x	laminae → no laminae
Photo	x	abrupt layer of shell fragments above contact, consistently spaced laminae → inconsistently spaced, lakeward dipping laminae, brown → grey	x	laminae → no laminae, brown → light brown
Peel	x	abrupt layer of shell fragments above contact, consistently spaced laminae → inconsistently spaced, lakeward dipping laminae	x	laminae → no laminae
<b>2032</b>	<b>S-F Contact</b>	<b>Explanation</b>	<b>F-D Contact</b>	<b>Explanation</b>
Mean	x	fine → normally graded	x	normally graded → fine
D(99)	x	fine → normally graded	x	normally graded → fine
Skewness	x	fine → normally graded	x	normally graded → fine
Sorting	x	well sorted → moderately well sorted to well sorted	x	less well sorted → well sorted
X-plots			x	grouping in Sorting, Skewness, and D(99) vs Mean
Visual	x	abrupt layer of shell fragments above contact, horizontal laminae → lakeward dipping laminae	x	laminae → no laminae
Photo	x	abrupt layer of shell fragments above contact, horizontal laminae → lakeward dipping laminae, brown → grey	x	laminae → no laminae, brown → light brown
Peel	x	abrupt layer of shell fragments above contact, horizontal laminae → lakeward dipping laminae	x	laminae → no laminae
<b>2033</b>	<b>S-F Contact</b>	<b>Explanation</b>	<b>F-D Contact</b>	<b>Explanation</b>
Mean	x	fine → normally graded	x	normally graded → fine

D(99)	x	fine → normally graded	x	normally graded → fine
Skewness	x	fine → normally graded	x	normally graded → fine
Sorting	x	well sorted → moderately well sorted to well sorted	x	less well sorted → well sorted
X-plots				
Visual	x	abrupt layer of shell fragments above contact, consistently spaced laminae → inconsistently spaced laminae	x	laminae → no laminae
Photo	x	abrupt layer of shell fragments above contact, consistently spaced laminae → inconsistently spaced laminae, brown → grey	x	laminae → no laminae, brown → light brown
Peel	x	abrupt layer of shell fragments above contact, consistently spaced laminae → inconsistently spaced laminae	x	laminae → no laminae
<b>2034</b>	<b>S-F Contact</b>	<b>Explanation</b>	<b>F-D Contact</b>	<b>Explanation</b>
Mean	x	fine → normally graded	x	normally graded → fine
D(99)	x	fine → normally graded	x	normally graded → fine
Skewness	x	fine → normally graded	x	normally graded → fine
Sorting	x	well sorted → moderately well sorted to well sorted	x	less well sorted → well sorted
X-plots				
Visual	x	abrupt layer of shell fragments above contact, horizontal laminae → lakeward dipping laminae	x	laminae → no laminae
Photo	x	abrupt layer of shell fragments above contact, horizontal laminae → lakeward dipping laminae, brown → grey	x	laminae → no laminae, brown → light brown
Peel	x	abrupt layer of shell fragments above contact, horizontal laminae → lakeward dipping laminae	x	laminae → no laminae
<b>2035</b>	<b>S-F Contact</b>	<b>Explanation</b>	<b>F-D Contact</b>	<b>Explanation</b>
Mean				
D(99)				
Skewness				
Sorting				
X-plots				
Visual	x	abrupt layer of shell fragments above contact, inconsistently spaced, horizontal laminae → consistently spaced, horizontal to lakeward dipping laminae	x	laminae → no laminae
Photo	x	abrupt layer of shell fragments above contact, inconsistently spaced, horizontal laminae → consistently spaced, horizontal to lakeward dipping laminae, grey → brown	x	laminae → no laminae, brown → light brown
Peel	x	abrupt layer of shell fragments above contact, inconsistently spaced, horizontal laminae → consistently spaced, horizontal to lakeward dipping laminae	x	laminae → no laminae
<b>2036</b>	<b>S-F Contact</b>	<b>Explanation</b>	<b>F-D Contact</b>	<b>Explanation</b>
Mean	x	fine → normally graded	x	normally graded → fine

D(99)	x	fine → normally graded	x	normally graded → fine
Skewness	x	fine → normally graded	x	normally graded → fine
Sorting	x	well sorted → moderately well sorted to well sorted	x	less well sorted → well sorted
X-plots	x	groupings in all graphs	x	groupings in all graphs
Visual	x	abrupt layer of shell fragments above contact, inconsistently spaced laminae → consistently spaced laminae	x	laminae → no laminae
Photo	x	abrupt layer of shell fragments above contact, inconsistently spaced laminae → consistently spaced laminae, grey → brown	x	laminae → no laminae, brown → light brown
Peel	x	abrupt layer of shell fragments above contact, inconsistently spaced laminae → consistently spaced laminae	x	laminae → no laminae
<b>2037</b>	<b>S-F Contact</b>	<b>Explanataion</b>	<b>F-D Contact</b>	<b>Explanation</b>
Mean			x	normally graded → fine
D(99)			x	normally graded → fine
Skewness				
Sorting				
X-plots			x	grouping in Sorting, Skewness, D(99) vs Mean
Visual				
Photo			x	brown → light brown
Peel				
<b>2038</b>	<b>S-F Contact</b>	<b>Explanataion</b>	<b>F-D Contact</b>	<b>Explanation</b>
Mean	x	fine → normally graded	x	normally graded → fine
D(99)			x	normally graded → fine
Skewness			x	normally graded → fine
Sorting	x	well sorted → moderately well sorted to well sorted	x	less well sorted → well sorted
X-plots			x	grouping in Sorting, Skewness, D(99) vs Mean
Visual	x	laminae → no laminae, silt layer → no silt layer	x	laminae → no laminae
Photo	x	laminae → no laminae, grey → brown	x	laminae → no laminae, brown → light brown
Peel	x	laminae → no laminae	x	laminae → no laminae
<b>2039</b>	<b>S-F Contact</b>	<b>Explanataion</b>	<b>F-D Contact</b>	<b>Explanation</b>
Mean	x	fine → normally graded	x	normally graded → normally graded
D(99)	x	fine → normally graded	x	normally graded → normally graded
Skewness	x	fine → normally graded	x	normally graded → normally graded
Sorting	x	well sorted → moderately well sorted to well sorted		
X-plots	x	groupings in all graphs	x	groupings in all graphs
Visual	x	abrupt layer of shell fragments above contact, inconsistently spaced laminae → consistently spaced laminae	x	laminae → no laminae

Photo	x	abrupt layer of shell fragments above contact, inconsistently spaced laminae → consistently spaced laminae, grey → brown	x	laminae → no laminae, brown → light brown
Peel	x	abrupt layer of shell fragments above contact, inconsistently spaced laminae → consistently spaced laminae	x	laminae → no laminae
<b>2040</b>	<b>S-F Contact</b>	<b>Explanation</b>	<b>F-D Contact</b>	<b>Explanation</b>
Mean	x	fine → normally graded	x	normally graded → fine
D(99)	x	fine → normally graded	x	normally graded → fine
Skewness	x	fine → normally graded	x	normally graded → fine
Sorting	x	well sorted → moderately well sorted to well sorted	x	less well sorted → well sorted
X-plots				
Visual	x	abrupt layer of shell fragments above contact, inconsistently spaced laminae → consistently spaced laminae	x	laminae → no laminae
Photo	x	abrupt layer of shell fragments above contact, inconsistently spaced laminae → consistently spaced laminae, grey → brown	x	laminae → no laminae, brown → light brown
Peel	x	abrupt layer of shell fragments above contact, inconsistently spaced laminae → consistently spaced laminae	x	laminae → no laminae